



Deposited via The University of Leeds.

White Rose Research Online URL for this paper:

<https://eprints.whiterose.ac.uk/id/eprint/169823/>

Version: Accepted Version

Article:

Scotese, CR, Song, H, Mills, BJW et al. (2021) Phanerozoic Paleotemperatures: The Earth's Changing Climate during the Last 540 million years. *Earth-Science Reviews*, 215. 103503. ISSN: 0012-8252

<https://doi.org/10.1016/j.earscirev.2021.103503>

Crown Copyright © 2021 Published by Elsevier B.V. This manuscript version is made available under the CC-BY-NC-ND 4.0 license <http://creativecommons.org/licenses/by-nc-nd/4.0/>.

Reuse

This article is distributed under the terms of the Creative Commons Attribution-NonCommercial-NoDerivs (CC BY-NC-ND) licence. This licence only allows you to download this work and share it with others as long as you credit the authors, but you can't change the article in any way or use it commercially. More information and the full terms of the licence here: <https://creativecommons.org/licenses/>

Takedown

If you consider content in White Rose Research Online to be in breach of UK law, please notify us by emailing eprints@whiterose.ac.uk including the URL of the record and the reason for the withdrawal request.

1
2
3
4
5
6
7
8
9
10
11
12
13
14
15
16
17
18
19
20

Phanerozoic Paleotemperatures: The Earth’s Changing Climate during the Last
540 million years

by

Christopher R. Scotese, Department of Earth and Planetary Sciences, Northwestern University, Evanston, IL,
60208, cscotese@gmail.com

Haijun Song, State Key Laboratory of Biogeology and Environmental Geology, School of Earth Sciences, China
University of Geosciences, Wuhan, 430074, China, haijunsong@cug.edu.cn

Benjamin J.W. Mills, School of Earth and Environment, University of Leeds, Leeds, LS2 9JT, UK,

and Douwe G. van der Meer, CNOOC International, 945 Bunker Hill Road, Houston, Tx 77024, USA

11/25/2020

21

22 **Abstract**

23 This study provides a comprehensive and quantitative estimate of how global temperatures have
24 changed during the last 540 million years. It combines paleotemperature measurements
25 determined from oxygen isotopes with broader insights obtained from the changing distribution of
26 lithologic indicators of climate, such as coals, evaporites, calcretes, reefs, and bauxite deposits. The
27 waxing and waning of the Earth's great polar icecaps have been mapped using the past distribution
28 of tillites, dropstones, and glendonites. The global temperature model presented here includes
29 estimates of average global temperature (GAT), changing tropical temperatures (ΔT° tropical), deep
30 ocean temperatures, and polar temperatures. Though similar, in many respects, to the temperature
31 history deduced directly from the study of oxygen isotopes, our model does not predict the extreme
32 high temperatures for the Early Paleozoic required by isotopic investigations. The history of global
33 changes in temperature during the Phanerozoic has been summarized in a "paleotemperature
34 timescale" that subdivides the many past climatic events into 8 major climate modes; each climate
35 mode is made up of 3-4 pairs of warming and cooling episodes (chronotemps). A detailed narrative
36 describes how these past temperature events have been affected by geological processes such as
37 the eruption of Large Igneous Provinces (LIPS) (warming) and bolide impacts (cooling). The
38 paleotemperature model presented here allows for a deeper understanding of the interconnected
39 geologic, tectonic, paleoclimatic, paleoceanographic, and evolutionary events that have shaped our
40 planet, and we make explicit predictions about the Earth's past temperature that can be tested and
41 evaluated. By quantitatively describing the pattern of paleotemperature change through time, we
42 may be able to gain important insights into the history of the Earth System and the fundamental
43 causes of climate change on geological timescales. These insights can help us better understand the
44 problems and challenges that we face as a result of Future Global Warming.

45

46

47 Keywords: paleoclimate, paleotemperature, Phanerozoic, climate change, climate history, ice age,
48 icehouse, hothouse, Hirnantian Ice Age, Permo-Carboniferous Ice Age, End Triassic Extinction, K/T
49 Extinction, K/T Impact Winter, PETM, Pleistocene Ice Age, Future Global Warming, $\delta^{18}\text{O}$, $\delta^{13}\text{C}$

50

51

Part I. Introduction, Methods, and Discussion

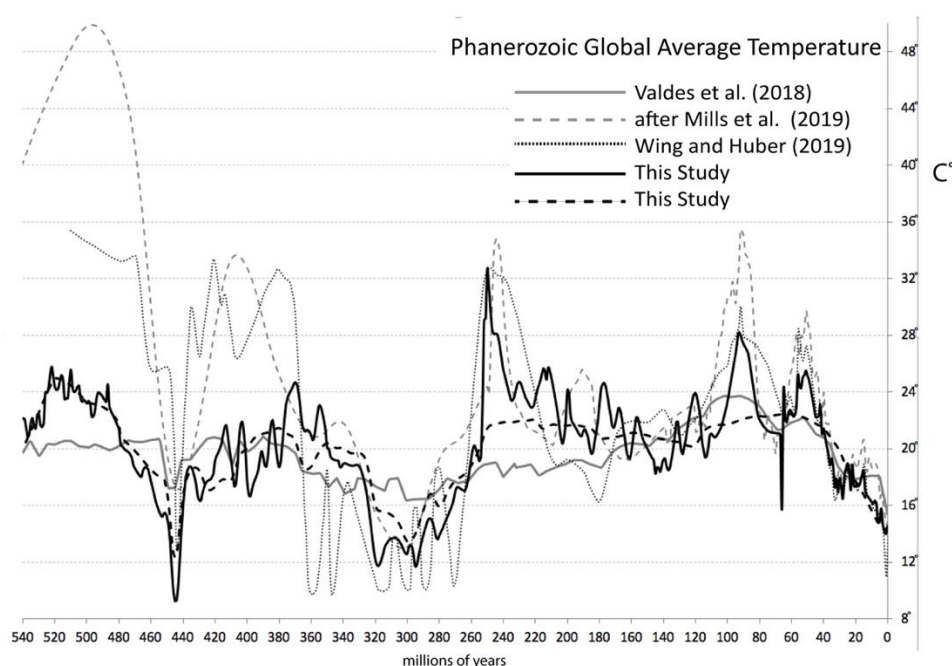
52 1. Introduction

53 There have been several recent studies of the Earth's changing temperature during the Phanerozoic,
54 e.g. Grossman (2012a&b); Veizer and Prokoph, (2015); Scotese (2016); Mills et al. (2019); Henkes et
55 al. (2018); Wing and Huber (2019); Verard and Veizer (2019); Song et al. (2019); Grossman and
56 Joachimski, 2020). All of these studies are based on oxygen isotope measurements of $\delta^{18}\text{O}$ in
57 carbonate or apatite microfossils. The first extensive compilation of oxygen isotope data assembled
58 by Veizer and Hoefs (1976) and Veizer et al. (1986, 1999, 2000) has been used by other researchers
59 to characterize temperature change at a variety of temporal and geographic scales (Royer et al.,
60 2004; Prokoph et al., 2008; Grossman, 2012 a&b). Recently, two comprehensive, global Phanerozoic
61 compilations of oxygen isotope paleotemperatures have been assembled (Song et al., 2019 and the
62 PALects database, Grossman et al., 2018).

63 Urey (1951) and Emiliani (1955) were the first scientists to appreciate the utility of oxygen isotopes.
64 For every 4.3°C increase in temperature, there is a 0.1% decrease in the amount of ^{18}O (Epstein and
65 Mayeda, 1953) used to produce the calcium carbonate of the foraminifera's shell. By measuring the
66 ratio of ^{18}O to ^{16}O , also referred to as $\delta^{18}\text{O}$, it is possible to estimate the temperature at which the
67 calcium carbonate was produced. Savin et al. (1975), Savin (1977), Miller et al. (1987), Zachos et al.,
68 (2001, 2008) and Cramer et al. (2009) used the changing ratios of $^{18}\text{O}/^{16}\text{O}$ in benthic foraminifera to

69 describe the changing temperature of the world's oceans and the growth of the polar icecaps. For an
70 excellent summary of the science of oxygen isotopes see Grossman (2012a).

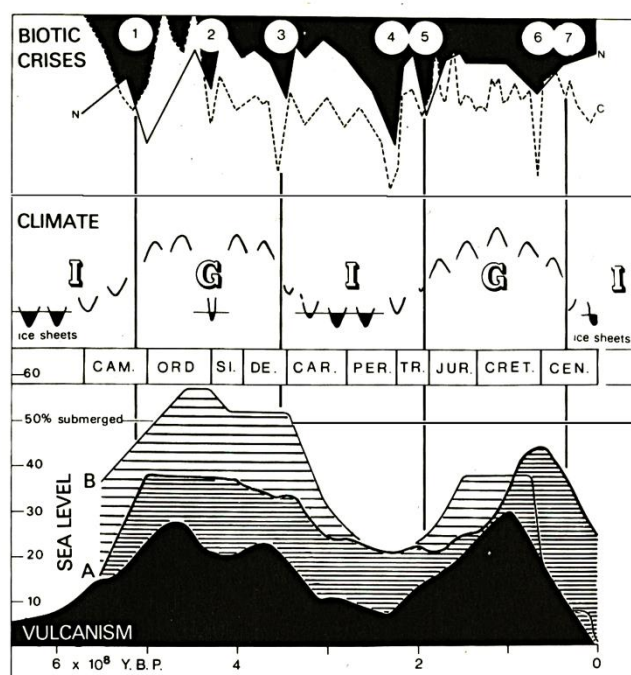
71 The oxygen isotope record is strongly biased towards tropical regions and measurements of
72 temperature derived from localities above 40° N or S are sparse; therefore, paleotemperature curves
73 that exclusively use $\delta^{18}\text{O}$ data (Song et al., 2019; Verard and Veizer, 2019; Veizer and Prokoph, 2015;
74 Grossman, 2012a&b; Royer et al. 2004) are measurements of tropical temperature, not global
75 temperature. Only the Phanerozoic paleotemperature curves of Scotese (2016), Mills et al., (2019,
76 2020), Wing and Huber (2019), and Valdes et al. (2018) (Figure 1), either adjust the isotopic
77 temperatures to compensate for the difference between tropical and global temperatures or use
78 non-isotopic temperature information (e.g., HadCM3 paleoclimate model simulations, Valdes et al.,
79 2020).



80 Figure 1. Estimates of Phanerozoic Global Average Temperature (GAT). Sources: Wing and Huber (2019), Valdes et al. (2018), Mills et al. (2019), and This study.

81 These curves are in good agreement and show the classic “double hump” Phanerozoic temperature
82 history shown in Figure 2 (Fischer, 1981, 1982, 1984; Frakes, et al., 1992, fig. 11.1; Scotese et al.,
83 1999; Summerhayes, 2015). Temperatures are high during the Early Paleozoic. Cooler temperatures
84 prevail during the Late Paleozoic, followed by warmer Mesozoic and early Cenozoic temperatures,

85 finally returning to cooler temperatures in the Late Cenozoic. This pattern is linked to the “Wegener
 86 Supercontinent” cycle (Nance et al., 2014; Van der Meer et al., 2014; 2017), namely: the breakup of
 87 the supercontinent, Pannotia, during the latest Precambrian (Powell et al., 1993; Powell, 1995;
 88 Scotese, 2009; Nance and Murphy, 2018), the formation of Pangea during the late Paleozoic (~300
 89 Ma), its subsequent breakup (~200 Ma), and the assembly of the modern continental configuration.



90 Figure 2. “Double Hump” pattern of Phanerozoic Climate (Fischer, 1981; 1982), I = Icehouse, G = Greenhouse .

91 Specific features that the curves in Figure 1 share in common are:

- 92 1) A broad sinusoidal pattern with peaks near 20 Ma, 50 Ma, 90 Ma, 245 Ma, 370 Ma, 420 Ma, and
- 93 500 Ma, with the highest peaks occurring at, 90 Ma, and 245 Ma.
- 94 2) Broad troughs link the 370 Ma and 245 Ma peaks and the 245 Ma and 90 Ma peaks.
- 95 3) The three youngest peaks (i.e. 90 Ma, 50 Ma, and 20 Ma) decrease, stepwise, in height.
- 96 4) The coherence of the curves breaks down during the middle and early Paleozoic. Some curves
- 97 rapidly trend toward higher isotopic temperatures.

98 5) The temperatures between 330 Ma and 290 Ma (Permo-Carboniferous Ice Age), are $\sim 14^{\circ}\text{C}$ on
99 average, but fluctuate 6°C with a period of ~ 10 million years.

100 6) A sharp “dip” occurs at in all curves at 445 Ma (Hirnantian Ice Age).

101 The pre-Carboniferous portions of these temperature curves can be divided into two groups: the
102 “hothouse” middle and early Paleozoic versions (Valdes et al., 2018; this study), and the “extreme
103 hothouse” middle and early Paleozoic versions (Mills et al., 2019; Wing and Huber, 2019).

104 It should be emphasized that the paleotemperature curve that we will present here is a “model” of
105 Phanerozoic temperature change. No one line of evidence, such as, lithologic indicators of climate,
106 oxygen isotopic measurements, or CO_2 proxy information (Foster et al., 2017) is sufficient to
107 estimate past temperatures. We combine multiple, independent lines of evidence to produce a
108 synthetic, multi-disciplinary model that describes how global temperature may have varied during
109 the last 540 million years. The temperature predictions made by this model can be used to form
110 hypotheses that can be tested by the acquisition of new $\delta^{18}\text{O}$ temperature data, by other
111 independent measurements of paleotemperature (e.g., Tex 86 or clumped isotope data), as well as
112 the expected effects of temperature on the evolution of life and the environment.

113

114 **2. Methods**

115 **2.1 Derivation of the Phanerozoic Global Average Temperature Curve**

116 Our Phanerozoic Global Average Temperature Curve has been produced by combining: 1) estimates
117 of the changing pole-to-Equator temperature gradient obtained from lithologic indicators of climate
118 (i.e. paleo-Köppen belts), and 2) estimates of tropical changes in temperature obtained from oxygen
119 isotopes. The temperatures obtained from oxygen isotope measurements have been summarized
120 and sometimes temperatures have been modified to better agree with the geological and
121 paleontological record.

122 We only schematically illustrate the extremely rapid (<1 million years), high amplitude temperature
123 fluctuations that occurred during the coldest intervals. These dramatic temperature fluctuations are
124 triggered by variations in insolation due to changes in the three Milankovitch parameters (obliquity,
125 precession, and eccentricity). The effect of on short term climate are discussed in more detail in
126 Kump et al. (1999c), Ruddiman (2001), and Hay (2016).

127

128 **2.2 Estimates of Pole-to-Equator Temperature gradients derived by mapping Köppen Climate** 129 **Belts**

130 Long-term global temperature (>50 million years) is controlled by multiple tectonic and
131 environmental processes that drive the Earth's climate from icehouse to hothouse conditions and
132 vice-versa. The dominant factors are the level of greenhouse gases (principally CO₂), which are
133 regulated by volcanic outgassing and the draw down of CO₂ due to weathering (van der Meer et al.
134 2014, Torsvik et al., 2020) the geographic configuration of the continents and ocean basins
135 (paleogeography and paleoceanography), and the reflectivity of the Earth's surface (albedo). Many
136 of these factors are interconnected by a complex network of positive and negative feedback loops
137 that can accelerate or slowdown changes in long-term global temperature (Hay, 2016; Ruddiman,
138 2001).

139 In this paper we use the geologic record, specifically the paleogeographic distribution of lithologic
140 indicators of climate to map how the Earth's Pole-to-Equator temperature gradient has changed
141 through time. The expansion, contraction, and shifting position of the Earth's climatic belts
142 provides important insights into the changes in the Earth's long-term climate history.

143 Using modern temperature and rainfall records, we can map five very distinct climatic regions called
144 "Köppen Climate Belts" (Figure 3). The Köppen Climate Belts are defined by seasonal variations in
145 temperature and precipitation (Köppen, 1918). These variations give rise to regional climates and

146 create the mosaic of diverse environments that cover the Earth. These environments include: (A)
 147 tropical rainforests near the Equator, (B) desert belts at subtropical latitudes that transition into (C)
 148 warm temperate grasslands and forests. In the modern world, as we move poleward, warm-
 149 temperate regions are replaced by (D) seasonally warm/cold temperate regions and (E) finally frigid
 150 polar regions. These climatic zones extend over the oceans where they are primarily zonal. Each of
 151 these climatic zones is characterized by a distinctive, flora, fauna, land-cover, and geology.

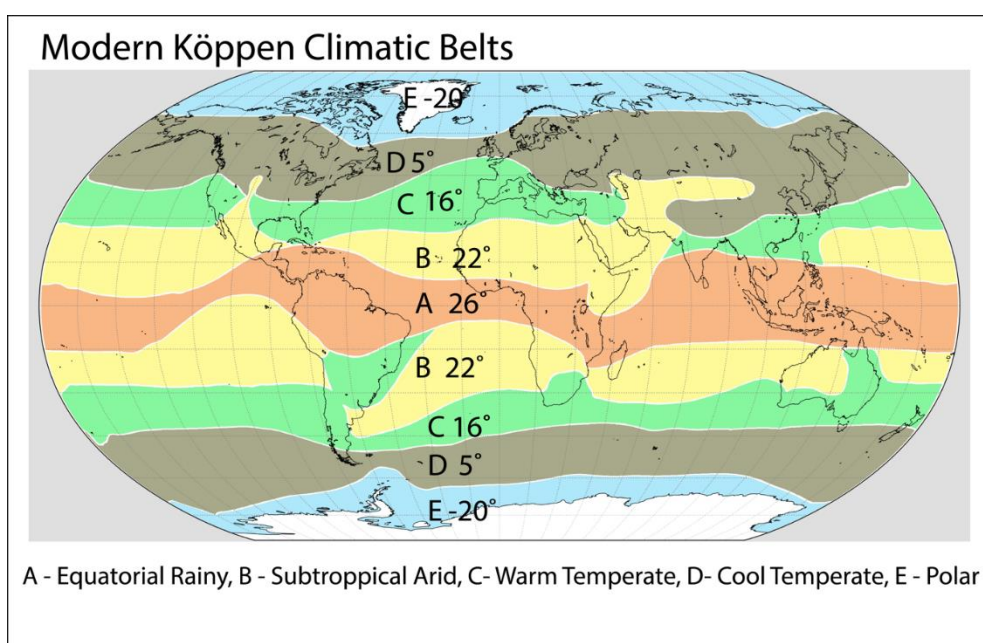
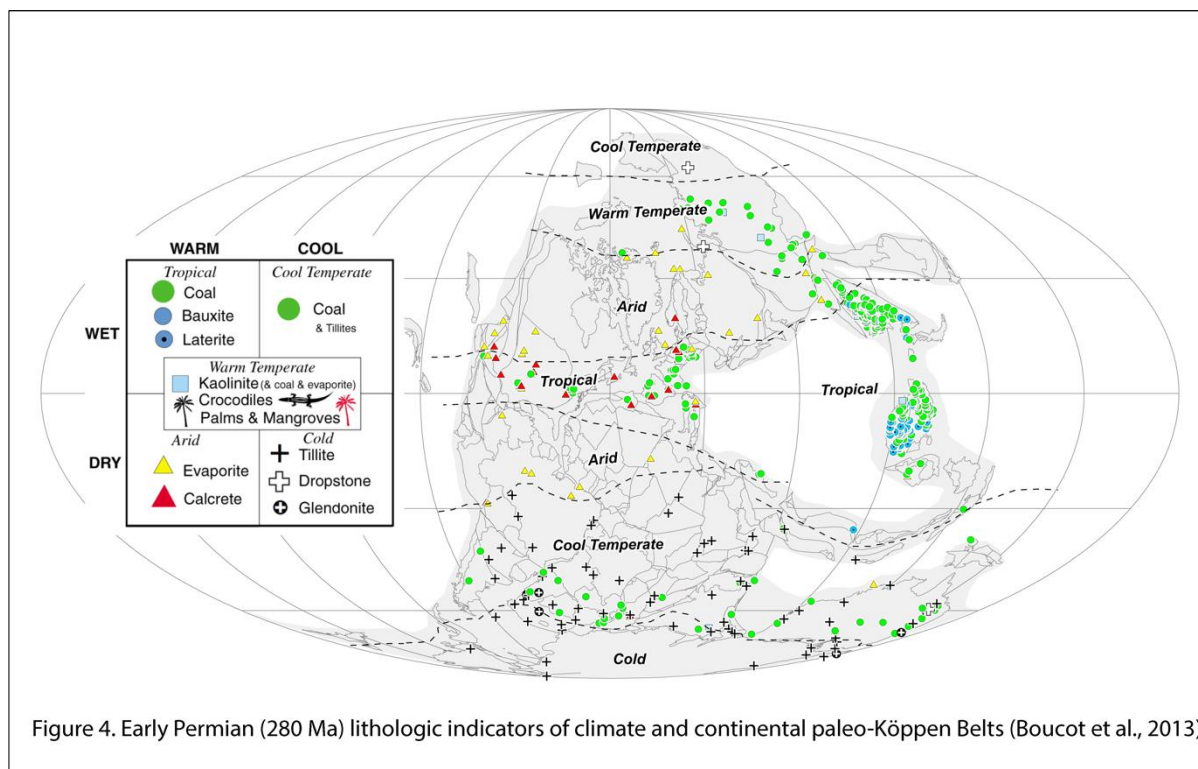


Figure 3. Modern Köppen belts and the average temperature of each belt.

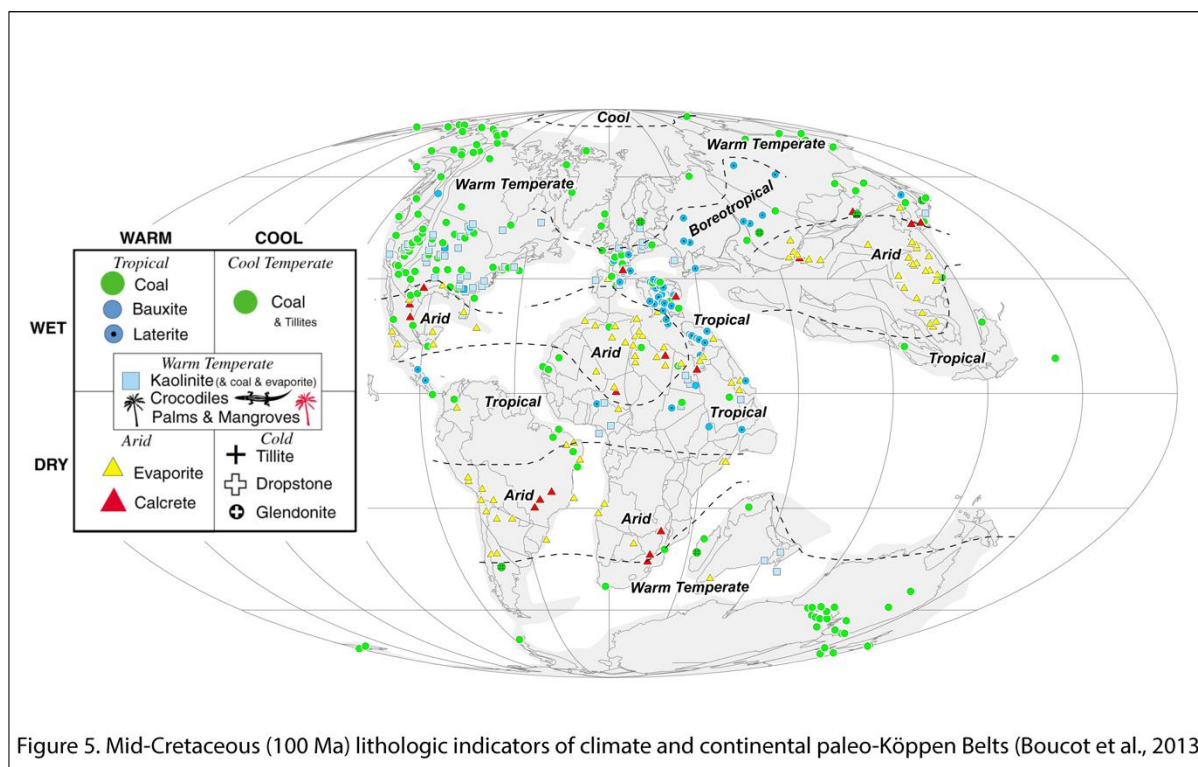
152

153 Using lithologic indicators of climate such as coals, evaporites, and glacial deposits, it is possible to
 154 map “paleo”– Köppen Climate Belts for ancient time periods (Ziegler et al., 2003; Boucot et al., 2013;
 155 Figures 4 and 5). Over the past 20 years, a global database of over 15,000 lithologic indicators of
 156 climate was assembled (Boucot et al., 2013). For a thorough discussion of both lithologic and
 157 biological indicators of climate, see Parrish, 1998; Boucot et al., 2013; and Cao et al., 2019. Other
 158 important lithologic indicators of climate are: soil minerals such as bauxite, an aluminum ore which
 159 forms in warm, wet climates; calcrete, or caliche, which forms in semi-arid regions; and kaolinite
 160 which forms in regions with climates that are sometimes wet and sometimes dry (warm temperate
 161 climate belt). Dropstones, like tillites, are important indicators of frozen lakes or sea ice. A
 162 glendonite it is a pseudomorph of ikaite, a low temperature, hydrated polymorph of CaCO_3 that

163 forms at temperatures $<4^{\circ}$ C. Recent experimental data suggests that it may also form at higher
 164 temperatures under special conditions (Tollefsen et, 2020). The legend inset on Figures 4 and 5
 165 summarizes the association of the various lithologic indicators of climate with warm/cool and
 166 wet/dry environmental conditions.



167



168

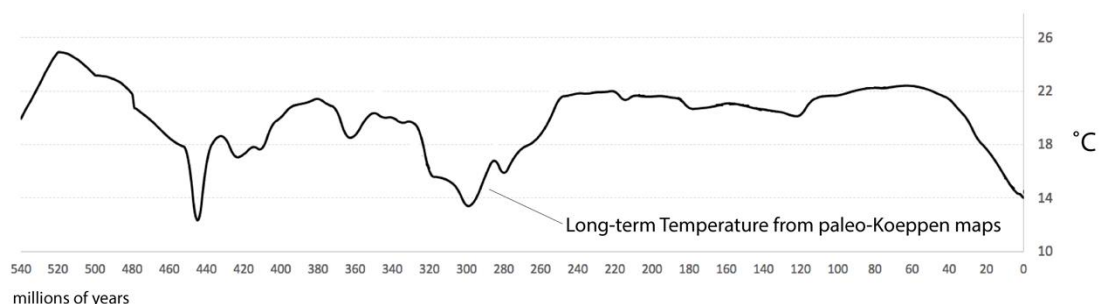
169 Bauxites, as a general rule, reflect tropical-subtropical humid, monsoonal conditions. Their modern
 170 occurrence is almost entirely restricted to the Equatorial Wet Belt. The occurrence of bauxite
 171 deposits in northern Europe and Siberia during the late Jurassic, Cretaceous, Paleocene, and Eocene
 172 times (Boucot et al., 2013), is one of the strongest geological indications of warm and wet conditions
 173 at high latitudes.

174 When we plot these lithologic indicators of climate on a set of paleogeographic maps we find that
 175 there have been times (e.g., Early Permian, Figure 4) when the Earth's climate was much like the
 176 present-day "icehouse" world. An icehouse world is simply defined as a time when the Earth is
 177 covered by permanent ice at either pole. For permanent ice to accumulate in the polar regions (>67°
 178 N & S) the temperatures must remain below freezing during the summer months. In other words,
 179 the global average temperature (GAT) must be less than around 18°C and the average annual
 180 temperature of the polar region must be below -5 °C. Though the tropics remain relatively warm
 181 (26°C) in an icehouse world, the polar regions are frigid (-5°C to - 50°C).

182 There are also have been times when there was no ice above the polar circle – even during the
 183 winter (e.g., Late Cretaceous, Figure 4). During these “hothouse” times, the average temperature of
 184 the Earth was generally above 20°C (68°F) and the polar regions were relatively warm (5°C to 15°C)
 185 and no ice could accumulate. It is a well-established fact that no polar ice existed during the
 186 Paleocene-Eocene Thermal Maximum (55.6 Ma; McInerney and Wing, 2011) or the Cenomanian-
 187 Turonian Thermal Maximum (93 Ma; Ziegler et al., 1985).

188 The long-term temperature curve (Figure 6) was calculated by mapping past extent of the five major
 189 Köppen belts using lithologic indicators of climate (tillites, dropstones, glendonites, high latitude
 190 mangroves, palms, and crocodiles; temperate coal, evaporites, calcretes, tropical coals, bauxites,
 191 and laterites (Boucot et al., 2013)). These paleoclimatic reconstructions, spaced at intervals of 5
 192 million years, were used to characterize changes in global temperature along a spectrum of climatic
 193 states ranging from Severe Icehouse (GAT = 10° - 14°C) to Extreme Hothouse (GAT = 22° - 26°C;
 194 Figure 5). The complete set of more than 100 paleo-Köppen maps illustrating the distribution of
 195 lithologic indicators of climate are provided in the Supplemental Materials (Part 3).

Figure 6. Long-Term Phanerozoic temperature trend calculated by estimating the changing area of paleo-Köppen belts (see Supplementary Materials for data and details of calculations).



197 The average temperatures of the modern Köppen belts was calculated using the global temperature
 198 model of Legates and Wilmott (1990). The Equatorial Rainy Belt has a Mean Annual Temperature
 199 (MAT) of 26°C; the Subtropical Arid Belt’s MAT is 22°C; the Warm Temperate Belt’s MAT is 16°;
 200 Cool Temperate Belt’s MAT is 5 °C; and the North & South Cold Polar Belts’ MAT average -20°C. The
 201 Global Average Temperature (GAT) was then estimated by summing the areas of the 5 major Köppen

202 climatic belts on each of the paleoclimatic reconstruction and then multiplying that area by the MAT
203 of that Köppen belt. For example, for the modern world (Figure 3): the Equatorial Rainy Belt (A)
204 covers 23% of the Earth's surface, the Arid Belt (B) covers 28%, the Warm Temperate Belt (C) covers
205 20%, the Cool Temperate Belt (D) covers 20%, and the Polar Belt (E) covers 9%. The present-day
206 global average temperature (GAT) = $.23*(26^{\circ}\text{C}) + .28*(22^{\circ}\text{C}) + .20*(16^{\circ}\text{C}) + .20*(5^{\circ}\text{C}) + .09*(-20^{\circ}\text{C})$,
207 which simplifies to $(5.98^{\circ}\text{C} + 6.16 + 3.2 + 1.0 - 1.8)^{\circ}\text{C} = 14.5^{\circ}\text{C}$.

208 On the mid-Cretaceous paleoclimatic reconstruction (Figure 5): the Equatorial Rainy Belt covers 25%
209 of the Earth's surface, the Subtropical Arid belt covers 29%, the Warm Temperate Belt covers 44%,
210 the Cool Temperate Belt covers 2%, and the Cold Polar Belt covers 0%. The GAT = $.25*(26^{\circ}\text{C})$
211 $+ .29*(22^{\circ}\text{C}) + .44*(16^{\circ}\text{C}) + .02*(5^{\circ}\text{C}) + 0.0$, which gives 20°C . The Boreotropical belt, which is strictly
212 a climatic feature of hothouse worlds is assigned the same average temperature as the Arid Belt.

213 In a similar fashion, the global average temperature for the Early Permian (280 Ma, Figure 4) was
214 calculated as follows: GAT = $.20*(26^{\circ}\text{C}) + .29*(22^{\circ}\text{C}) + .16*(16^{\circ}\text{C}) + .30*(5^{\circ}\text{C}) + .05*(-20^{\circ}\text{C})$, which equals
215 14.6°C . The global average temperature during the early Permian icehouse was similar to the
216 present-day icehouse.

217 Global temperatures were calculated in this manner for 100 Phanerozoic reconstructions of paleo-
218 Köppen belts (one map \sim 5 million years). For an in-depth discussion of the data and methodology
219 used see the Supplementary Materials. The resulting long-term global temperature curve is shown in
220 Figure 6.

221 The estimates of global temperature obtained in this manner, do not provide a precise or detailed
222 measurement of how the Earth's temperature has changed through time. The width of the Köppen
223 belts are only approximate and are poorly known for older time periods, especially the Early
224 Paleozoic. Though we assume a zonal pattern for the oceans, there are certainly major distortions
225 caused by ocean currents and upwelling (Figure 3). Most importantly, the temperatures assigned to

226 each of the Köppen belts are based on modern icehouse values and may not reflect temperatures in
227 past hothouse worlds.

228 Despite these limitations, the Köppen approach does provide one important bit of information. This
229 procedure tells how the Pole-to-Equator temperature gradient has changed through time. The
230 relative widths of the equatorial wet and the subtropical arid belt do not change significantly
231 through time because they are controlled by Hadley Cell Circulation. The changing in Pole-to-Equator
232 temperature gradient is due nearly exclusively due to the changing width of the Warm Temperate,
233 Cool Temperate and Polar Belts.

234 In icehouse worlds, like the present-day, Pole-to-Equator temperature gradient is very steep. The
235 temperature falls $.75^{\circ} - 1^{\circ}$ C per degree of latitude as we move towards the Pole (e.g., if we start at
236 30° C at the Equator, we end up with temperatures of -40° C to -60° C at the pole). During hothouse
237 worlds (e.g., Cenomanian-Turonian Thermal Maximum, 93 Ma), the pole-to-Equator temperature
238 gradient was much shallower, approximately $.20^{\circ} - .33^{\circ}$ C per degree of latitude. That means that if
239 we start out at 30° C at the Equator, the temperature at the Pole would still be well above freezing
240 (0° to 12° C).

241 Figure 7 illustrates the possible range of ancient Pole-to-Equator gradients. The plus signs lie along
242 the modern Pole-to-Equator gradient and describe how temperatures change as a function of
243 latitude. In the present-day world, the temperature near the Equator is 26° C. The temperature
244 remains nearly constant in the subtropics ($0^{\circ} - 15^{\circ}$ latitude), and then begins to decrease rapidly.
245 Freezing temperatures are reached at 60° latitude; falling to -35° C at the Poles.

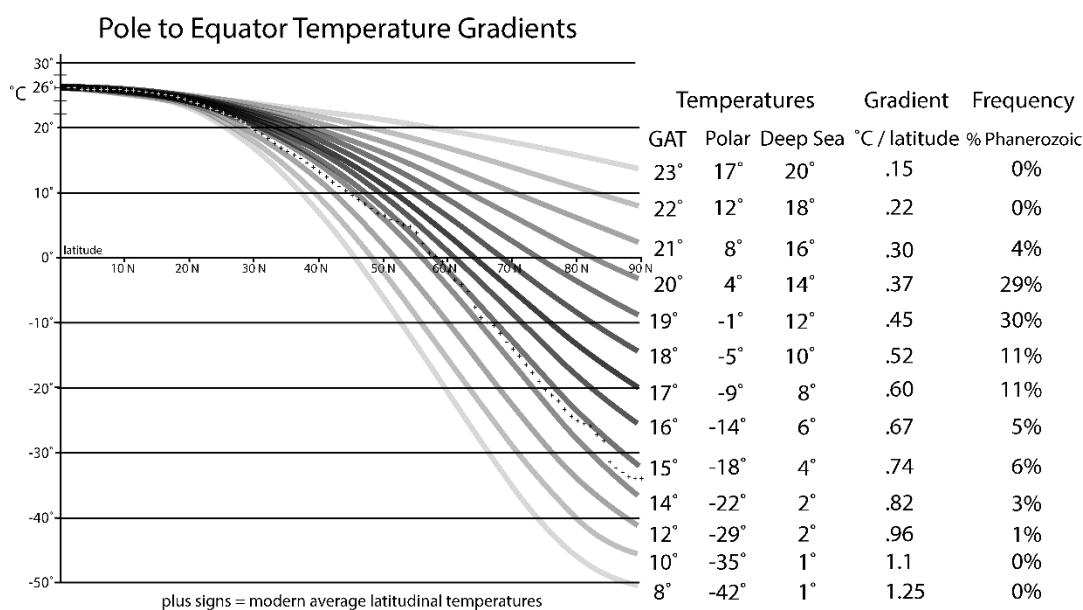


Figure 7. The polar temperature and the Pole to Equator temperature gradient for different Global Average Temperatures (GAT). Polar Temperature = average temperature above 67° latitude (N&S), Deep Sea = the average temperature at the bottom of the oceans (after Valdes et al., 2020). Pole to Equator Gradient = the average change in temperature for every one degree of latitude measured between 30° and 60° latitude. The Pole to Equator temperature gradient is shallow near the Equator and steepens rapidly near the Pole. The plus signs are the combined average temperatures for the present-day northern and southern hemispheres. Frequency % Phanerozoic = the percent of the time during the Phanerozoic characterized by this specific Pole-to-Equator temperature gradient. All of these calculations are based on an average tropical temperature of 26°C (15° N – 15° S).

246

247 The first column labelled “GAT” is the global average temperature obtained by the Köppen

248 technique. The adjacent curve is the Pole-to-Equator temperature gradient associated with that

249 GAT. The modern world (GAT = 14.5°C) falls between the 14°C and 15°C curves. The other columns

250 describe how the polar temperature, the temperature of the deep ocean and the latitudinal gradient

251 (between 30° - 60° latitude), change with each “GAT” curve. These topics will be discussed later. The

252 final column labelled, “Frequency % Phanerozoic”, records the frequency of these various GATs

253 during the Phanerozoic. Past hothouse worlds with global temperatures ranging between 19° - 20°C

254 have been the most frequent (~60%). Icehouse worlds with global temperatures similar to the

255 modern world (>15°C) are relatively rare (~10%). It should be noted that some very shallow Pole-to-

256 Equator gradients (GAT > 21°C), though theoretically possible, have probably not been achieved.

257 Conversely, Pole-to-Equator gradients associated with GATs below 10° C, have only been seen in the

258 Snowball Earth worlds of the late Precambrian (Hoffman and Schrag, 1998; 2000; 2002 ; 2009).

259 Though these estimates of Global Average Temperature are based on a methodology rooted in the
260 modern icehouse world, it is possible to make adjustments to these GATs so that they also reflect
261 temperature changes in past hothouse worlds. As can be seen in Figure 7, all of the Pole-to-Equator
262 temperature gradient curves are set to 26°C at the Equator. This equatorial temperature is certainly
263 lower than the equatorial temperatures during hothouse times. In the next section we describe how
264 we used oxygen isotopic data to estimate the change in tropical temperatures through time.

265

266 **2.3 Global Temperature Change (~10 - 20 million years) derived from Oxygen Isotopic Data**

267 In addition to the gradual change in global temperature recorded by the changing pole-to-Equator
268 gradient, we know that the Earth's temperature has varied significantly over periods of 10 – 20
269 million years. The evidence for these temperature changes comes from the measurements of the
270 ratio of $^{18}\text{O}/^{16}\text{O}$ (also referred to as $\delta^{18}\text{O}$) in the shells and bones secreted by marine organisms
271 (Figure 8).

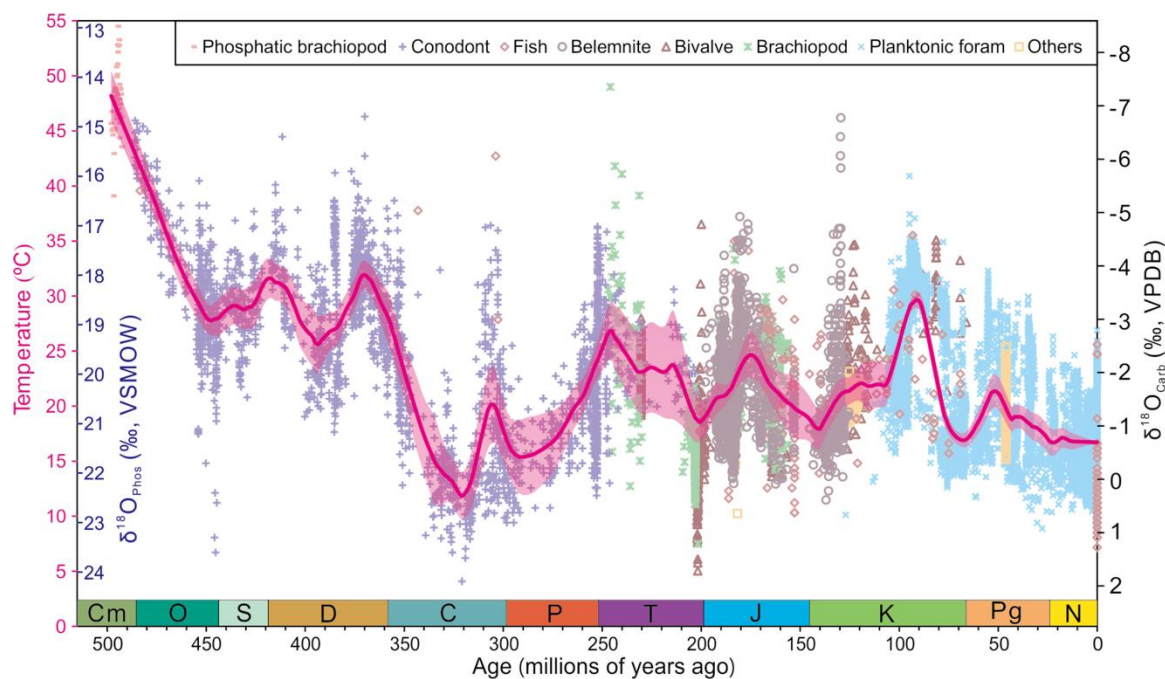


Figure 8. Raw and mean values of oxygen isotopes from phosphatic and carbonate fossils for reconstructing sea surface temperatures over the past 500 million years (modified after Song et al., 2019). The scale of $\delta^{18}\text{O}_{\text{Phos}}$ is used for phosphatic fossils, i.e., phosphatic brachiopod, conodont, and fish. The scale of $\delta^{18}\text{O}_{\text{Carb}}$ is used for carbonate fossils, i.e., belemnite, bivalve, brachiopod, planktonic foraminifer, and others. Magenta curve represents the mean values of sea surface temperatures per million years. Shaded area represents 95% confidence intervals.

272

273 The solid black line in Figure 9A illustrates the isotopic temperature of seawater for the last 500
 274 million years based on a compilation of >22,000 oxygen isotope measurements (Song et al., 2019).
 275 Isotopic values were converted to temperature using the equation of Lécuyer (2013) for phosphate
 276 fossils and by using the equation of Hays and Grossman (1991) for carbonate fossils. Because the
 277 samples upon which this curve is based come entirely from tropical and subtropical latitudes (< 40°
 278 N&S), this curve is essentially an estimate of tropical temperatures through time.

279 Each dot in Figure 9A represents the average of all isotopic estimates of temperature that fall within
 280 a one million year interval. Error estimates of the average temperature calculation are given in Song
 281 et al. (2019). The best-fit curve in Figure 9A was obtained using the Savitsky-Golay smoothing
 282 technique which fits successive sub-sets of adjacent data points with a low-degree polynomial by the
 283 method of linear least squares (Savitsky and Glay, 1964). We found the Savitsky-Golay method did a
 284 better job honoring the data points than either the high-order polynomial or LOESS techniques
 285 traditionally employed.

286

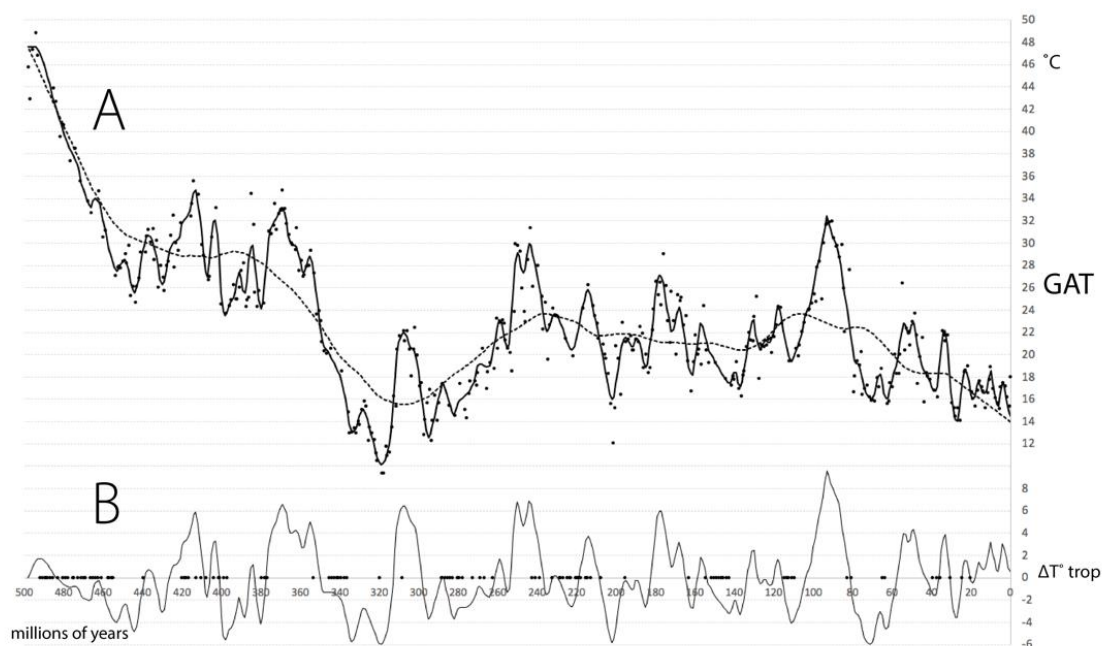


Figure 9. Phanerozoic Isotopic Temperature (Song et al., 2019). A. = Each dot represents the average of all temperatures that fall within a given one million year interval. The best-fit curve was obtained using the Savitsky-Golay smoothing technique (window 11-15, degree 4). B. Change in Tropical Temperature (ΔT^{trop}). The black dots along the x-axis are the times when no data are available.

287

288 Though the isotopic temperature curve is relatively flat for much of the Mesozoic and Cenozoic, the
 289 curve has a steep, linear negative slope during the early Paleozoic. The isotopic estimates of
 290 temperature for these times appear to be much higher (up to +24°C difference at 500Ma) than the
 291 temperatures obtained from lithologic indicators of climate.

292 It should be noted that the isotopic temperatures illustrated in this curve do not take into account
 293 regional variations in the isotopic composition of seawater, or proposed Phanerozoic changes in the
 294 ^{18}O ^{16}O ratio of seawater. Some researchers believe that there is a long-term trend in the average
 295 isotopic composition of seawater (Veizer, 2000; Prokoph et al., 2008; Verard and Veizer, 2019).

296 Others vehemently disagree (Grossman, 2012 a&b). This debate has been going on for more than 30
 297 years. It seems incredible that the average temperature of the tropical oceans could have been as
 298 high as 50°C (122° F) during the early Paleozoic and late Precambrian. This implies that diurnal or
 299 seasonal temperatures were much higher. Even in extreme cases, modern organisms cannot survive
 300 when seawater temperatures reach 40°C (104°F) (Fraenkel, 1960). Verard and Veizer (2019) propose

301 that a systematic decrease in plate tectonic activity during the last 540 million years may have
302 systematically increased the ratio of ^{18}O to ^{16}O in seawater; however, they admit that the details of
303 the correlation are poor and that tectonic activity prior to the formation of Pangea is not well-
304 known. It may be possible that the $\delta^{18}\text{O}$ composition of seawater has not remained constant, nor has
305 it gradually changed in a quasi-linear fashion. Rather the $\delta^{18}\text{O}$ could have varied non-monotonically
306 through time.

307 Upon reflection, what may be important is not the “absolute” temperature provided by the isotopic
308 data, but rather the “relative” change in temperature at shorter timescales. For our purposes, the
309 most useful information that can be gleaned from the isotopic temperature record is the change in
310 the tropical temperatures through time (i.e., the $\Delta T^{\circ}_{\text{trop}}$), Figure 9B. In order to calculate the $\Delta T^{\circ}_{\text{trop}}$,
311 we first estimated the long-term isotopic temperature signal by averaging the isotopic data using a
312 60 million year running-average. We chose 60 million years because it best approximated the long-
313 term temperature signal from the Köppen analysis. The 60 million year running average was then
314 subtracted from the best-fit isotopic tropical temperature estimates (Figure 9A, black line) to obtain
315 the $\Delta T^{\circ}_{\text{trop}}$ value (Figure 9B).

316

317 **2.4 Modifying the Isotopic Estimates of Changing Tropical Temperatures Using Geological and** 318 **Paleontological Constraints**

319 The isotopic temperature of seawater can be affected by multiple environmental conditions:
320 hypersalinity or hyposalinity, the presence of continental ice caps, or the water depth at which
321 sampled organisms originally resided (Grossman2012a,b). In this section we review the isotopic
322 estimate of tropical temperature described in the previous section and make modifications based on
323 geological and paleontological constraints.

324 Figure 10 illustrates the changing temperature of the Tropics (ΔT° trop) based on isotopic
 325 measurements (dotted line). Superimposed on the dotted line are colored lines that represent
 326 seven time intervals when the “raw” isotopic estimates of tropical temperature that do not agree
 327 with geological or paleontological information and therefore, must be adjusted or modified. These
 328 seven intervals are: the Cambrian, 540 – 485 Ma; the latest Ordovician, 445 -443 Ma; parts of the
 329 Permo-Carboniferous, 340 – 275 Ma; the Triassic, 252 – 200 Ma; the Early Cretaceous, 125 Ma – 95
 330 Ma; the latest Cretaceous, 80 – 65 Ma; and the Cenozoic (65 – 0 Ma).

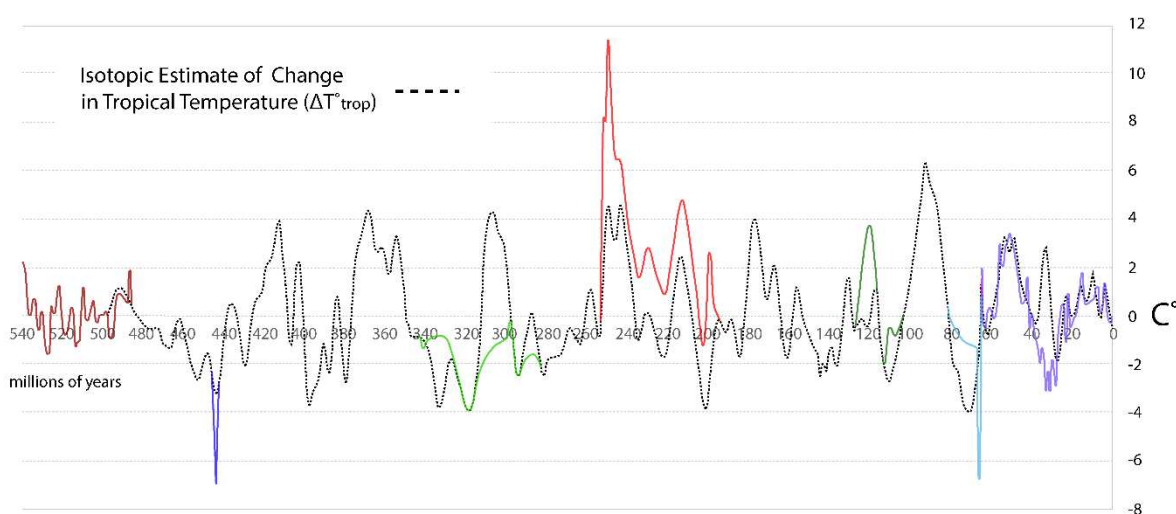


Figure 10. Modifications to the Phanerozoic Isotopic Temperature Curve. The dashed line is the isotopic temperature curve (see Figure 8). The colored lines represent modifications and adjustments made to that curve based on geological and paleontological constraints.

331

332 The procedure that we used to determine whether in isotopic measurements require modification
 333 was initially developed at a workshop convened by Scott Wing and Brian Huber at the Smithsonian
 334 National Museum of Natural History (April, 2017 & 2018). At those meetings a multidisciplinary
 335 group of more than 20 earth scientists convened at the Museum to refine a Phanerozoic
 336 paleotemperature curve that eventually became part of an exhibit on Global Warming in the
 337 Museum’s Earth History Hall (Wing and Huber, 2019). During that meeting participants were invited,
 338 based on their geological and paleontological knowledge and expertise, to make additions and
 339 revisions to the proposed Phanerozoic temperature curve which was posted as a wall-sized display.
 340 The results of that collaborative effort are illustrated in Figure 1 (Wing and Huber, 2019). The
 341 criteria used to modify or adjust the isotopic estimate of temperature included the addition of

342 ephemeral events which have not been sampled in the isotopic record (e.g., KT Impact Winter,
343 Permo-Triassic Thermal Maximum), the elimination of spurious thermal maxima during times of
344 icehouse conditions (e.g., late Pennsylvanian thermal maximum), and the elimination of cooling
345 events that would require large, permanent ice caps during times of hothouse conditions (e.g., latest
346 Cretaceous cooling). This same basic procedure was used by the authors to modify and adjust the
347 raw isotopic estimates of temperature so that they better agreed with geological and
348 paleontological constraints. In the following section, we describe the changes that have been made
349 to the raw isotopic estimates and the reasons for these changes.

350 **2.4.1 Cambrian, 540-485 Ma.**

351 There is sparse isotopic data older than 500 million years (Bergmann et al., 2018b; Hearing et al.,
352 2018; Henkes et al., 2018). The data that is available indicates that tropical temperatures were in
353 excess of 40°C; as noted previously, this is problematic (Fraenkel, 1960). For a more detailed
354 discussion of global temperatures during the Cambrian, see section 5.2.

355 The dark red curve in Figure 10 is a speculative estimate of temperature changes based on the
356 carbon isotope record. They coincide with 10 proposed Cambrian $\delta^{13}\text{C}$ isotopic excursions (Zhu et
357 al., 2006). The covariance of $\delta^{13}\text{C}$ and $\delta^{18}\text{O}$ trends has long been noted (Wenzel and Joachimski,
358 1996; Jenkyns et al., 2002). Approximately 80% of the positive $\delta^{13}\text{C}$ excursions are correlated with
359 warmer temperatures (hyperthermals). The correlation is generally attributed to the causal
360 relationship between higher ocean temperatures, the formation of deep water anoxia, and the
361 subsequent preservation of organic carbon.

362 **2.4.2 Latest Ordovician (Hirnantian, 445-443 Ma)**

363 The isotopic estimates of tropical temperatures during the Hirnantian Ice Age (see section 5.3), show
364 a notable dip of 3°C. We have exaggerated the dip in temperature to help explain the growth of the
365 massive, Hirnantian south polar ice cap that extended well into the Ordovician tropics (~35° S).

366 2.4.3 Permo-Carboniferous Icehouse

367 Evaporitic anomalies are known to affect the isotopic measurements made in the great subtropical
 368 epeiric seas of the Paleozoic (Mii et al., 1999). Because evaporation preferentially removed the
 369 lighter isotope of oxygen (^{16}O), the observed isotopic temperature measurements obtained from
 370 organisms living in these evaporitic seas are erroneously too cool. Conversely, freshwater is rich in
 371 ^{16}O , so isotopic estimates of temperature made in areas that receive a large influx of freshwater are
 372 erroneously too warm.

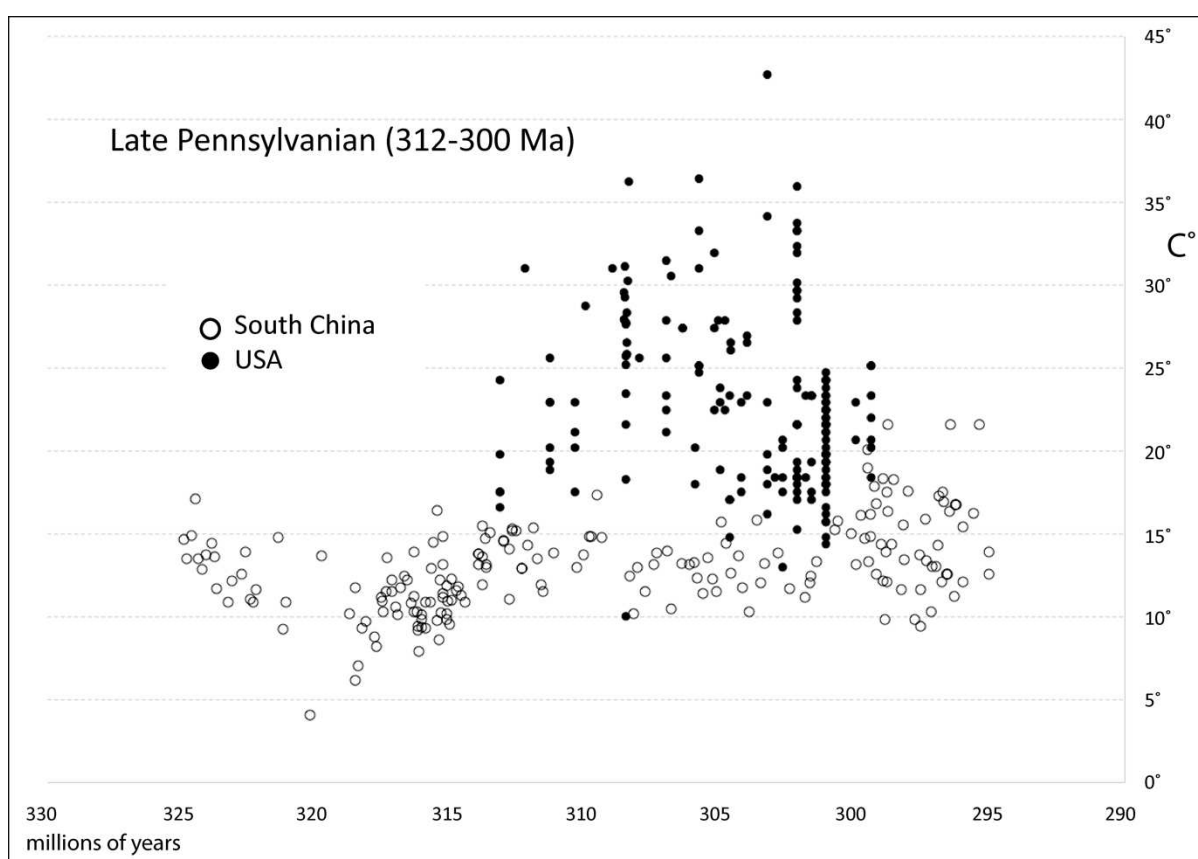


Figure 11. Comparison of isotopic temperature data from the late Pennsylvanian of South China (open dots) and the USA (black dots) (Song et al., 2019).

373

374 As Figure 10 shows, a broad temperature peak (dotted line) sits in the middle of the Permo-
 375 Carboniferous Ice Age. A closer examination of the isotopic temperature record reveals that the
 376 isotopic data for the late Pennsylvanian come primarily from South China and the USA (Figure 11).
 377 The isotopic temperatures for China (Chen et al., 2013; 2016) and the USA (Luz et al., 1984;

378 Joachimski et al., 2006; Elrick and Scott, 2010; Rosenau et al., 2014) are very different. The average
379 temperature for the USA data is $\sim 25^{\circ}\text{C}$, whereas the average temperature for South China is $\sim 13^{\circ}\text{C}$.
380 This difference in temperature cannot be explained in terms of latitudinal position. 310 million years
381 ago, both of these regions straddled the paleo-Equator (Scotese, 2014). The difference in isotopic
382 temperatures is more likely due to environmental differences. In the USA, the influx of fresh water
383 rich in ^{16}O from the rising Central Pangean mountain ranges may have altered the $^{18}\text{O} / ^{16}\text{O}$ ratio,
384 making the seawater “lighter”, giving a false, warmer isotopic temperature. We invoke a similar
385 explanation to explain the much smaller thermal anomaly in the early Permian (~ 285 Ma).

386 As described above, evaporitic anomalies may cause isotopic temperatures to appear “too cool”.
387 We can speculate that this phenomenon may explain the cooler than expected temperatures during
388 the early Carboniferous (~ 335 Ma).

389 We have applied an ad hoc correction of $4\text{-}5^{\circ}\text{C}$ to the mid-Pennsylvanian isotopic measurements to
390 bring them into line with the geological observations. This adjustment keeps temperatures below
391 the global temperature required to form permanent polar ice caps (see section 3.2). A more modest
392 adjustment of $2\text{-}3^{\circ}\text{C}$ was applied to the earliest Permian (295 – 285 Ma) because extensive south
393 polar glacial deposits indicate the Permo-Carboniferous glacial maximum occurred during the latest
394 Carboniferous – earliest Permian (see section 5.5). Conversely, the isotopic temperatures for the
395 Visean appear to be much too cold suggesting that the Visean represented the depths of the Permo-
396 Carboniferous Ice Age. This is not the case, the Visean was one of the warmest intervals of the
397 Carboniferous (Mii et al., 1999). Consequently, isotopic temperatures have been increased a modest
398 $2\text{-}3^{\circ}\text{C}$.

399 **2.4.1 Triassic and early Jurassic (252 – 200 Ma)**

400 Three adjustments to the average isotopic temperature were made for the Triassic. The Permo-
401 Triassic Extinction was the greatest mass extinction of the Phanerozoic (see section 5.6). The kill
402 mechanism was massive, global warming (see section 3.1.2). It is likely that average global

403 temperatures reached 40°C (Sun et al., 2012). The sharp spike in temperatures at the Permo-Triassic
404 have been adjusted accordingly.

405 Global temperatures peaked during the earliest Triassic, fell sharply during the early Triassic (Sun et
406 al., 2012), and extreme hothouse conditions did not ameliorate until the mid-Triassic (Ladinian; see
407 section 5.6). The averaged isotopic temperatures for the late Triassic and early Jurassic are far too
408 low and erroneously suggest possible icehouse conditions. This anomaly is probably due to the fact
409 that some of the isotopic measurements come from belemnites and clams that once inhabited
410 deeper, cooler waters (Dera et al., 2011; Wierzbowski and Joachimski, 2007). To remedy this
411 mismatch between isotopic and geologic evidence, global temperatures were increased by 2-3 °C.
412 Finally, the end of the Triassic was marked by a major extinction event that was most likely triggered
413 by the eruption of the Central Atlantic Magmatic Province (see sections 3.2 and 5.6). There is no
414 oxygen isotope record of this relatively brief event (1-2 million years; Ernst, 2014). To explain the
415 extinction event and other paleontological evidence of global warming, we have added a narrow
416 thermal spike at 200-201 Ma.

417 **2.4.5 Early Cretaceous (130 – 105 Ma) and latest Cretaceous (80 – 65 Ma).**

418 The Late Jurassic – earliest Cretaceous is generally considered to be a relatively cool period with
419 evidence of intermittent polar ice. Towards the end of this interval (~120 Ma), massive volcanic
420 eruptions took place in the Central Pacific (Greater Ontong Java Plateau), along the southern margin
421 of Africa, and forming the Kerguelen Plateau (see section 3.2 for details). The oldest Cretaceous
422 oceanic anoxic event, OAE1a, the Selli/Goguel Thermal Maximum is coincident with these LIP events.
423 Because this oceanic anoxic event is thought to have been triggered by significant global warming,
424 we have added a thermal peak at ~120 Ma. This early Aptian warming was followed by a “cold snap”
425 in the late Aptian – early Albian (see section 5.8). The little “bump” that precedes the Cenomanian-
426 Turonian Thermal Maximum represents the Paquier/Urbino Thermal Maximum (OAE1b) (see Table
427 6).

428 2.4.6 Cenozoic (65 – 0 Ma)

429 The classic record of deep ocean temperatures based on benthic foraminifera assembled by James
 430 Zachos (Figure 12, Zachos et al., 2001, 2008; Westerhold et al., 2020) provides a framework for
 431 describing the temperature fluctuations during the Paleocene-Eocene Hothouse and the Late
 432 Cenozoic Icehouse (Koeberl and Montanari, 2009).

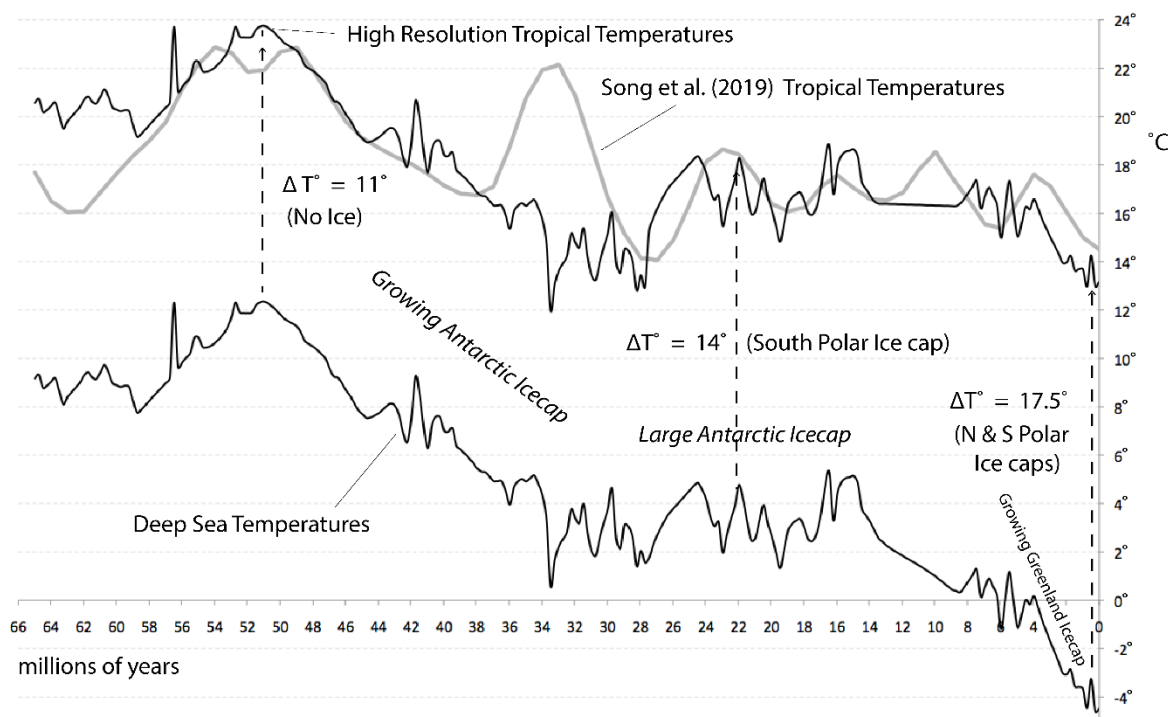


Figure 12. Comparison of Cenozoic deep ocean isotopic temperatures and tropical temperatures A. gray line = low resolution Tropical Temperatures (this study), and the black line = high resolution Δ Tropical Temperatures for the Cenozoic. B. isotopic temperatures from deep ocean, benthic foraminifera (Zachos et al., 2001, 2008; Westerhold et al., 2020).

433

434 The temporal resolution of the Phanerozoic isotopic temperature record from the tropics (Figure 9A)

435 is one control point per million years. While this resolution is adequate for older geological periods,

436 it does not permit a detailed description of Cenozoic temperature changes. We can improve the

437 Cenozoic portion of the temperature curve if isotopic information from deep ocean, benthic

438 foraminifera are used (Zachos et al., 2001, 2008; Westerhold, 2020). The isotopic record from

439 benthic foraminifera provides a nearly continuous record of deep sea temperature changes from

440 beginning of the Cenozoic to the present-day and has a temporal resolution of $\sim 100,000$ years.

441 As illustrated in Figure 12, we have converted the Cenozoic deep ocean temperatures to a high
442 resolution estimate of global average temperatures by superimposing the high-resolution deep
443 ocean temperature curve on our low-resolution estimate of tropical temperatures. This was done by
444 adding $\sim 11^{\circ}\text{C}$ to the pre-ice, Paleogene- early Oligocene portion of the deep ocean temperature
445 curve (65 Ma – 28 Ma), as well as adding $\sim 14^{\circ}\text{C}$ to the early and mid-Miocene portion of the deep
446 ocean temperature curve (28 – 14 Ma). The late Miocene to Recent portions of the temperature
447 curve (14 – 0 Ma) were transposed using linear approximation.

448 The overall shape and amplitudes of the superimposed curves are in remarkable agreement (Figure
449 12). The only significant mismatch is the late Eocene – early Oligocene (33 – 38 Ma) portion of the
450 curve. The Oligocene portions of the transposed deep ocean temperature are 6° - 8° C cooler than
451 isotopic tropical temperatures, which is certainly anomalous. We have chosen to use the updated
452 high resolution Cenozoic tropical temperatures when building our model of Cenozoic global average
453 temperatures.

454 It should be noted that the methods that Hansen et al. (2013) have used to estimate global average
455 temperatures from deep sea temperatures were not used. Though the results he obtained for the
456 Neogene are identical to our estimates, his methodology overestimates global temperatures when
457 applied to hothouse climates.

458 **2.4.7 Summary of Modifications to the Isotopic Temperature Curve**

459 In summary, $\sim 30\%$ of the Phanerozoic isotopic paleotemperature curve was modified using
460 geological and paleontological criteria. In most cases, $2\text{-}3^{\circ}\text{C}$ were added to or subtracted from the
461 isotopic temperatures. Three notable exceptions are the Hirnantian Ice Age (-4°C), the Permo-
462 Triassic Extinction Event ($+7^{\circ}\text{C}$), and the KT Impact Winter (-6°C). Two new thermal maxima were
463 added (200Ma, CAMP; 124 Ma, OAE1a), three problematic apparent thermal maxima were removed
464 (315-295 Ma; 285-275Ma, and 40-30 Ma), and two anomalous apparent cool episodes were either
465 reduced (80-65Ma) or eliminated (340-330 Ma).

466 In addition, a high-resolution isotopic curve was used to represent Cenozoic temperatures (see
 467 section 5.9) and Cambrian carbon isotope excursions were used as a proxy for temperature (see
 468 section 5.2).

469

470 2.5 Combining the Estimates of the Changes in the Pole-to-Equator temperature gradient with the

471 Revised $\Delta T^{\circ}_{\text{trop}}$ curve derived from Oxygen Isotope Data

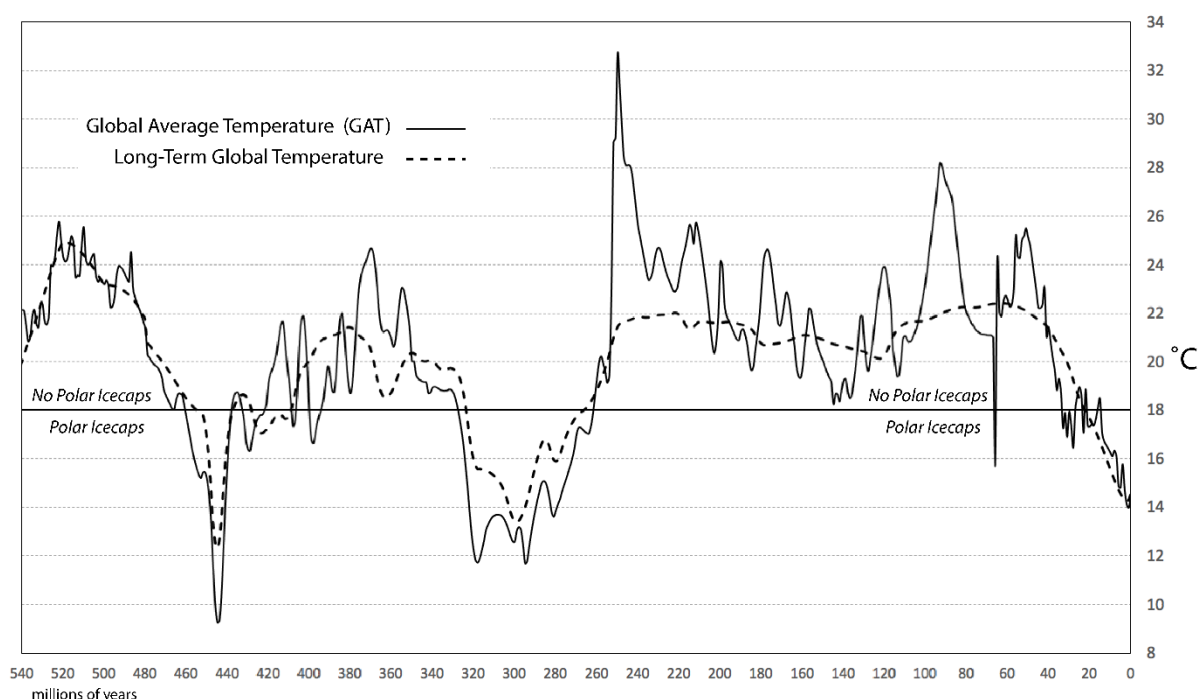


Figure 13. Phanerozoic Global Average Temperature (GAT), blackline = Global Average Temperature, dashed line = Long-term temperature change derived from changes in the pole-to-Equator temperature gradient calculated from the changing area of Köppen Climatic Belt (see Figure 6). When the Global Average Temperature is below 18°C large polar icecaps can form. When the Global Average Temperature is above 18°C large polar icecaps are unlikely to form.

472

473 In the final step of our methodology, we combine the estimates of Global Average Temperature
 474 obtained from the changes in the Pole-to-Equator temperature gradient (Figure 6) with the revised
 475 changing temperature of the Tropics ($\Delta T^{\circ}_{\text{trop}}$) (Figure 10). The combined geological and isotopic
 476 temperature curve (Figure 13) is similar in many respects to the curve derived solely from isotopic
 477 data (Figure 9A), but also differs in several important ways.

-
- 478 1. The Paleogene portion of the isotopic temperature curve is $\sim 1.5^{\circ}\text{C}$ cooler than the geologic
479 temperature curve.
- 480 2. The isotopic temperature curve, overall, tends to indicate slightly warmer temperatures (e.g peak
481 of the Cenomanian-Turonian thermal high).
- 482 3. The late Carboniferous through Triassic, and the late Jurassic - early Cretaceous portions of the
483 isotopic temperature curve are $1.5^{\circ} - 2^{\circ}\text{C}$ warmer than the geologic temperature curve.
- 484 4. The mid-Ordovician through Devonian portion of the isotopic temperature curve is significantly
485 warmer than the geologic temperature curve ($> 6^{\circ} - 8^{\circ}\text{C}$).
- 486 5. The Cambrian and early Ordovician temperatures indicated by the isotopic temperature curve are
487 nearly double the geologically-inferred ($\sim 50^{\circ}\text{C}$ versus $\sim 25^{\circ}\text{C}$, respectively).

488

489 **3. Discussion**

490 A central thesis of this paper is that changes in the Earth's temperature during the Phanerozoic have
491 been caused by factors that act on different time scales. This is not a new idea but rather goes back
492 to the archetypical insights of Alfred Fischer (Fischer, 1981, 1982, 1984), who recognized climatic
493 oscillations and cycles in the biosphere. We recognize three major timescales of temperature
494 change. Long-term changes in temperature (>50 million years) are due to global changes in the rates
495 of volcanic CO_2 degassing associated with seafloor spreading and subduction, as well as long-term
496 changes in the weathering of continents. Long-term changes in temperature (>50 million years) are
497 modeled by mapping the extent of ancient climatic belts (Köppen belts) which vary in response to
498 changes in the Pole-to-Equator temperature gradient. Medium-term changes in temperature (10 –
499 20 million years) can be deduced from changes in the isotopic temperature of the tropical seas.

500 How well does our Phanerozoic temperature model (Figure 13) match the geological record? In the
501 next section we compare the composite Phanerozoic temperature curve with a variety of geological

502 phenomena including: LIP eruptions, bolide impacts, the formation of permanent ice caps, and
503 changes in tropical, deep ocean, and polar temperatures during the Phanerozoic. We also discuss top
504 priorities for future research.

505 **3.1 Short-Term Global Temperature Excursions (< 1 to several million years) due to LIP Eruptions** 506 **and Bolide Impacts**

507 We know that very rapid excursions in temperature can be caused by a variety of tectonic and
508 geological phenomena. For example, global temperatures can rise rapidly due to the release of vast
509 amounts of CO₂ into the atmosphere by eruptions from Large Igneous Provinces (LIP) (Clapham and
510 Renee, 2019). In Figure 14, the black rectangles represent the timing and relative magnitude of 21
511 major LIP eruptions (Ernst, 2014; Ernst and Youbi, 2017). Conversely, temperatures can fall rapidly,
512 creating short-lived icehouse worlds, due to major bolide impact events (e.g., K/T boundary Impact
513 Winter or possibly the Hirnantian Ice Age). Very large impact events (crater size > 150 km) may also
514 trigger large igneous eruptions that create a period of global warming that follows impact-related
515 cooling (e.g., Chicxulub impact event). In Figure 14, the circles illustrate the timing and crater size of
516 the largest, well-established impact events (Spray, 2020).

517

518 **3.2 Large Igneous Provinces (LIPs)**

519 The slow and steady release of CO₂ from the volcanism that accompanies subduction and seafloor
520 spreading is one of the major factors that determine the Earth's thermal equilibrium. This thermal
521 equilibrium changes slowly because the plates move slowly and the continents erode slowly. In
522 contrast, LIPs erupt rapidly, release tremendous amounts of CO₂ and consequently warm the Earth
523 rapidly. The amount of global warming depends on the volume of CO₂ released and the amount of
524 CO₂ in the atmosphere (i.e., climate sensitivity; Royer, 2016). A major LIP eruption during a period of
525 icehouse climate will have a much greater effect than the same LIP eruption during a period of

526 hothouse climate. The warming effects of LIPs will continue as long as voluminous eruptions
 527 continue, often for several million years. Beginning soon after eruption, the weathering of subaerial
 528 basalts may remove CO₂ from the atmosphere reducing global temperatures to near pre-eruption
 529 levels. The rate at which this occurs depends, in part, on the climatic setting of the LIP (Walker et al.,
 530 1981; Berner et al. 1983; Marshall et al. 1988; Raymo et al. 1988; Worsley & Kidder 1991; Bluth &
 531 Kump 1991; Otto-Bliesner 1995; Gibbs et al. 1999; Berner 2004; Nardin et al. 2011; Godd ris et al.
 532 2012, 2014)

533

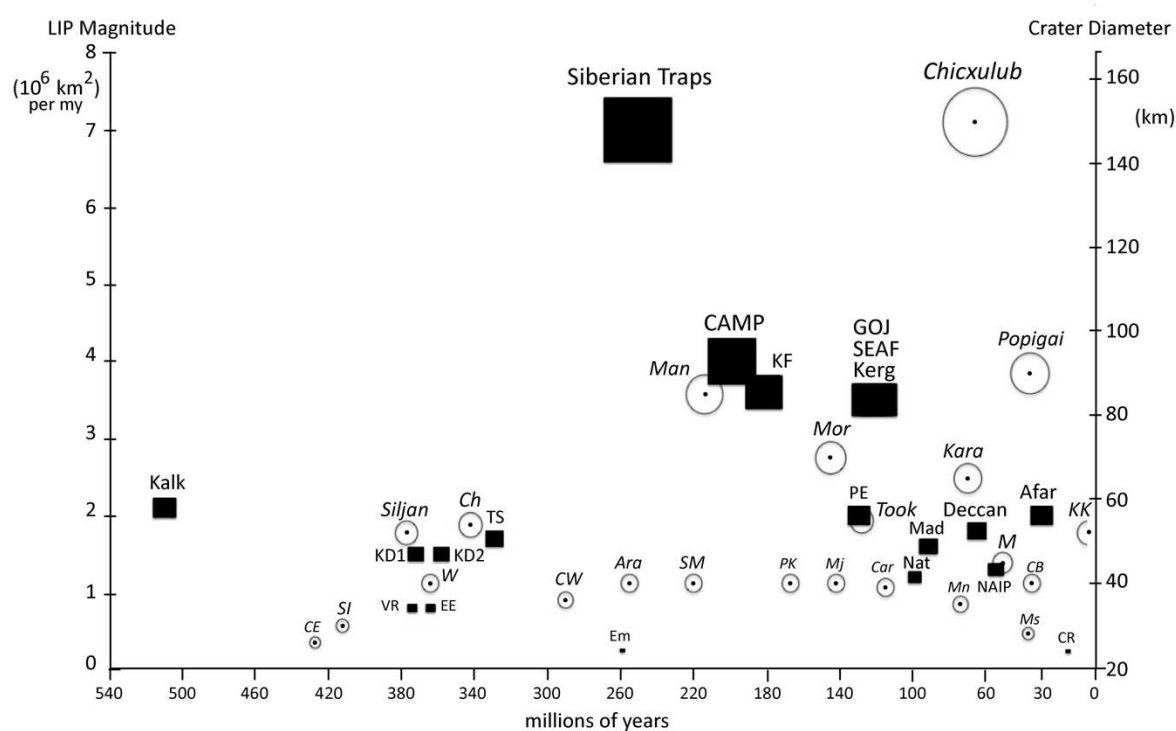


Figure 14. Timing and magnitude of Large Igneous Provinces (rectangles) eruptions and bolide impacts (circles). The size of the rectangles indicates the relative eruptive intensity (10⁶ km²/my) (left-hand scale). See Table 1 and 2 for abbreviations. Sources: Ernst (2014), Spray (2020).

534

535

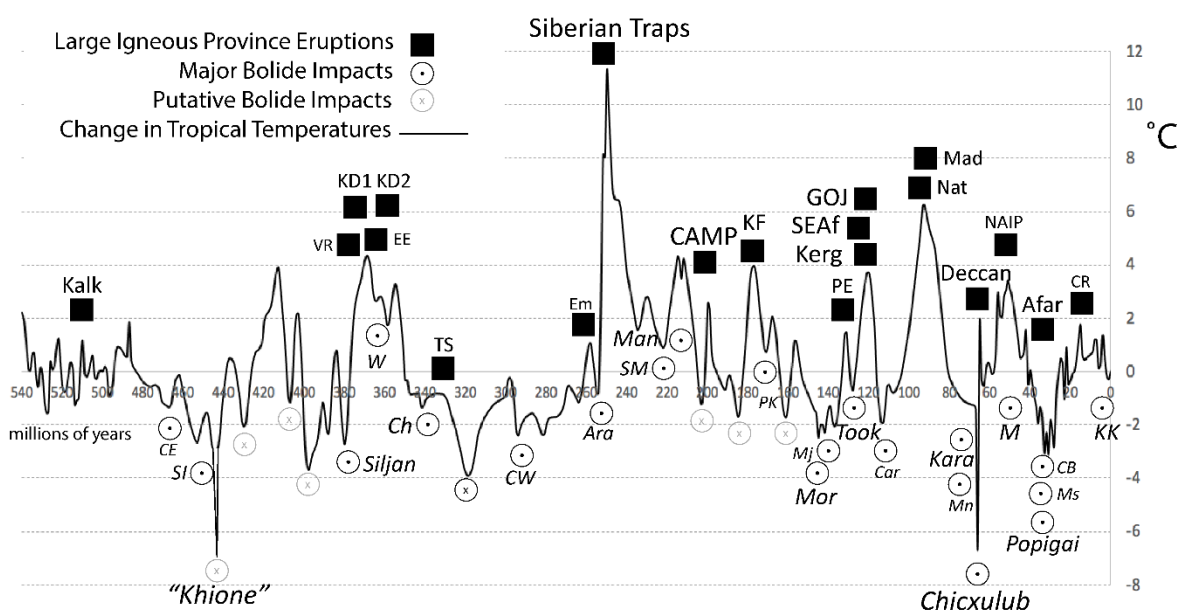


Figure 15. Comparison of the timing of LIPS (black squares, Table 1), large bolide impacts (circles with dots, Table 2), and putative large impact events (light gray circles with x's) with the changes in Tropical Temperature (ΔT^{trop}). The size of the lettering is roughly proportional to the size of the LIP or bolide impact. See Table 1 and 2 for abbreviations. Sources: Ernst (2014), Spray (2020).

536

537

538 Table 1 lists 21 of the largest Phanerozoic Large Igneous Provinces (Ernst, 2014; Ernst and Youbi,

539 2017). They are also plotted as black squares in Figure 15. It is clear from a cursory look at Figure 15

540 that there is a strong correlation between warm periods and the eruption of LIPs. 19 of the 21 major

541 LIPS fall within periods of global warming. Most notable are the correlation between: 1) the West

542 Siberian Traps and the Permo-Triassic Thermal Maximum (252 Ma); 2) the correlation between the

543 Barremian-early Aptian Warm Period (125 – 116 Ma) and the synchronous eruptions that formed

544 the Greater Ontong Java plateau (Taylor, 2006), the Southeast African oceanic plateaus, and the

545 Kerguelen Plateau; 3) the Viluy rift and the mid-late Devonian Hangenberg Thermal Maximum (375 –

546 355 Ma); 4) the Karoo-Ferrar LIP and the Toarcian Thermal Maximum (180 Ma) and; 5) the late

547 Paleocene early Eocene Warm Period (58 – 55 Ma) and the eruption of the North Atlantic Igneous

548 Province (NAIP). The one major exception was the East Africa eruptions (Afar LIP) which took place

549 during the period of intense of late Eocene -early Oligocene cooling. Reluctantly, we have excluded

550 the Caribbean LIP (Sullivan et al., 2020) from consideration because the origin of the underlying

551 lithosphere is certainly older (Jurassic?) than the purported age of the LIP (90 Ma), and the age of
552 the surfacing volcanics is not well-constrained.

553 As has been noted by numerous authors, (Kidder and Worsley, 2010; Wignall, 2001, 2015; Rampino
554 and Self, 2015; Bond and Grasby, 2017; Ernst and Youbi, 2017; Clapham and Renne, 2019; Rampino
555 et al., 2019; McKenzie and Jiang, 2019; Schobben et al., 2019; Suarez et al., 2019), the global
556 warming caused by the eruption of large LIPS has often resulted in mass extinctions. LIP eruptions
557 correlate with extinction events during the middle Cambrian (Kalkarindji, 510 Ma); at the Frasnian-
558 Famennian boundary (Kellwasser extinction, 373-372 Ma); during the latest Devonian (Hangenberg
559 extinction, 359-358 Ma); at the Triassic-Jurassic boundary (CAMP, 201 – 200 Ma); the Toarcian
560 extinction (Karoo – Ferrar LIP, 183 – 181 Ma); the Eocene-Oligocene boundary extinction (Afar- E.
561 African Rift, 31 – 29 Ma); not to mention the two greatest extinction events of all time, the Permo-
562 Triassic Mass Extinction (West Siberian Traps, 252 Ma – 251 Ma) and the K/T Extinction (Deccan
563 Traps, 66 Ma – 65 Ma).

564 Though the geochemistry of LIP lavas indicate that most LIPS are derived from deep mantle sources,
565 there remains the possibility that a few of the largest LIPS (e.g., West Siberian Traps, CAMP, and the
566 Greater Ontong Java Plateau ; Ernst, 2014; Ernst and Youbi, 2017) may have been produced by
567 extremely large impact events (crater size > 200 km). Any craters produced by these gigantic impact
568 events would probably have been obscured by the subsequent voluminous volcanic eruptions.

569

570 **3.3 Bolide Impacts**

571 Table 2 lists 29 bolide impact events that generated craters greater than 25 km in diameter (Spray,
572 2020). Figure 14 illustrates the relative size of these craters and the timing of the impact events.

573 The amount of energy generated by an impact event is described by the equation (Hughes, 2003;
574 Rampino, 2020):

575 $E = 9.1 \times 10^{24} D^a$, where E = is the kinetic energy of the bolide impact in ergs, and D = the diameter
576 of the resulting crater.

577 Proposed values for the exponent, a , range from 2.59 (Hughes, 2003) to 3.89 (Melosh, 1989). In
578 either case, it is clear that the energy associated with an impact event correlates with the cube of
579 the impact crater diameter.

580 The amount of aerosols, SO_4 , and particulate matter injected into the atmosphere is primarily a
581 function of the energy associated with the impact event. Whether a bolide lands on continental
582 crust or oceanic crust may also affect the character of the impact event. In either case, the cooling
583 effect of impact events drops off rapidly as the size of the bolide decreases. It has been suggested
584 that after the impact of the bolide that formed the Chicxulub crater (150 km), the global mean
585 temperature would have dropped $7^\circ - 12^\circ C$ (Vellekoop et al., 2014). By comparison, the impact
586 event that formed the Manicouagan crater in Quebec, which is approximately half the size of the
587 Chicxulub crater, would have generated only $2.5^\circ C$ of cooling. Impact events that produce craters
588 that are less than 25 km in diameter cause negligible amounts of global cooling ($< 1^\circ C$).

589 As illustrated in Figure 15, there are remarkable number of Phanerozoic bolide impacts (circles) that
590 coincidentally occurred during periods of major global cooling (18 of 22). The most notable are the
591 Puchezh-Katunki impact (167 Ma, Middle Jurassic Cool Interval), the Morokweng, Mjolnir and
592 Tookoonooka impacts (145 - 128 Ma, Tithonian- early Barremian Cool Interval), and the Carswell
593 impact (115 Ma, Aptian – Albian Cold Snap). Though the timing of these impact events and the
594 periods of cooling appears to be entirely coincidental, we cannot rule out the possibility that these
595 intense, short-lived cooling events may have triggered ice-albedo feedbacks (Park and Royer, 2011)
596 that accelerated cooling processes already underway.

597 A quick scan of Figure 15 reveals that there are several relatively brief periods of rapid global cooling
598 ($-2^\circ C$ to $-12^\circ C$) that may have been triggered by a bolide impact, but no crater has been associated
599 with these cooling events. This, of course, is not surprising due to the incompleteness of the

600 geological record. The craters that formed during these impact events may have been eroded,
601 tectonically destroyed, or buried beneath a thick pile of sediments. There are no positively identified
602 impact craters in the oceanic basins (Gersonde et al. 1997). Impact events older than 180 million
603 years would have taken place on oceanic crust that has been subducted. Given the proportion of the
604 area of continental crust versus the area of oceanic crust, we would expect that, during the last 540,
605 million years the deep oceans of the Earth were hit by > 20 bolides that could have generated impact
606 craters >50 km in diameter. One or two of these oceanic impacts could have been as large, or larger,
607 than the Chicxulub crater (>150 km).

608 It is possible that as yet unknown bolide impacts may have caused some of the cooling events shown
609 in Figure 15. The most notable putative impact is the “Khione” impact event which could have
610 triggered the latest Ordovician ice age (444 Ma) and mass extinction (Brenchley et al., 1994; Kump et
611 al., 1999a; Sheehan, 2001; Finnegan et al., 2011). The “Khione” (key-OH-nay) impact event is named
612 after the daughter of the Greek god, Boreas, god of winter. Khione is the goddess of snow. The
613 Hirnantian icehouse is especially interesting because it was very short-lived, yet very intense. Ice
614 sheets extended from the South Pole to a paleolatitude of nearly 35°S (Boucot et al., 2013). The
615 Hirnantian Ice Age is anomalous because it occurred during a time of relatively high global
616 temperatures (GAT = 20° - 22° C).

617 Other putative oceanic impact events may have caused the rapid drops in global temperature that
618 are observed during the early Devonian (Pragian, 407 Ma), latest Triassic (Rhaetian, 203 Ma), early
619 Jurassic (Pliensbachian, 184 Ma), and mid-Oligocene (28 Ma). These speculative impacts are
620 indicated by the gray circles with x's in Figure 15.

621 As noted earlier, Figure 15 compares the chronology of LIP eruptions (squares) and bolide impacts
622 (circles) with the changes in global temperature. In Tables 1 and 2 we have estimated the
623 magnitude of the warming and cooling effects of these LIP eruptions and bolide impacts,
624 respectively (Black and Gibson, 2019; Vellekoop et al., 2014; Kamber and Petrus, 2019; Suarez et al.,

2019). Large LIP eruptions nearly all have significant warming effects (i.e. several degrees centigrade). The cooling effects of most impacts are negligible. Several impacts were large enough that they should have had a noticeable effect on global temperatures (Sudbury, Popigai, Acraman, and Manicouagan). The Chicxulub impact (K/T boundary) and the putative Khione-type impacts undoubtedly had profound effects on global climate, extinction, and the evolution of life.

3.4 Icehouse Worlds

During the past 720 million years, the Earth's climate has transitioned from a frigid icehouse to a steaming hothouse seven times. Three of these icehouse periods took place during the late Precambrian (the Sturtian icehouse, 720 – 660 Ma; the Marinoan icehouse, 635 Ma; and the Gaskiers icehouse, 585 Ma (Ogg et al., 2016). During icehouse intervals, large permanent icecaps occupied either the northern or southern polar regions, or both. These times of icehouse conditions are recorded by glacial debris and tillites on land, dropstones in adjacent deep sea sediments that were released by melting icebergs, and glendonites in shallow marine environments where the temperature of the bottom waters is within a few degrees of freezing (Boucot et al., 2013).

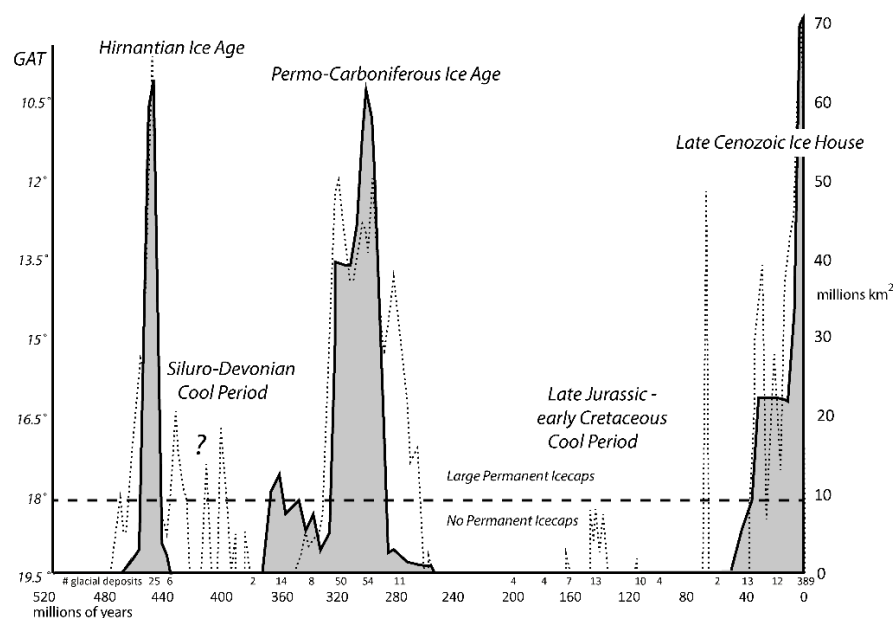


Figure 16. Phanerozoic Ice Ages. gray = global area of snow and ice cover (106 km²), dotted line = snow and ice predicted by Global Average Temperatures (GAT < 18°C, Figure 12), numbers = number of glacial deposits (tillites, dropstones, and glendonites, Boucot et al., 2013). Note inverted temperature scale (left side).

640 Figure 16 plots the geological record of tillites, dropstones, and glendonites, as well as the area of
641 permanent ice cover during the Phanerozoic (gray shading). Figure 16 also plots the global average
642 surface temperature (GAT) during these icehouse intervals (dotted line). As expected, there is a good
643 correspondence between the times when there is geological evidence for icehouse conditions and
644 the times when the GAT is below 18°C (dashed line). Permanent polar ice caps can only form if the
645 global average temperature is less than 18°C. At that global temperature, the average annual
646 temperature of the polar region (>67° N&S) is not warm enough during the summer months to melt
647 the winter snow and ice. Without a complete summer thaw, snow and ice can accumulate and large
648 ice caps can grow rapidly. Conversely, a large, permanent polar ice cap cannot form if the average
649 global temperature is greater than 20°C (68°F). At that temperature, the average annual
650 temperature of the polar regions is ~7°C, too warm for a permanent ice cap to form. A transition
651 zone exists when global temperature ranges between 18°C and 20°C. Snow and ice will be present
652 during the winter months and patches of permanent ice may develop close to the Pole or at high
653 elevations (>500 m).

654 The last three major icehouse intervals (Hirnantian Ice Age (450-444 Ma), Late Paleozoic Icehouse
655 (360 – 285 Ma), and the Late Cenozoic Icehouse (45 – 0 Ma) represent 23% of Phanerozoic time.
656 However, the paleotemperature model presented here predicts that there may have been additional
657 time intervals when icecaps may have existed, albeit briefly. If we accept the correlation of
658 temperature and area shown in Figure 16 at face value, then the largest of these icecaps may have
659 been the half the area of East Antarctica (434 – 385 Ma), the smallest icecaps may have been twice
660 the area of Greenland (150 - 111 Ma). Several of these brief icehouse interludes are plausible
661 because they occur during cool (but not frigid) intervals: 1) the Wenlock Cool Interval (434-326 Ma,
662 2) the Pragian Cool Event (411-406 Ma), (3) the Early-Middle Devonian Cool Interval (401-385 Ma),
663 and 4) the Callovian Cool Event (166-164 Ma), Tithonian-Early Barremian Cool Interval (150-128 Ma).
664 There are sparse, high latitude tillites, dropstones, and glendonites supporting the Jurassic-
665 Cretaceous, and Aptian - Albian cool periods (Boucot et al., 2013). Much of the Siluro-Devonian is

666 considered to be a cool period, but there are no known glacial deposits from this time interval
 667 (Boucot et al., 2013).

Tropical Temperature Global Average Temperature Deep Ocean Temperature Average Polar Temperature

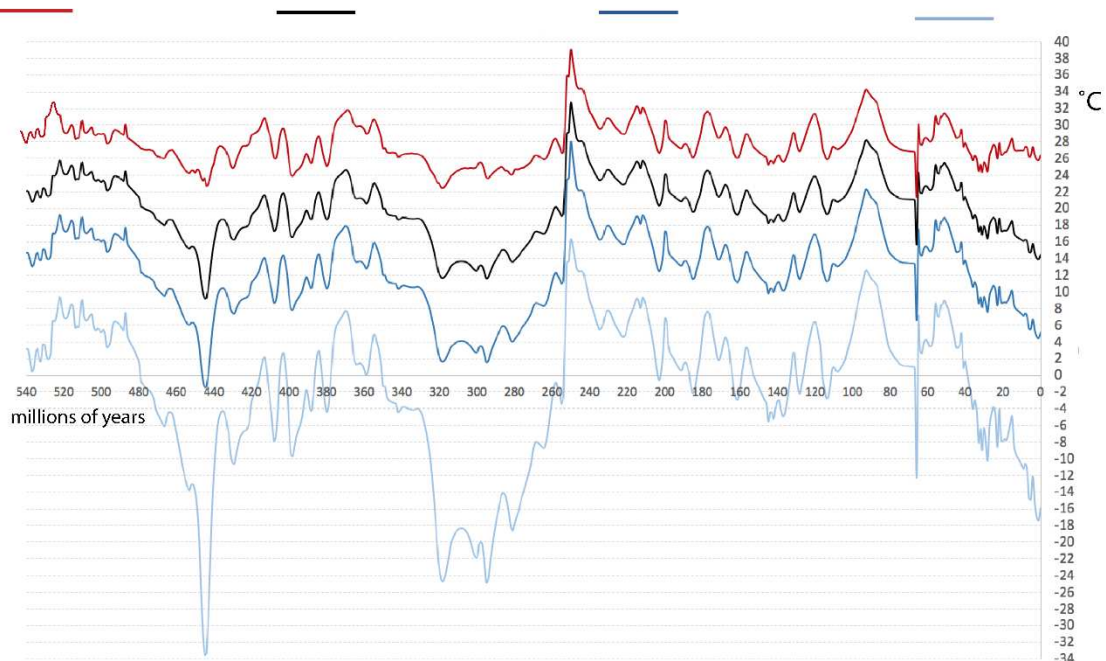


Figure 17. Tropical, Global Average, Deep Ocean, and Polar Temperatures. (a) red line = tropical temperature (15 N - 15 S), (b) black line = global average temperature (GAT), (c) blue line = deep ocean temperatures (after Valdes et al., 2020), (d) light blue line = polar temperature (> 67 N&S).

668

669 3.5 Tropical Temperatures

670 Estimating the Phanerozoic history of tropical temperature is straight-forward. Since we know the
 671 change in tropical temperature ($\Delta T^{\circ}_{\text{trop}}$, Figure 10), and the present-day average tropical
 672 temperature (26°C ; Legates and Wilmott, 1990), then the ancient tropical temperature is simply the
 673 sum of the present-day tropical temperature (26°C) and the change in tropical temperature ($\Delta_{\text{trop}}T^{\circ}$).

$$674 \text{ Tropical Temperature} = 26^{\circ}\text{C} + \Delta T^{\circ}_{\text{trop}}$$

675 For example, the predicted average temperature of the tropical seas during the Paleocene-Eocene
 676 Thermal Maximum (55.6 Ma) was $26^{\circ}\text{C} + 5^{\circ}\text{C} = 31^{\circ}\text{C}$.

677 The predicted mean temperature of the tropical seas back to 540 Million years is 28°C. Tropical
678 temperatures, for the most part, are modeled to have fluctuated between 25°C and 32°C (Figure 17),
679 with the exception of two periods of extreme warmth (Permo-Triassic (~39°C) and Cenomanian-
680 Turonian (~34°C)) and three intervals of extreme cold (Hirnantian(~23°C), Permo-Carboniferous Ice
681 Age (~23°C), K/T impact winter (~22°C))

682

683 **3.6 Deep Ocean Temperatures**

684 During hothouse times, the temperature gradient in the oceans is reduced and the temperature of
685 deep ocean waters can be as high as 20°C (Valdes et al., 2020). During icehouse times, cold bottom-
686 water is produced adjacent to the polar ice caps and this cold, salty water sinks to the depths of the
687 ocean basins and refrigerates the oceans. In the modern world, the cool North Atlantic and North
688 Pacific bottom waters, and the colder circum-Antarctic bottom-waters form at latitudes of 60° N&S
689 (Emiliani, 1954). We assume that this is the approximate latitude where cold deep ocean waters
690 would have originated in the past. We realize that factors, such as the formation of warm, hyper-
691 saline bottom-water in the wide epeiric seas of the middle and early Paleozoic (Chamberlin, 1906;
692 Brass et al., 1982) may also played an important role. Though this estimate of deep ocean
693 temperatures is simplistic and imprecise, it generally agrees with the deep ocean temperatures
694 obtained through climate modeling (Valdes et al., 2020).

695 **3.7 Polar Temperatures**

696 Polar Temperatures were calculated by averaging the temperatures in the polar region above 67°
697 latitude. The results are shown in Figure 17. For example if the Global Average Temperature (GAT) is
698 14.5°C (modern value), then the average temperature of the polar region (above 67° latitude) is a
699 very cold -20 °C. On-the-other-hand, during a hothouse interval like the PETM, the average polar
700 temperature was above 8°C (Figure 17).

701 It seems rather remarkable that the mean temperature of the polar regions back to 540 Million
702 years is $\sim 0^{\circ}\text{C}$. This implies that the polar regions have hovered between ice-free and ice-covered
703 conditions. Average Polar temperatures, for the most part, have fluctuated between 12°C and -12°C ,
704 with the exception of three periods of extreme warmth (Cambrian hothouse ($\sim 14^{\circ}\text{C}$), Permo-Triassic
705 extinction ($\sim 17^{\circ}\text{C}$), and the Cenomanian-Turonian Thermal Maximum ($\sim 13^{\circ}\text{C}$)) and four intervals of
706 extreme cold (Hirnantian Ice Age ($\sim -32^{\circ}\text{C}$), Permo-Carboniferous Icehouse ($\sim -24^{\circ}\text{C}$), the KT Impact
707 Winter ($\sim -30^{\circ}\text{C}$) and Late Cenozoic Icehouse ($\sim -20^{\circ}\text{C}$). Throughout most of the Phanerozoic the
708 average temperature of the southern polar region (-4°C) has been considerably colder than the
709 average temperature of the northern hemisphere (4°C). Only for a brief interval in the Late Permian
710 was the northern hemisphere colder than the southern hemisphere.

711 **3.8 Top Priorities for Future Research**

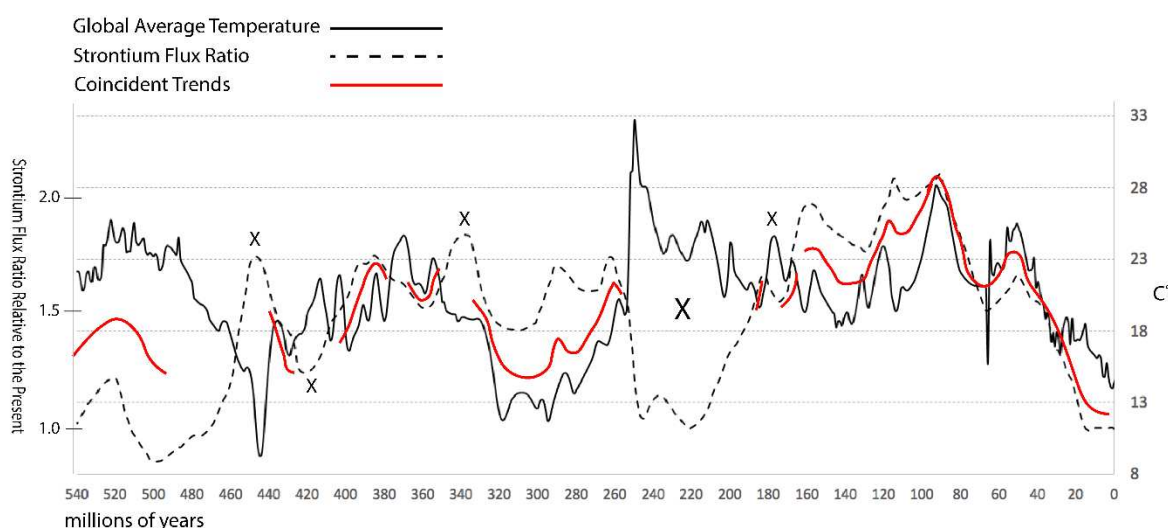
712 There are several important issues and areas of research that need further investigation, these
713 include: variations in the isotopic record due to insufficient sampling in time and space and the
714 fundamental changes in the Earth System that have driven temperature change.

715 **3.8.1 Insufficient Sampling in Time and Space**

716 As is the case for any geological investigation, due to the incompleteness of the geological record,
717 there are bound to be gaps in the record of isotopic temperature. The temporal record of isotopic
718 measurements compiled by Song is $\sim 80\%$ complete. That is to say, average isotopic temperatures
719 have only been calculated for 400 of the 500 one million years intervals of the Phanerozoic. The data
720 density can be directly viewed in Figure 9. The black dots along the x-axis in Figure 9B are the times
721 for which there are no isotopic temperature measurements. The missing data is not randomly
722 distributed. There are large data gaps during the: late Eocene (36 - 40 Ma), early Albian (110 - 115
723 Ma), Kimmeridgian -Tithonian (157-143 Ma), Norian (213 - 229 Ma), late Cisuralian (278 - 289 Ma),
724 early Viséan (336 - 346 Ma), Emsian (396 - 406 Ma), earliest Devonian (417- 420 Ma), and early and

725 middle Ordovician (455 - 495 Ma). We recommend that these gaps in the data record be priority
726 targets for future research.

727 The sampling of isotopic temperature measurements is also geographically sparse. Most of the
728 sample sites are highly clustered and there are few sample sites from paleolatitudes above 40° N or
729 S. Though the data set can be accurately characterized as “tropical”, the possibility remains that for
730 some time periods the isotopic samples may be biased either towards the Equator, or away from the
731 Equator. As we saw in the case of the late Pennsylvanian data, it is also important to identify
732 environmental variables such as salinity or ocean circulation that may affect the isotopic
733 temperature. One of our future research goals is to carefully analyze the isotopic temperature
734 database for these kinds of geographic and environmental biases (Judd et al., 2020).



735 Figure 18. Comparison of Phanerozoic global average temperatures (black line) with strontium flux ratio relative to the present-day flux (dashed line). Red line highlights when the two trends were coincident.

736 3.8.2 Modeling the Fundamental Causes of Global Temperature Change

737 Correcting the isotopic artifacts and improving the temporal and geographic sampling of isotopic
738 data are important, but they do not address fundamental questions regarding the ultimate causes of
739 changes in the Earth’s temperature. Long-term changes in temperature (>50 million years) and
740 medium-term changes in temperature (10-20 million years) are primarily driven by the slow and

741 inexorable changes brought on by plate tectonics and continental weathering (van der Meer et al.
742 2014; Berner, 1994; Brune et al., 2017).

743 To the first order, the amount of CO₂ released into the atmosphere is proportional to the rates of
744 seafloor spreading and subduction (van der Meer et al., 2014). The isotopic composition of the
745 oceans, in particular the ratio of ⁸⁷Sr/⁸⁶Sr, can be used as a proxy for the rate of sea floor
746 spreading (van der Meer et al. 2017). New ⁸⁶Sr is introduced into the oceans by the weathering of
747 new basaltic oceanic lithosphere which is rich in non-radiogenic, depleted upper mantle-derived
748 ⁸⁶Sr. On-the-other-hand, continental sources are richer in ⁸⁷Sr, which is a decay product of ⁸⁷Rb.

749 Faster periods of seafloor spreading introduce more ⁸⁶Sr into the oceans. This decreases the ratio of
750 ⁸⁷Sr to ⁸⁶Sr of seawater. In Figure 18, the non-radiogenic strontium flux ratio (van der Meer et al.
751 2017) ratio relative to the present (dashed line) is compared to our estimate of Phanerozoic global
752 temperatures (solid line).

753 There appears to be a remarkably good correlation between the global temperature and non-
754 radiogenic strontium flux. For 65% of the Phanerozoic, when the ratio of ⁸⁷Sr/⁸⁶Sr in the oceans
755 rose or fell (red line), global temperatures also rose or fell. The correlation is especially good for the
756 last 180 million years (breakup of Pangea) and during the Permo-Carboniferous Ice Age (assembly of
757 Pangea, 320 Ma – 255 Ma). For other time intervals, the isotopic and temperature records are in
758 partial agreement (e.g., Cambrian, 540 – 500 Ma; Devonian – early Carboniferous, 400 – 345 Ma).

759 However, there are also significant time intervals when the isotopic and temperature record are
760 completely out-of-synch (marked by X's). Most notable are the Hirnantian Ice Age and the Triassic
761 Hothouse. This suggests that there are other factors besides the volcanic degassing of CO₂ that drive
762 global temperature change. E.g. during the Hirnantian Ice Age, a massive bolide impact and
763 subsequent positive ice-albedo feedbacks might have cooled the Earth despite the fact that plate
764 tectonic activity was high at the time. During the Triassic, on-the-other-hand, the increased degree

765 of aridification due to extreme hothouse temperatures ($>40^{\circ}\text{C}$) and mega-monsoonal desertification
766 across the interior of Pangea may have slowed down chemical weathering and allowed CO_2 to build
767 up in the atmosphere which increased global temperatures.

768 We can speculate that other geological processes that occur with rates of change that match the
769 temperature peaks and troughs might also have produced the observed pattern of Phanerozoic
770 temperature change. For example, mountain building and unroofing, periods of ophiolite obduction
771 and subsequent chemical weathering, the opening of oceanic gateways, and some evolutionary
772 events (e.g., the emergence of land plants) all occur on timescales comparable to the rates of change
773 seen in the ΔT_{trop} curve. A careful and systematic analysis of the evolutionary, paleogeographic,
774 tectonic, paleoceanographic, and environmental changes that may have driven global temperatures
775 will continue to be a fruitful area of research.

776

777 **Part II. Phanerozoic Paleotemperature Timescale**

778 **4. A Phanerozoic Paleotemperature Timescale**

779 The main goal of our research has been to construct a continuous record of temperature change
780 during the last 540 million years (Figures 19-21). In the second half of this paper, we document this
781 record of temperature change with specific paleotemperature events that are analogous to the
782 “golden spikes” (GSSP) of the geological timescale (Gradstein et al., 2012). In some ways, this
783 paleotemperature timescale is similar to the linear magnetic reversal time scale that was assembled
784 at the beginning of the plate tectonic revolution more than 50 years ago. However, instead of
785 normal and reverse magnetic polarity events, the paleotemperature timescale is defined by
786 “warming” and “cooling” temperature intervals called “chronotemps”. Our preliminary attempt to
787 identify these warm and cool intervals is illustrated by the cool (black) and warm (white)
788 subdivisions of the global average temperature curve (Figure 19-21).

789 The Phanerozoic paleotemperature timescale can be subdivided into 24 pairs of warm and cool
790 intervals. It should be noted that the resolution of this version of the timescale is 1 million years;
791 rapid temperature excursions shorter than a million years (e.g. PETM, K/T Impact Winter) are not
792 well-resolved. The cool sections of the temperature timescale are labeled c1 – c24. Some of these
793 cooling events are well-known like the Pleistocene Ice Age (c1) or the Hirnantian Ice Age (c22). Other
794 cool intervals are more speculative (c6, Aptian-Albian Cold Snap) and require further investigation.
795 Similarly, the warm intervals are labeled w1 – w24. Some of these warming events are well-known
796 like the Permo-Triassic Thermal Maximum (w13) and the Toarcian Warm Interval (w9). Other warm
797 intervals are more speculative. Also, there is no strict equivalence between two cool intervals or two
798 warm intervals. Two cool intervals may have very different minimum, maximum, and average
799 temperatures (Tables 3 – 7). The same is true for the warm intervals.

800 Each warm and cool time interval is illustrated in Figures 19-21 and supporting references are given
801 in Tables 3-7. These tables provide precise information about the name of each interval, the start
802 time and end time, the Tropical Temperature, the Polar Temperature, and the Global Average
803 Temperature (GAT) of each interval, as well as the timing of major LIP eruptions and bolide impacts.
804 Key citations for each chronotemp are also provided. Each interval may contain several discrete
805 short-term temperature events or excursions. For example during the Paleocene-Eocene hothouse
806 (W5, PEH), there were several thermal maxima, the PETM (W5.9, Paleocene-Eocene Thermal
807 Maximum), EETM (W5.6, Early Eocene Thermal Maximum), and METM (W5.1, Middle Eocene
808 Thermal Maximum). Conversely, a few temperature intervals may be grouped into a larger,
809 geologically meaningful temperature interval; for example, the Late Paleozoic Icehouse (C13-C17)
810 consists of the cool intervals: C13 (Late Permian Cooling), C14 Mid-Permian Cool Interval, C15
811 (Permo-Carboniferous Icehouse), C16 (Early Mississippian Cooling), and C17 (Famennian-Earliest
812 Tournaisian Ice Age), as well as the intervening warm intervals.

813 We have tried to standardize the names and abbreviations used to describe the various
814 chronotemps depending on the length of a temperature event (icehouse, ice age, cool interval, cool
815 event), its magnitude (e.g. thermal maximum, glacial maximum), or if the chronotemp represents a
816 transition between warm or cool time intervals (e.g. warming or cooling). Often discrete
817 temperature intervals are connected by prolonged periods of warming or cooling (e.g Eocene-
818 Oligocene Transition). We have used a gray scale gradient in Figures 19-21 to schematically
819 represent the rate of cooling or warming.

820 We do not use the term “climate” as part of the naming convention to avoid confusion with broader
821 climatic considerations (i.e., precipitation, temperature gradients, equability, etc.), and have avoided
822 the use of other somewhat pejorative terms such as “optimum”. Also, whenever possible we have
823 used a specific stage name (e.g., Cenomanian-Turonian Thermal Maximum) rather than a more
824 generic geological description (e.g., Cretaceous Thermal Maximum). We also prefer the term
825 “interval” rather than “period” because of the geological connotation of the latter term. “Events”
826 tend to be temperature phenomena that last only a few million years or less. “Excursions” are
827 events that depart from the norm, i.e, a warm event during a cool interval.

828 Unfortunately, in our attempt to rationalize and standardize the naming conventions, older more
829 established names that have precedence have been mostly discarded (e.g., the Mid-Miocene
830 Climatic Optimum (MMCO) has become the Middle Miocene Thermal Maximum (MMTM).

831 What are the advantages to dividing the timescale into discrete temperature events and giving each
832 of them a number and a name? Some may argue that our state of knowledge is still too primitive
833 and that attempting to build a paleotemperature timescale is premature. We would argue that by
834 constructing a paleotemperature timescale, even if this first version is imperfect, we now have a
835 structure that can be built upon, refined, corrected, and expanded. Also having a paleotemperature
836 timescale is essential if we are to understand the tempo and mode of climate change during Earth
837 history. By characterizing, in a quantitative way, the pattern of paleotemperature change through

838 time, we may be able to gain important insights into the history of the Earth System and the
839 fundamental causes of climate change.

840 **5. Climate Modes of the Phanerozoic**

841 **5.1 Introduction**

842 In this section we will review the evidence used to construct the Phanerozoic Paleotemperature
843 Timescale (Tables 3-7, Figures 19-21). The 24 pairs of warm and cool temperature intervals listed in
844 Tables 3-7 can be grouped into eight distinct “climate modes” (after Frakes, 1989; Frakes et al.,
845 1992; Vaughan, 2007). Four of these climatic groups represent four warm periods in Earth history
846 (Cambro-Ordovician, Siluro-Devonian, Triassic, and mid Cretaceous-Paleogene), three climatic
847 groups represent cold periods in Earth History (Late Ordovician-Silurian, Late Paleozoic, and Late
848 Cenozoic), and one “cool” period made up of mixture of cool and warm intervals (Jurassic – early
849 Cretaceous). These warm and cool modes are similar to the eight warm and cool modes outlined by
850 Frakes et al., (1992). The only major differences are: the Famennian/Tournaisian Ice Age is included
851 in the Late Paleozoic Icehouse, the early Mesozoic warm mode includes only the Triassic, and the
852 Jurassic – Early Cretaceous Cool Period includes the entire Jurassic. The average global temperature
853 during the cool climate modes is 16 °C, the average global temperature during the warm climate
854 modes is ~20°C, and the average temperature during the mixed or mild mode is 17.5°C which is close
855 to the average temperature of the Phanerozoic (18°C). It should be noted that the global
856 temperatures during these climatic modes are not entirely warm or entirely cool, but rather
857 alternate between relatively cooler and relatively warmer times.

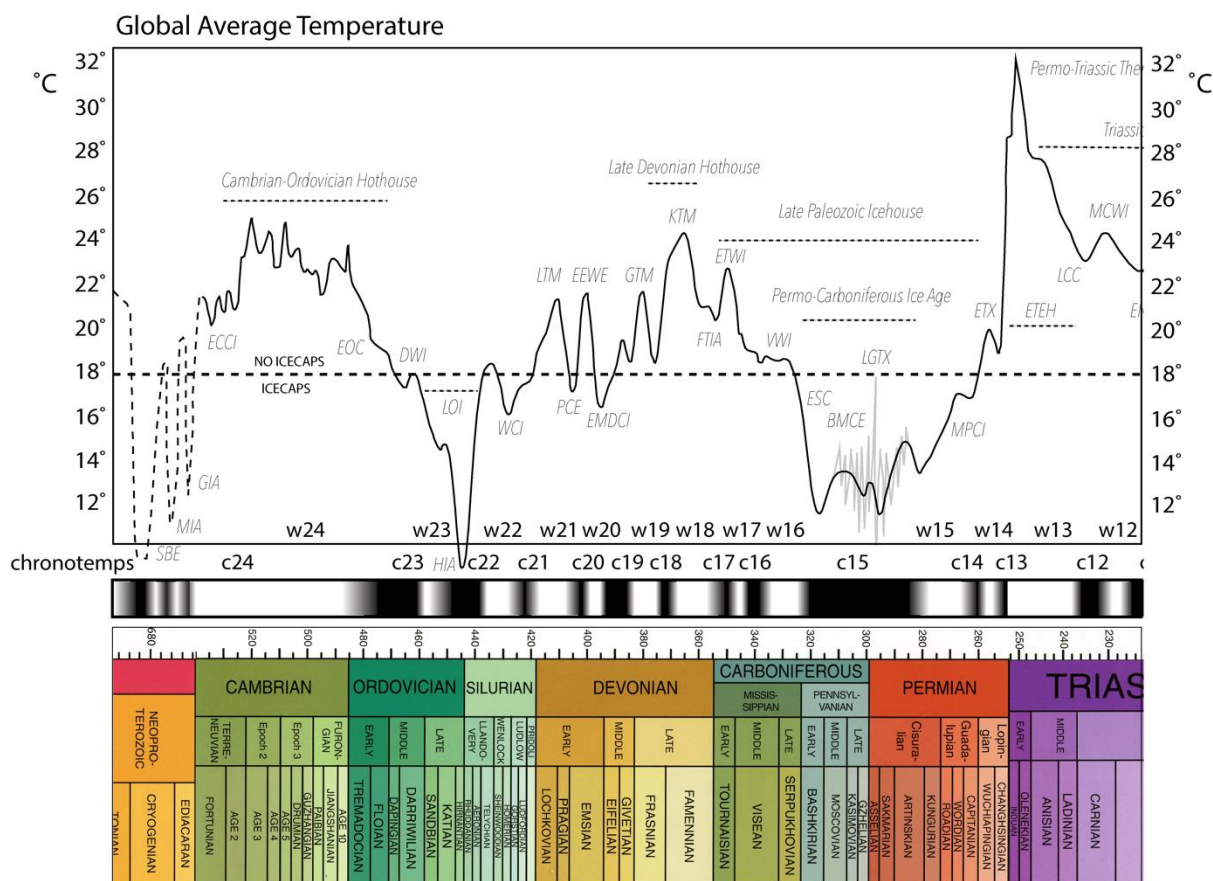


Figure 19. A Paleozoic Paleotemperature Timescale. white = warm time intervals, black = cool time intervals. Solid black line = Global Average Temperatures (GAT), < 18°C = large permanent, icecaps, > 18°C = no large, permanent icecaps. Light gray jagged lines = a schematic representation of >50 glacial/interglacial cycles during the Permo-Carboniferous. Timescale = International Chronostratigraphic Chart v2020/01. Refer to Table 3 for more information and sources of data for each chronotemp and abbreviations.

858

859 5.2 Cambro-Ordovician Hothouse (W23 – C24, 458–541 Ma), Table 3, Figure 19

860 The Cambro-Ordovician warm climate mode starts at the base of the Cambrian (541 Ma) and
 861 extends through most of the Ordovician (late Darwillian, 458 Ma). Global temperatures were
 862 highest during the Cambrian and cooled during the early Ordovician. There is uncertainty regarding
 863 the maximum temperatures during the Cambrian because the interpretation of early Paleozoic $\delta^{18}\text{O}$
 864 values remains controversial.

865 Measurements of the isotopic composition of early Paleozoic seawater are enriched in the lighter
 866 isotope of oxygen (^{16}O). This apparent enrichment has given rise to two explanations: 1) the
 867 composition of seawater has become systematically enriched in the heavier isotope of oxygen (^{18}O)

868 through time (Kasting et al., 2006; Jaffres et al., 2007) or 2) the composition of seawater has
869 remained constant (Henkes et al., 2018) and therefore the lighter $\delta^{18}\text{O}$ values accurately reflect
870 warmer paleo-temperatures during the early Paleozoic and late Precambrian. Recent studies of the
871 $\delta^{18}\text{O}$ composition of Precambrian oceans suggest that the composition of seawater has been
872 systematically enriched in the heavier isotope of oxygen (^{18}O) (Galili et al., 2019; Hodel et al., 2018)
873 and therefore, isotopic temperatures for the Early Paleozoic and late Precambrian may be in error.

874 The proponents of the “hot” early Paleozoic temperature model suggest that prior to the Darwillian,
875 tropical sea surface temperatures were $8^\circ - 10^\circ$ warmer than modern tropical sea surface
876 temperatures. This interpretation is supported by clumped isotope estimates of tropical
877 paleotemperatures for the late Precambrian ($>50^\circ\text{C}$; Bergmann et al., 2018a), late Cambrian (32°C),
878 early Ordovician (36°C), and middle Ordovician ($\sim 40^\circ\text{C}$; Bergman et al., 2018b; Henkes et al., 2018).

879 Measurements of $\delta^{18}\text{O}$ from pristine, phosphatic euconodont fossils from England give
880 temperatures of $20^\circ - 25^\circ\text{C}$ for near polar latitudes ($>70^\circ\text{S}$, Hearing et al., 2018). The equivalent
881 temperature at tropical latitudes would have been $> 40^\circ\text{C}$. According to “hot” model, temperatures
882 would have exceeded 50°C during the latest Precambrian (Ediacaran; Bergmann et al., 2018a; see
883 Figure 5).

884 The “cool” early Paleozoic temperature model proposes that Cambro-Ordovician tropical
885 temperatures were only modestly elevated ($28^\circ - 32^\circ\text{C}$) in comparison to modern average tropical
886 sea surface temperatures (26°C) and that cool temperate conditions ($4^\circ - 12^\circ\text{C}$) prevailed near the
887 poles (Figure 17). This interpretation is consistent with the occurrence of bauxites (Boucot et al.,
888 2013) and “Bahamian-type” carbonates at low latitudes and the restriction of archaeocyathid reefs
889 to tropical and subtropical latitudes (McKerrow et al., 1992). During the early Paleozoic, temperate
890 and polar latitudes were characterized by clastic facies with strata containing unweathered mica
891 flakes indicative of cooler temperatures (Boucot et al., 2013). The late Cambrian and early

892 Ordovician world was latitudinally subdivided into four distinct trilobite provinces - Bathyruid,
893 Dikelocephalinid, Ptychopygine/Megalaspid, and Calymenacean-Dalmanitacean (Cocks and Fortey,
894 1990; McKerrow et al., 1992) - indicating a moderate pole-to-equator temperature gradient. Landing
895 et al. (2020) also noted that trilobites first appeared in the warm shelf environments of Siberia and
896 Laurentia and later spread to the cooler, higher latitude waters of Baltica and Gondwana. In the
897 “cool” temperature model, global temperatures increased during the middle and late Cambrian as
898 the continental cratons were flooded and the resulting decrease in the planetary albedo warmed the
899 Earth (Landing and Westrop, 2004; Landing, 2012).

900 Temperatures continue to fall during the middle Ordovician (Trotter and Barnes, 2008). Trotter and
901 Barnes (2008) proposed that sustained, cooler tropical temperatures (26°-30°C) provided a more
902 hospitable environment for evolutionary innovation and may have been the impetus for the Great
903 Ordovician Biodiversification Event (GOBE; Webby et al., 2004).

904 As noted earlier (section 3.1.2.1), the ~2° temperature fluctuations during the Cambrian shown in
905 Figure 19 are speculative. They coincide with 10 proposed Cambrian $\delta^{13}\text{C}$ isotopic excursions (Zhu
906 et al., 2006). It should be noted that the global synchronicity of some of these excursions (in
907 particular TOCE and REOCE) has been disputed (Landing, personal communication). The covariance
908 of $\delta^{13}\text{C}$ and $\delta^{18}\text{O}$ trends has long been noted (Wenzel and Joachimski, 1996; Jenkyns et al., 2002).

909 Approximately 80% of the positive $\delta^{13}\text{C}$ excursions are correlated with warmer temperatures
910 (hyperthermals). The correlation is generally attributed to the causal relationship between higher
911 ocean temperatures, the formation of deep water anoxia, and the subsequent preservation of
912 organic carbon.

913 **5.3 Late Ordovician – Silurian Icehouse (C21 – C22, 426-458 Ma), Table 3, Figure 19**

914 The most spectacular, short-term cooling event of the Phanerozoic is the Hirnantian Ice Age (445 –
915 441 Ma; Brenchley, et al., 1994; Sheehan and Coorough, 1990; Sheehan, 2001; Finnegan et al.,

916 2011). Whether the Hirnantian Ice Age (C22) was preceded by a prolonged, stepwise cool-down is
917 still debated. Biostratigraphic (Brenchley et al., 1994) and geochemical data (Finnegan et al., 2011)
918 indicate that the maximum glacial advance was very short-lived (less than one million years; Ling et
919 al., 2019). The repercussions of the Hirnantian Ice age were felt worldwide and left indelible
920 signatures in the geochemical, paleontological (Sheehan and Coorough, 1990; Finnegan et al., 2012),
921 and sedimentary rock record .

922 The widespread occurrence of latest Ordovician tillite deposits (Beuf et al., 1971; Boucot et al., 2013)
923 indicates that ice sheets covered ~50% of Gondwana and extended to latitudes of ~35 S. The
924 enormous extent of snow and ice cover increased the Earth's albedo and triggered ice-albedo
925 feedbacks that rapidly cooled the Earth. The asymmetric latitudinal disposition of the Earth's land
926 masses during the late Ordovician, namely the fact that no large continents occupied the northern
927 hemisphere, probably prevented the Earth from slipping into another "Snowball Earth". Only thin
928 sea-ice accumulated on the freely circulating, open northern oceans. This meant that during the late
929 Ordovician, the northern hemisphere remained relatively warm and prevented a runaway Snowball
930 Earth-like global freeze.

931 Multiple explanations have been proposed for the cause of the Hirnantian Ice Age. Crowley and
932 Baum (1991, 1995) suggested that the growth of the Gondwana ice cap was facilitated by the
933 combination of increased precipitation and cold temperatures along the northern margin of
934 Gondwana. Other authors have invoked increased chemical weathering of young mountains
935 (Taconic ranges) or recently obducted ophiolites that lead to a drawdown in atmospheric CO₂, which
936 promoted globally cooler temperatures (Kump et al., 1995, 1999b,c; Swanson-Hysell and
937 Macdonald, 2017; Landing, 2018). This effect may have been enhanced by the evolution of simple,
938 non-vascular land plants (Lenton et al., 2012).

939 A more spectacular explanation, as discussed in section 3.3, is that the Hirnantian Ice Age was
940 triggered by a bolide impact as large or larger than the Chicxulub impact. There is no geologic record

941 of this massive impact on the continents. Though the impact site may be buried under younger
942 continental strata, it is more likely that the Khione impact targeted the late Ordovician ocean basin
943 and that the impact crater was subsequently subducted. This hypothesis was first proposed in 1986
944 by Kent Colbath who noted the rapid extinction of tropical acritarch genera in the southern
945 Appalachian basin and their subsequent replacement with more cosmopolitan taxa in the earliest
946 Silurian. The extinction of warm, shallow water tropical faunas during the latest Ordovician and
947 their replacement by cool-water benthic taxa or cosmopolitan planktonic taxa has been confirmed
948 by numerous other studies (Sheehan, 2001). The Hirnantian extinction event ranks second in terms
949 of taxonomic severity (~46% marine genera extinct). Only the Permo-Triassic Extinction (58% marine
950 genera extinct; Sepkoski, 1996; Bambach et al., 2004) was more cataclysmic.

951 Though some snow and ice in the polar regions of South America (central Brazil and Bolivia) lingered
952 into the earliest Silurian (Grahn and Caputo, 1992; Grahn and Gutierrez, 2001; Díaz-Martínez and
953 Grahn, 2007), rapid warming during the Llandovery (W22) was followed by a period of slow
954 ecological recovery. The remainder of the early-middle Silurian was characterized by a moderate
955 pole-to-equator temperature gradient which was cool by early Paleozoic standards but warmer than
956 today's world (Moore et al., 1994). Most early and middle Silurian tropical taxa were widely
957 distributed (i.e., cosmopolitan) with the exception of the high latitude, cool-water brachiopods,
958 *Clarkeia* (southern hemisphere; Boucot, 1990; Benedetto and Sanchez, 1996) and *Tuviella* (northern
959 hemisphere; Cocks, 1972). Three carbon isotopic excursions occurred during the middle and late
960 Silurian. Two of these excursions (Ireviken and Mulde) bracket the Wenlock and may have been
961 caused by the growth of ephemeral, south polar ice caps (Brand et al., 2006).

962

963 **5.4 Siluro-Devonian Hothouse (W18 – W21, 365-426 Ma) Table 4, Figure 19**

964 The late Silurian through late Devonian hothouse includes four warm intervals (W21 – W18)
965 separated by three relatively cool episodes (C20 – C18). There is no geological evidence for

966 permanent polar icecaps during any of the cool intervals (Boucot et al., 2013). The following
967 summary of the Siluro-Devonian warm mode is based on the isotopic evidence summarized by
968 Joachimski et al. (2009), the biogeographic information synthesized by Stock (2005), the lithologic
969 indicators of climate assembled by Boucot et al. (2013), and a comprehensive synthesis of the
970 Frasnian-Famennian crisis by Racki (2020).

971 The Siluro-Devonian Warm Interval spans the early Ludlow to early Lochkovian time interval
972 (Joachimski et al., 2009; Munnecke et al., 2010; Trotter et al., 2016). It is followed by a pair of brief
973 cooling and warming events during the Pragian (C20) and early Emsian (W20), respectively. The
974 Pragian Cool Event coincides with a widespread fall in sea level (~100m) during the earliest Devonian
975 and the resulting unconformity marks the end of the Tippecanoe Supersequence. This fall in sea
976 level is seen on most continents, but is especially prominent on North America (Schuchert, 1910,
977 1955; Sloss, 1963).

978 After a brief warming event in the early Emsian, temperatures continued to fall during the
979 remainder of the Emsian and into the middle Devonian (Eifelian – middle Givetian; Joachimski et al.,
980 2004, 2009; van Gelderin et al., 2006). The Early-Middle Devonian Cool Interval (C19, GAT = 18.7°C)
981 was followed by a brief, rapid rise in temperature during the late Givetian (W19, Givetian Thermal
982 Maximum, GAT = 21.2°C). Late Givetian warming coincided with the Taghanic onlap (Brett et al.,
983 2009), the start of a global transgressive cycle that would culminate with the highest sea level of the
984 Paleozoic (late Frasnian; Haq et al., 1987; Haq and Schutter, 2009). Global temperatures cooled
985 briefly during the early Frasnian but rose steadily through the remainder of the Frasnian, culminating
986 in the Kellwasser Thermal Maximum (W18.2, 372.5 Ma). A recent synthesis of Frasnian and
987 Famennian isotopic, paleontologic, and tectonic information (Racki, 2020) provides numerous
988 detailed insights into the paleoclimatic events that took place across the Frasnian-Famennian
989 boundary.

990 According to Racki (2020), the Kellwasser Event, also known as the Frasnian-Famennian Extinction
991 Event, can be subdivided into two pairs of rapid warming/cooling events. The first event, the Early
992 Kellwasser Event (373 Ma), may have been triggered by the eruption of the Vilui and Kola LIPS (see
993 Table 1). Shortly thereafter, continued volcanic eruptions (Pripyat-Dneiper-Donets LIP) triggered a
994 second episode of rapid warming and cooling (Late Kellwasser Event; 372 Ma). An alternate
995 hypothesis invoking a bolide impact has also been proposed (McLaren, 1970, 1983). The combined
996 Kellwasser Extinction Event was the fourth most severe extinction event when measured in terms of
997 ecological severity (McGhee et al., 2013). It is associated with highest sea level of the Paleozoic
998 (Johnson, 1988; Johnson et al., 1985; Sandberg et al., 2000) as well as with a dramatic increase in
999 $^{87}\text{Sr}/^{86}\text{Sr}$ composition of seawater (Zhang et al., 2020). For a more detailed account of the Frasnian-
1000 Famennian Extinction Event see McGhee(1996, 2005), Racki(2005), and Sandberg(2000, 2002).

1001 The isotopically inferred temperature events outlined above are in good agreement with the
1002 paleoclimatic conditions inferred from paleobiogeography and lithologic indicators of climate.

1003 According to Boucot et al. (2013), the global climatic gradient during the Early Devonian through to
1004 the Eifelian was “moderate”, resulting in cool but not freezing temperatures in temperate latitudes.
1005 Like much of the earlier Paleozoic, the high southerly latitudes of Gondwana were characterized by
1006 an exclusively clastic facies with unweathered mica flakes and a distinctive cool-water fauna
1007 (Malvinokaffric province). Conodonts (Girard et al., 2005) and reef-like stromatoporoids (Stock,
1008 2005), which preferred warm waters, were absent from the cooler, temperate shallow seas of
1009 central and southern Gondwana. Global temperatures warmed in the Givetian and Frasnian; and the
1010 Malvinokaffric province was eliminated, replaced by warmer water faunas. Faunas at low latitudes
1011 became less endemic and more cosmopolitan (Stock, 2005). Temperatures continued to warm
1012 throughout the Frasnian and Famennian, until the onset of the Late Famennian Ice Age (discussed in
1013 the next section).

1014

1015 **5.5 Late Paleozoic Icehouse (C13 – C17, 253-365 Ma) Table 4, Figure 19**

1016 Spanning more than 100 million years, the Late Paleozoic Icehouse was the longest interval of cold
1017 climates during the Phanerozoic. Polar ice existed, more or less continuously, at either the South or
1018 North Poles with the exception of brief warming events during the Mississippian (Tournaisian and
1019 Visean Warm intervals, W17 and W16, respectively), latest Pennsylvanian (Latest Gzhelian Thermal
1020 Excursion, C15.3,) and late Permian (Emeishan Thermal Excursion, W14). Global average
1021 temperatures ranged from 13°C during the depths of the Permo-Carboniferous Ice Age to ~22°C
1022 during the Early Tournaisian Warm Interval, the warmest time period during the Carboniferous or
1023 Permian.

1024 The Late Paleozoic Icehouse began in the latest Devonian with the formation of a short-lived,
1025 medium-sized south polar icecap (Caputo et al., 2008). This ice cap, centered in Brazil, stretched
1026 from the proto-Andean mountains, eastward to Rio de Janeiro and Gabon, and northeastward into
1027 equatorial west Africa and Niger. The Famennian Ice Age (C17) lasted less than 5 million years and is
1028 correlated with the widespread extinction of marine faunas. This late Devonian extinction event
1029 ranks fourth in terms of taxonomic severity (50% genera lost; McGhee et al., 2013).

1030 During the early Mississippian (Tournaisian), global climate first warmed (W17), then cooled
1031 dramatically (C16; Grossman et al., 2008). Throughout the remainder of the Mississippian,
1032 Gondwana moved steadily northward across the South Pole. Ice sheets contracted, then expanded,
1033 moving southward into south-central Argentina. The south polar ice cap nearly vanished during the
1034 Visean Warm Interval (W16), retreating to the highlands of the proto-Andes of Bolivia and western
1035 Argentina, as well as into the remnants of the Pan-African mountain ranges in southeastern Brazil
1036 and southwest Africa (Fielding et al., 2008).

1037 These latest Devonian and Mississippian machinations were just a prelude to the impending Permo-
1038 Carboniferous Ice Age (313 – 291 Ma.) Beginning in the early Serpukhovian (latest Mississippian, 330
1039 – 326 Ma), the world began to cool once again. However, this time it would remain cool, with Global

1040 Average Temperatures (GAT) less than 18°C for nearly 80 million years. Starting in the earliest
1041 Pennsylvanian (Bashkirian, 323.2 Ma), a large ice cap began to develop at the South Pole and grew
1042 equatorwards reclaiming the southern reaches of the Amazon basin, crossing south-central Africa,
1043 and extending across Antarctica and most of Australia (Mory et al., 2008). Though often portrayed
1044 as a single, large Ice sheet (Scotese et al., 1999), the South Polar Ice Cap was actually composed of
1045 several growing, glacial nuclei (Fielding et al. 2008, 2010; Montañez and Poulsen, 2013) that
1046 coalesced and expanded equatorwards reaching latitudes of 35° south by the mid-Pennsylvanian
1047 (315.2 Ma, Moscovian).

1048 Beginning in the early Moscovian (~313 Ma), the growing South Polar Ice Cap began to rhythmically
1049 wax and wane in synchrony with the changes in the shape of Earth's orbit (Milankovitch cycles;
1050 Milankovitch, 1920; Kump et al., 1999b; Hay, 2016) that regulated the amount of solar energy
1051 received by the Earth. The expansion and contraction of the South Polar Ice Cap caused cyclical
1052 changes in sea level. Paired transgressions and regressions, separated by ~400,000 years, pulsed
1053 across the broad, flat continental cratons generating more than 55 repeating sedimentary packages
1054 called "cyclothems" (Wanless and Weller, 1932). Cyclothems have been mapped across the mid-
1055 continent of North America (Illinois and Mid-Continent Basin; Heckel, 2013) and, to a lesser extent,
1056 the Appalachian basin. Cyclothems have also been identified in similar aged rocks in Donets Basin of
1057 the Ukraine (Montañez et al., 2007; 2016).

1058 The cyclothems are direct evidence of Permo-Carboniferous glacial-interglacial cycles (Wanless and
1059 Shepherd, 1936; Heckel, 1994, 2008; Montañez and Poulsen, 2013) and are identical in nature to
1060 glacial-interglacial sedimentary sequences deposited during the Pleistocene Ice Age (C1.3). The
1061 oldest cyclothems in the mid-continent are middle Pennsylvanian in age (Desmoinesian /early
1062 Moscovian, ~313 Ma; Heckel, 2013). During one particularly warm interglacial episode, the Latest
1063 Gzhelian Thermal Excursion (C15.3), global temperatures may have warmed sufficiently to have
1064 temporarily reduced or eliminated the South Polar Ice Cap (Davydov et al., 2010). However,

1065 whatever the cause, the warmth did not last and glacial-interglacial cycles resumed in earnest. The
1066 youngest cyclothems are early Permian in age (late Sakmarian, 291 Ma). Cyclothems bracket the
1067 coldest phase of the Permo-Carboniferous Ice Age (C15.2, GAT = 13°C) and disappear shortly after
1068 the Permo-Carboniferous Glacial Maximum (C15.1, 299 – 293, early Asselian – early Sakmarian;
1069 Montañez and Poulsen, 2013).

1070 The deep oceans were “refrigerated” during much of the Carboniferous and early Permian (Valdes et
1071 al., 2020). Cold bottom-waters generated by the seasonal melting of the South Polar Ice Cap filled
1072 the oceans with near-freezing waters from the bottom up. Along some continental margins, this
1073 cold bottom-water was carried to the surface by upwelling. Glendonites formed in shallow marine
1074 sediments where the temperatures were < 4°C (De Lurio and Frakes, 1999). Glendonites occur in
1075 association with the shallow water carbonates of the Rundle Group of western Canada which was
1076 located near the equator during the Visean (Brandley and Krause, 1994). At south polar latitudes,
1077 numerous glendonites are found in fine-grained clastic sediments deposited along the margins of
1078 Gondwana (Boucot et al., 2013). In addition, the thermal continuity of these cool shelf and deep
1079 shelf environments allowed early Permian marine faunas to migrate freely between cool temperate
1080 southern latitudes, across the tropics, and into cool temperate northern latitudes (Waterhouse and
1081 Shi, 2013; Shi, 2001).

1082 By the middle Artinskian (285 Ma), global temperatures had warmed (W15) signalling the end of the
1083 Permo-Carboniferous Ice Age (Ziegler et al., 1997). Though the large South Polar Ice Cap was gone
1084 for good, intermontane glaciers inhabited the highlands of eastern Australia, the Trans-Antarctic
1085 Ranges of Eastern Antarctica (Frank et al., 2015), and the far northern, mountainous reaches of
1086 Siberia until the end of the Permian.

1087 Though the coldest portion of the Late Paleozoic Icehouse was over, the Permian remained a “cool”
1088 world, with a moderate pole-to-equator temperature gradient (.75°C per 1 degree of latitude). An
1089 exception was the Emeishan Thermal Excursion (W14), which occurred 260 million years ago during

1090 the late Capitanian. As the name implies, this brief thermal excursion was the result of the eruption
 1091 of the Emeishan flood basalts in southwestern China (Ernst, 2014; Rampino and Shen, 2019). The
 1092 Emeishan eruption was precursor to the much more massive West Siberian eruptions that would
 1093 end the Late Paleozoic Icehouse, terminate the Paleozoic Era, and cause the greatest extinction
 1094 event of all time (Erwin, 1993, 1995, 2006).

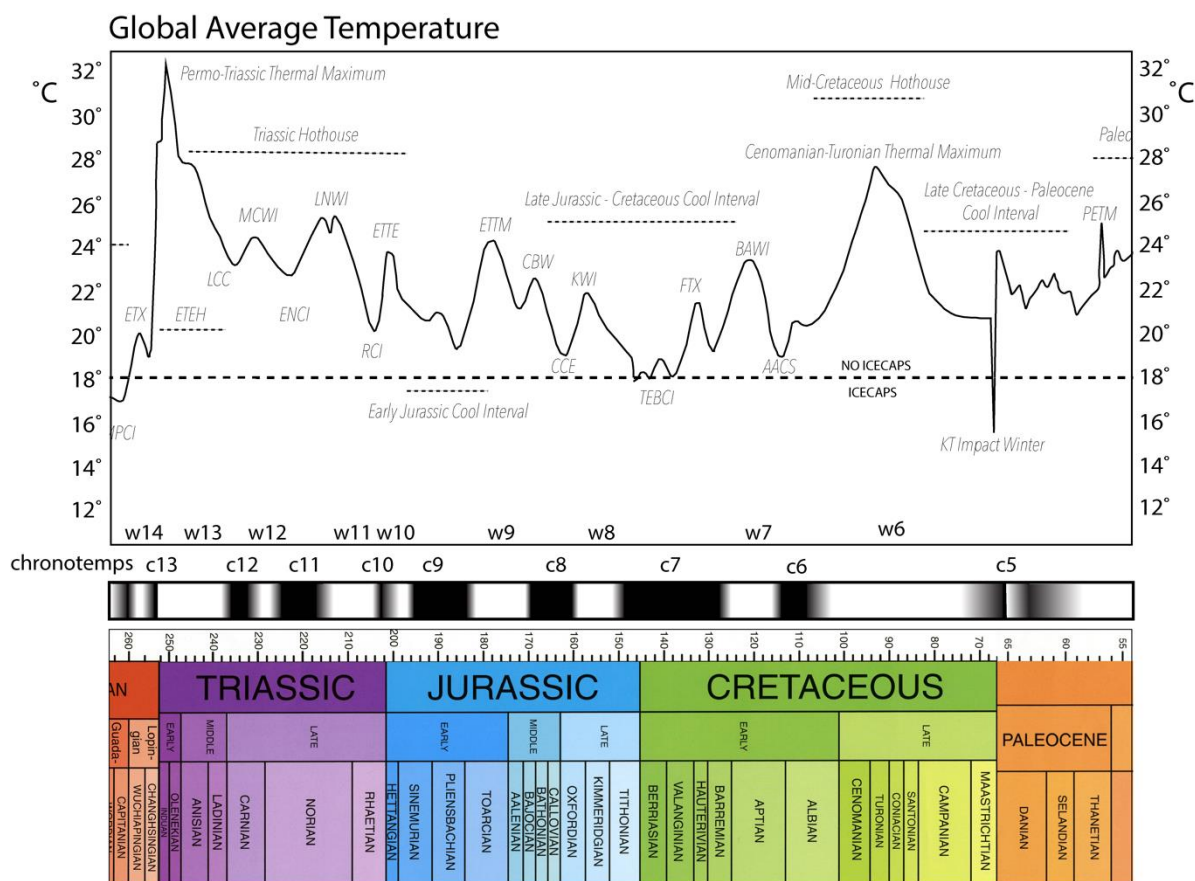


Figure 20. A Mesozoic Paleotemperature Timescale. white = warm time intervals, black = cool time intervals. Solid black line = Global Average Temperatures (GAT), $< 18^{\circ}\text{C}$ = large, permanent icecaps, $> 18^{\circ}\text{C}$ = no large, permanent icecaps. Timescale = International Chronostratigraphic Chart v2020/01. Refer to Table 3 for more information and sources of information for each chronotemp and abbreviations.

1095

1096 5.6 Triassic Hothouse (W10 – W13, 253 – 199 Ma), Table 5, Figure 20

1097 At the beginning of the Mesozoic Era, the Earth was an extreme hothouse world with average
 1098 tropical temperatures approaching 40°C . It is now widely accepted that the extreme global warming
 1099 that ended the Late Paleozoic Icehouse was caused by the voluminous eruption of the West Siberian
 1100 Large Igneous Province (LIP) (Ernst, 2014). During a brief interval (~ 1 million years) at the Permo-

1101 Triassic boundary (252.1 Ma; Kamo et al., 2003), more than 15 million km³ of basaltic lava flowed
1102 from rifts beneath the West Siberian basin (Reichow et al., 2005, 2009; Saunders et al., 2005) and
1103 the Putorana and Tunguska plateaus. This outpouring buried more than 50% of Siberia (7 million
1104 km²) under a mantle of basaltic lava 1-4 km deep (maximum 6.5 km). The primordial, mantle-
1105 derived CO₂ released by these eruptions was supplemented by additional CO₂ derived from the
1106 combustion of thick, buried coal deposits (late Carboniferous – early Permian) that lay along the
1107 subterranean path of the erupting volcanics. The Permo-Triassic Mass Extinction is marked by a $\delta^{13}\text{C}$
1108 spike (Gruszczynski, et al., 1989; Grossman, 1994; Scholle, 1995).

1109 The combined primordial and coal-derived CO₂ (~5000 gigatons) more than doubled atmospheric
1110 levels of CO₂. As a result, tropical temperatures surged from ~25°C prior to the eruption to nearly
1111 40°C. This "Super Hothouse" global warming parched life on land and led to the formation of an
1112 anoxic "Strangelove" ocean (Hsu et al., 1985; Kump, 1991; Hotinski et al., 2001; Zhang et al., 2001;
1113 Grice et al., 2005; Heydari et al., 2008).

1114 As the atmosphere warmed rapidly, the greatest effect was felt near the poles. The cold polar air
1115 masses warmed and the cold surface waters at high latitudes, which were the oceanographic engine
1116 that had previously filled the Late Permian oceans with cold oxygenated bottom water, began to
1117 warm and the engine stalled. As the oceans warmed, they became stratified and began to stagnate.
1118 Organic carbon accumulated in the deep ocean, using up any available oxygen. Anoxia set in (Song
1119 et al., 2014). The first ocean to become anoxic from top to bottom was the landlocked PaleoTethys
1120 Ocean (Wignall and Hallam, 1992; Şengör and Atayman, 2009). The NeoTethys soon became anoxic;
1121 the deeper more isolated portions of Panthalassa (between the Panthalassic mid-ocean ridge and
1122 western North America, -were the last to become toxic. The poisonous waters from PaleoTethys,
1123 NeoTethys, and Panthalassa spilled onto the shelves and the Late Permian benthic, neritic, and
1124 planktonic fauna began to die out. The oceans belched great volumes of CH₄ into the atmosphere

1125 and the level of atmospheric oxygen fell. As temperatures rose even higher, the food chain
1126 collapsed and many complex marine ecosystems were wiped out forever.

1127 On land the conditions were just as extreme. The equatorial regions baked. Average summer
1128 temperatures in the subtropical regions of Pangea exceeded 40 degrees C. Near the poles,
1129 temperatures were warm and seasonal changes were nearly eliminated. The movement of warm air
1130 masses and ocean currents into the polar regions made any attempt at winter cooling impossible.

1131 The interior of Pangea, 1000's of kilometers distant from any source of water, was an intolerably
1132 hot, abiotic desert.

1133 A few isolated habitats may have been refugia from the killing heat. Mountains that poked up into
1134 the westerly trade winds still received abundant rainfall during the winter months. The young peaks
1135 of the Cape Mountains in South Africa, where our burrowing mammal-like reptilian ancestors clung
1136 to life, was such a refugia. In the oceans, species that could tolerate the warmer sea surface
1137 temperatures or that could retreat to the cooler, deeper environments on shelf-edge and slope, also
1138 survived. Most importantly, some species that were able to reproduce rapidly and (e.g.
1139 microgastropods) were able to take advantage of the favourable conditions that sporadically
1140 appeared.

1141 The Permo-Triassic Mass Extinction dwarfs all other mass extinction events. During the Permo-
1142 Triassic Mass Extinction, 57% of all marine families went extinct (Sepkoski, 1989), and an estimated
1143 96% of all marine species were extinguished (Raup, 1979), though time percentage has been revised
1144 downwards to 81% by Stanley (2016). At the individual level, this means that 90 - 99% of all living
1145 things were wiped out. The Permo-Triassic Mass Extinction killed more species in low latitudes and
1146 led to a reduced latitudinal diversity gradient in the Early Triassic (Song et al., 2020). Though the
1147 extinction event appears to be geologically "instantaneous" for most taxonomic groups (especially
1148 brachiopods, bryozoans, crinoids, tabulate and rugose corals), arguments have been made that

1149 other taxa were already in decline (e.g. trilobites, graptolites, conodonts). For these "perched"
1150 fauna, the massive warming event was the coup de grace.

1151 Details of the rapid rise and fall of temperatures during the Early Triassic (252-247 Ma) have been
1152 described by Sun et al. (2012). The Early Triassic Extreme Hothouse (W13) was not a single spike, but
1153 rather a series of ups and downs. The Permo-Triassic Thermal Maximum (W13.4, 253-251 Ma) was
1154 followed by a 4°C fall in temperature (W13.3, Dienerian Cooling, 251-249 Ma), a 6°C rise in
1155 temperature (W13.2, Latest Smithian Thermal Maximum, 249-248 Ma), and finally a 6°C fall in
1156 temperature by the end of the Early Triassic (W13.1, Latest Olenekian Cooling, 248-247 Ma).

1157 The severity of the extinction event is revealed by subsequent "gaps" in the fossil record. Plants and
1158 animals were not able to quickly re-establish the complex ecosystems that prevailed before the
1159 extinction event. There are no significant coal deposits (i.e. no complex rainforest ecosystems) until
1160 20 million years after the mass extinction event ("coal gap"; Veevers et al., 1994; Looy et al., 1999).
1161 The Permo-Triassic Mass Extinction Event wiped out diverse tropical and temperate rainforest flora.
1162 It is interesting to note that the forests and scrublands were replenished by a new stock of plants
1163 (pteridosperms and conifers) that evolved from xerophytic ancestors (Zechstein flora) that were
1164 "pre-adapted" to the hot, dry conditions that prevailed in the Early Triassic (Looy et al., 1999;
1165 Hochuli et al., 2010).

1166 In the early Triassic oceans, there were similar reef and chert "gaps". In the shallow marine seas and
1167 on far-flung oceanic atolls, there were no coral reefs (Stanley, 2003). Reef ecosystems did not
1168 become re-established until the Middle Triassic (Ladinian), approximately 14 million years after the
1169 Permo-Triassic mass extinction wiped out tabulate and rugose corals (Flügel, 2002). These new reefs
1170 were built by a new type of coral animal (scleractinians) whose Permian ancestor was a soft-bodied
1171 "anemone-like" anthozoan that did not build limestone reefs. The radiolarian plankton were
1172 similarly wiped out, resulting in the absence of bedded-chert deposits in the deep oceans.

1173 Global temperatures fell during the Middle Triassic, reaching moderate hothouse temperatures
1174 (24°C) by the end of the Anisian (Trotter et al., 2015). These less extreme temperatures facilitated
1175 the re-establishment of tropical and temperate rainforests, coral reefs, and radiolarian plankton.
1176 The cooling trend continued through the remainder of the Middle Triassic (Ladinian) and into the
1177 early Late Triassic (C12, Ladinian-Carnian Cooling, 242-233 Ma; Trotter et al., 2015). Dense forests of
1178 the tree-like lycopod, *Pleuromania*, grew near the poles (Ziegler et al., 1994). The pattern of growth
1179 rings in *Pleuromania* indicates that these plants grew at rates 10 – 100 times faster than modern
1180 trees (Taylor et al., 2000). This suggests that though the climate was highly seasonal, light rather
1181 than temperature was the limiting growth factor.

1182 During the middle Carnian, temperatures warmed (Rigo and Joachimski, 2007; Trotter et al., 2015;
1183 Sun et al., 2016), rainfall increased and the once extensive carbonate platforms along the margins of
1184 southwestern Tethys were flooded by clastic deposits carried onto the continental shelf by hyper-
1185 active river systems (Dal Corso et al., 2018a,b). This dramatic change in climate is known as the
1186 “Carnian Pluvial Event” (W12.1, 233-230 Ma; Ruffell et al., 2015; Ogg, 2015). It has been proposed
1187 that these climatic events were triggered by the formation of the Wrangellian oceanic plateau and
1188 associated volcanic islands (Greene et al., 2008; 2009 a, b, 2010). The CO₂ released by the eruption
1189 of these basalts warmed the atmosphere which in turn intensified the Pangean monsoonal weather
1190 system (Parrish, 1993) and brought more moisture to the interior of the continent. This rainfall fed
1191 new river systems that transported vast amounts of sand, silt, and mud to oceans.

1192 The arrival of huge amounts of sediments shut-down carbonate factories, promoted deep water
1193 anoxia, and increased environment stress. During the Carnian Pluvial Event (CPE), important
1194 ammonite groups became extinct (Balini et al., 2010), conodonts went through a major crisis (Rigo et
1195 al., 2007; Martinez-Perez et al., 2014), and other groups such as bryozoans and crinoids show a
1196 sharp decline (Simms and Ruffell, 1989). On the continents, new floras evolved that were adapted to
1197 wetter conditions (Roghi et al., 2010; Preto et al., 2010; Mueller et al., 2016a,b). After this event,

1198 modern conifers and bennetitaleans evolved (Willis and McElwain, 2002; Kustatscher et al., 2018)
1199 and dinosaurs emerged as the dominant and most diverse terrestrial fauna (Benton, 1993; Bernardi
1200 et al., 2018).

1201 The Mid-Carnian Warm Interval (W12, 234-227 Ma), which included the Carnian Pluvial Interval, was
1202 followed by the Early Norian Cool Interval (C11, 227-217 Ma; Trotter et al., 2015). Global
1203 temperatures spiked again during the late Norian, (W11, 214-209 Ma; Trotter et al., 2015), before
1204 cooling off slightly at the end of the Triassic (C10, Rhaetian Cool Interval, 209-201; Trotter et al.,
1205 2015). The dip in temperatures during the late Norian can be attributed to a brief cooling excursion
1206 triggered by the Manicouagan impact (W11.1 214 Ma; Spray, 2020).

1207 At the end of the Triassic and into the earliest Jurassic (201.3 Ma), flood basalts erupted across a
1208 large portion of North America, South America, Africa, and southern Europe (estimated area ~10
1209 million km²; Marzoli et al., 1999; McHone and Puffer, 2003; Hames et al., 2003). During a brief
1210 episode of ~600,000 years), the Central Atlantic Magmatic Province (CAMP) released approximately
1211 80,000 gigatons of CO₂ into the atmosphere (Whiteside et al., 2010; Torsvik et al., 2020). This
1212 exhalation of greenhouse gases increased global temperatures 3° - 6° C (McElwain et al., 1999;
1213 Beerling and Berner, 2002; Korte et al., 2009; Dera et al., 2011) giving rise to the brief End Triassic
1214 Thermal Event (W10, 201–199Ma). This rapid episode of global warming triggered the now familiar
1215 cascade of catastrophic environmental changes: increased terrestrial weathering and erosion
1216 Ahlberg et al. (2003), changes in ocean chemistry (i.e., mercury poisoning; Sanei et al., 2012) oceanic
1217 acidification (Hautmann, 2004, 2008; Clarkson et al., 2015), photic zone euxinia, falling marine
1218 productivity, and possible deep ocean anoxia (Isozaki, 1997).

1219 The End Triassic Extinction (ETE) is ranked third in terms of taxonomic severity, with an estimated
1220 73% extinction of marine genera (McGhee et al., 2013). The once widespread seed fern *Dicrodium*
1221 disappeared from the fossil record (van de Schootbrugge et al., 2009). There was a 90% species
1222 turnover in the terrestrial megaf flora (McElwain and Punysena, 2007). A “fern-spike” suggests

1223 widespread changes in vegetation across Europe and North Atlantic (van de Schootbrugge et al.,
1224 2007; Bonis et al., 2010). A number of non-marine clades of vertebrates went extinct, though marine
1225 reptiles and fish actually flourished (McCune and Schaeffer, 1986; Benton et al., 2013; Friedman and
1226 Sallan, 2012). The End Triassic Extinction was the most severe extinction crisis ever experienced by
1227 scleractinian corals (Flügel, 1994; Flügel and Kiessling, 2002; Kiessling et al., 2002) and was
1228 catastrophic for reef communities. Bivalves and ammonoids, though they were hit hard by the End
1229 Triassic Extinction, had been in decline throughout the latest Triassic (Rhaetian; Hallam, 2002). For
1230 excellent summaries of the events surrounding the End Triassic Extinction, see Preto et al. (2010),
1231 Whiteside and Grice (2016), Bond and Grasby (2017), and Torsvik et al. (2020).

1232

1233 **5.7 Jurassic – Early Cretaceous Cool Interval (C7 – C9, 199-128 Ma), Table 5, Figure 20**

1234 Not all climate modes can be neatly pigeon-holed as either a steaming hothouse world or a frigid
1235 icehouse world. The 71 million year interval from the beginning of the Jurassic (Hettangian, 199 Ma)
1236 through the Early Cretaceous (early Barremian, 128 Ma) is made up of more than 16 distinct warm
1237 and cool events (Table 5). Cooler events make up ~67% of this time interval and justify the
1238 designation “Jurassic – Early Cretaceous Cool Interval”, though the appellation, “Jurassic – Early
1239 Cretaceous Mixed Interval” would work as well.

1240 The Jurassic - Early Cretaceous Cool Interval is made up of three cool, but not cold, intervals
1241 separated by two warm intervals. Both of these warmer intervals, the Toarcian Warm Interval (W9)
1242 and the Kimmeridgian Warm Interval were hothouse worlds with average global temperatures of
1243 22°C. The average global temperature during the Jurassic – Early Cretaceous Cool Interval was a
1244 relatively mild 17.5°C, which is close to the average temperature for the entire Phanerozoic (18°C).

1245 The Early Jurassic Cool Interval (C9, 199-183 Ma) and the Middle Jurassic Cool Interval (C8, 174 – 164
1246 MA) are both characterized by moderate pole-to-equator temperature gradients with annual
1247 average polar temperatures several degrees above freezing. Dropstones and glendonites found in
1248 northeastern Siberia (Boucot et al., 2013) are evidence of cold winters in the northern hemisphere
1249 during much of the early and middle Jurassic (late Pliensbachian – early Bathonian). The winter snow
1250 and ice, however, did not persist. The warm summers melted any seasonal snow and ice, preventing
1251 the growth of permanent ice caps in either hemisphere (Sellwood and Valdes, 2006).

1252 Distinctive Jurassic plant groups occupied different latitudinal climatic zones. The greatest diversity
1253 of plants occurred at mid-latitudes (40° N&S) where forest were composed a mixture of ferns,
1254 cycads, sphenopsids (like horsetails), pteridosperms (seed ferns), and conifers (Rees et al., 2000).
1255 The equatorial regions, which were sparsely populated, were hot and dry and dominated by
1256 xeromorphic (arid-adapted) forms, small-leafed conifers, and cycads. Large-leafed conifers and
1257 deciduous ginkgos grew in the polar regions (Rees et al., 2000). These plant groups suggest that the
1258 temperatures were seasonally cold, but not frigid. Estimates of tropical seawater temperatures
1259 from $\delta^{18}\text{O}$ measurements are 4° to 6 °C cooler than modern tropical temperatures (Dera et al., 2011)
1260 indicating a moderate pole-to-equator temperature gradient.

1261 The Early Jurassic Cool Interval (C9) was followed by the Toarcian Warm Interval (W9), during which
1262 temperatures spiked 4° - 8°C (Dera et al., 2011). This warm pulse has been attributed to increased
1263 atmospheric CO₂ arising from the eruption of the Karroo-Ferrar LIP (Pankhurst et al., 1998, 2000;
1264 Elliot et al., 1999; Courtillot and Renne, 2003; Jourdan et al., 2005; Ernst, 2014; Ernst and Youbi,
1265 2017). The global nature of this warming event is recorded by widespread oceanic anoxia (Toarcian
1266 OAE; Jenkyns et al., 2002; Jenkyns, 2010; van de Schootbrugge et al., 2013).

1267 Much has been made of the extremely arid conditions and unbearable heat of equatorial and
1268 subtropical Pangea (30N to 30 S). By modern standards, the climate at low latitudes during the

1269 Toarcian Warm Interval was unbearably hot. Average equatorial sea surface temperatures which
1270 were the warmest of the Jurassic exceeded 30° C and temperatures in the interior of Pangea often
1271 exceeded 40° C (Crowley, 1994). The intense summer heating of the large land areas north and
1272 south of the Equator strongly deflected the Intertropical Convergence Zone (ITCZ) during the
1273 summer months. This modification of the basic Hadley Cell circulation pattern has been called
1274 “mega-monsoonal” atmospheric circulation (Parrish 1993). Megamonsoons resulted in drier
1275 conditions along the Equator and the formation of a broader Subtropical Arid Belt.

1276 Though the equatorial and subtropical regions of Pangea were arid during the Early Jurassic, most of
1277 the world was covered by lush, habitable forest vegetation (Rees et al., 2000). Abundant Early
1278 Jurassic coal deposits are found in both the warm and cool temperate belts (up to 60 N& S) (Boucot
1279 *et al.*, 2013). Bauxite deposits, indicative of warm and wet conditions, are found in Europe and west
1280 central Asia (Kazakhstan) (30N - 45N).

1281 The early Jurassic Toarcian hothouse (W9) was followed by a relatively cool period during the middle
1282 Jurassic (Jenkyns et al., 2002; Dera et al., 2011). In a rare turnabout, during the early Jurassic, the
1283 South Polar region appears to have been warmer than the North Polar region. Dinosaurs and small
1284 flying reptiles, which would have had difficulty surviving freezing winters, inhabited the central
1285 Antarctica Transantarctic Ranges (Hammer and Hickerson, 1996); whereas dropstones and
1286 glendonites, indicative of freezing winter conditions, have been reported from Arctic Siberia (Boucot
1287 *et al.*, 2013; 70 N – 80 N).

1288 Global temperatures warmed again during the late Oxfordian and Kimmeridgian (W8, Kimmeridgian
1289 Warm Interval, Podlaha et al., 1998; Jenkyns et al., 2002; Dera et al., 2011). The “mega-monsoonal”
1290 atmospheric circulation that characterized the earlier Mesozoic (Parrish, 1993) was still in place, but
1291 showed signs of weakening. As the newly formed intra-Pangean ocean basins (Central Atlantic
1292 Ocean and Western Indian Ocean) widened, they brought new sources of moisture to the interior of
1293 Pangea. The influx of moisture from these young ocean basins dampened the severe, seasonal

1294 swings in temperature and precipitation that had plagued the dessicated core of Pangea since the
1295 Late Permian. For other climate model results for the Late Jurassic see Moore *et al.* (1992), Valdes
1296 and Sellwood (1992), Valdes (1994), Sellwood and Valdes (2006).

1297 The Kimmeridgian Warm Interval (164-150 Ma) was followed by a long interval characterized by
1298 cool, but not frigid, temperatures (Tithonian-early Barremian Cool Interval, C7, 150 – 128 Ma). The
1299 Tithonian-early Barremian Cool Interval was punctuated by isolated warm events (Weissert (136
1300 Ma) and Faraoni (131 Ma) thermal excursions).

1301 Global Climate during the earliest Cretaceous (Berriasian to Barremian) can be characterized as
1302 something “in-between” a hothouse and an icehouse (Frakes *et al.*, 1992). The average global
1303 temperature was about 17° C. This was five degrees warmer than the Late Cenozoic Icehouse (C1,
1304 12° C), but seven to nine degrees cooler than the Mid-Cretaceous – Paleogene Hothouse (W5-W6).

1305 Evidence for more temperate climatic conditions is based on the occurrence of dropstones,
1306 glendonites, and a few tillites (pebbly mudstones, Boucot *et al.*, 2013) in polar latitudes that co-
1307 occur with evidence of temperate forests (coal, plant fossils) and dinosaurs. Dropstones of Early
1308 Cretaceous age (Berriasian/Barremian) are widespread in South Australia, Queensland, New South
1309 Wales, and the Northern Territory of Australia (Boucot *et al.*, 2013). Glendonites occur in South
1310 Australia and New South Wales . In the northern hemisphere there are dropstones in Siberia and
1311 Svalbard, and glendonites in northern Siberia, Svalbard and the Arctic Islands (Grasby *et al.*, 2017;
1312 Brassell, 2009; Frakes and Francis, 1988; Frakes and Francis, 1990,1993; Frakes *et al.*, 1995; De Lurio
1313 and Frakes, 1999; Vickers *et al.*, 2019).

1314 The best interpretation for this mixture of cool and warm climatic indicators is that it was cold
1315 enough in the winters for lakes and rivers to freeze over. Snow covered the ground and there were
1316 glaciers at higher elevations. In the summer months it was warm enough to support the growth of
1317 lush vegetation and an influx of dinosaurs migrating in from warmer regions.

1318 It is interesting to note that the Kimmeridgian Anoxic Event is the only potential oceanic anoxic
1319 event for the time interval spanning the middle Jurassic (Aalenian, 174 Ma) to the early Barremian
1320 (128 Ma). It does not appear to be as widespread as the Cretaceous OAE events. The lack of anoxic
1321 basins during the earliest Cretaceous seems quite unusual in light of the fact that there were many
1322 “restricted” marine basins that would have been ideal habitats for anoxia to develop. The lack of
1323 OAEs may have been due to the fact that the bottom waters during the middle and late Jurassic
1324 through to the earliest Cretaceous were relatively well-oxygenated. The occurrence of glendonites
1325 at high latitudes during much of the Early Cretaceous indicates that cool, oxygen-rich bottom waters
1326 were being generated at polar latitudes preventing the bottom waters in lower latitudes from
1327 becoming anoxic.

1328 **5.8 Mid Cretaceous – Paleogene Hothouse (W5 – W7, 39.4-128 Ma), Table 6, Figure 20**

1329 If one imagines where the current phase of anthropogenic global warming is heading, one
1330 immediately thinks of the hothouse worlds of the Late Cretaceous and Eocene (Huber, 1998; Huber
1331 et al., 2000). During the Mid Cretaceous – Paleogene Hothouse global temperatures were indeed
1332 much warmer than the present-day (GAT = 28°C during the Late Cretaceous versus GAT = 15°C for
1333 the Modern). It remains to be seen whether we will succeed in warming the Earth to that degree,
1334 but at least we now know what a warmer world would look like.

1335 The Mid Cretaceous – Paleogene Hothouse is one of the best documented paleotemperature
1336 intervals. Table 6 lists some of the key references for this time interval and summarizes their
1337 primary conclusions regarding regional and global temperatures. The best single source for
1338 information about the Cretaceous portion of this hothouse interval is the O’Brien et al. (2017)
1339 summary of sea surface temperatures (SSTs) based on oxygen isotope and TEX₈₆ temperature
1340 estimates. The TEX₈₆ technique uses the lipid chemistry of the cell membrane of a common group of
1341 pelagic protokaryotes (Thaumarchaeota) to estimate temperatures (Schouten et al., 2002). The
1342 paleotemperatures are derived by measuring the ratio of key lipids (crenarchaeols). It has been

1343 noted that TEX₈₆ temperature estimates tend to be ~50% higher than $\delta^{18}\text{O}$ temperature estimates
1344 (O'Brien et al., 2017; Figure 8). Approximately 90% of the available TEX₈₆ paleotemperature
1345 estimates for the Cretaceous have been obtained from samples that are Aptian or younger in age.
1346 Moreover, there are very few $\delta^{18}\text{O}$ temperature estimates for times older than the mid-Albian
1347 (O'Brien et al., 2017). Fortunately, as noted earlier, geological evidence (glendonites, dropstones,
1348 and rare tillites) from the Early Cretaceous helps to fill in these data gaps.

1349 Both oxygen isotope and TEX₈₆ measurements identify an early Barremian – middle Aptian warm
1350 interval (W7, 128 – 118 Ma, GAT = 22°C), which was followed by a cooler period during the late
1351 Aptian-early Albian (C6, 118 – 111 Ma, GAT = 19°C), which preceded the rapid ramping up to a
1352 thermal maximum during the latest Cenomanian- earliest Turonian (W6.2, 94 – 93 Ma, GAT = 28°C).
1353 According to O'Brien et al. (2017), temperatures cooled gradually during the remainder of the Late
1354 Cretaceous reaching a minimum of ~21°C in the late Maastrichtian, just prior to the KT impact
1355 event.

1356 The Mid Cretaceous – Paleogene Hothouse (W6) began in the latest Barremian – earliest Aptian
1357 (~128 Ma) with two thermal events, the Hauptblatterton Thermal Event (W7.5; Mutterlose et al.,
1358 2009) and the oldest Cretaceous oceanic anoxic event, OAE1a, the Selli/Goguel Thermal Maximum
1359 (W7.4; Erba et al., 2015; Herrle et al., 2015; O'Brien et al., 2017). Average global temperatures
1360 during the Mid Cretaceous – Paleogene Hothouse was a ~23° C. Surface waters in the Cool
1361 Temperate regions (SST = 21-23°C) were only slightly cooler than the superheated tropical seas (29°
1362 C; O'Brien et al., 2017). Oceanic bottom waters were also much warmer than the present-day (9° -
1363 17° C; Valdes et al., 2020).

1364 The Selli/Goguel Thermal Maximum (OAE1a) is the first of nearly a dozen potential thermal spikes
1365 that characterize this time interval (see Table 3). The nature and origin of these OAEs has been
1366 much debated (Schlanger and Jenkins, 1976; Arthur and Sageman, 1994; Meyer and Kump, 2008).

1367 Previous notions that OAEs were simply the result of rapid rises in sea level (Arthur and Sageman,
1368 1994) or due to the stagnation of the ocean basins caused by thermohaline density stratification,
1369 have fallen out of favour. There are two current schools of thought. The first argues that the OAE's
1370 were "unusual", synchronous, global events. According to this argument, "catastrophic" tectonic
1371 events triggered "unusual" atmospheric, biologic, geochemical, and oceanographic conditions that
1372 promoted extensive deepwater anoxia that resulted in the formation of carbon-rich black shales
1373 (Total Organic Carbon often > 30%). Proponents of this school of thought argue that the following
1374 scenario may explain the widespread occurrence of the carbon-rich black shales associated with the
1375 early Aptian Selli/Goguel Thermal Maximum (OAE1a):

- 1376 • The eruption of the mid Cretaceous superplume (Larson, 1991; Larson and Erba, 1999)
1377 radically changed atmospheric and oceanic chemistry.
- 1378 • Greenhouse gases from the erupting lavas, (i.e. CO₂), warmed the Earth.
- 1379 • Increased warmth accelerated chemical weathering on land; consequently, a greater flux of
1380 nutrients was carried to the oceans.
- 1381 • Land-derived nutrients, together with a higher concentrations of biolimiting metals made
1382 available by increased hydrothermal activity associated with the extensive submarine
1383 eruptions (Duncan and Huard, 1997; Jones and Jenkyns, 2001) promoted greater marine
1384 productivity resulting in more carbon deposition.
- 1385 • The increased productivity depleted the available supply of oxygen in the water column,
1386 which led to basin-wide anoxic or dysoxic conditions.
- 1387 • Water-column anoxia, in turn, favoured the preservation of the carbon by inhibiting
1388 bacterial decay and carbon recycling.
- 1389 • The results were widespread carbon-rich black shales (Demaison and Moore, 1980)

1390 A second school of thought argues that the OAEs do not represent unusual or catastrophic, global
1391 events, but rather represent "business as usual". In other words, a certain constellation of biologic,

1392 geochemical, tectonic, atmospheric, and oceanographic conditions favour the development of local,
1393 basin-wide anoxia. The Cretaceous were unusual only in the sense that this constellation of
1394 favorable conditions was more likely to occur than one might have been expected. In essence the
1395 paleogeography of the Aptian/Albian (and Cenomanian/Turonian) was especially favourable for the
1396 formation of highly productive, anoxic basins that promoted “nutrient trapping” (Meyer and Kump,
1397 2008).

1398 These two schools of thought epitomize the classical conflict between “catastrophic” versus
1399 “uniformitarian” explanations of Earth processes. As in the case of most false dichotomies, each
1400 hypothesis may hold part of the answer. Each hypothesis may explain different aspects of the Earth
1401 System processes that produce oceanic anoxic events. The “catastrophic” hypothesis may be the
1402 best explanation for the rare, but truly global, “mega” OAE events (i.e. Selli/Goguel Thermal
1403 Maximum (OAE1a) and Cenomanian-Turonian Thermal Maximum (OAE2), whereas the
1404 “uniformitarian” hypothesis may be a better explanation for the more frequent, regional, and less
1405 intense OAE events (OAE1b, OAE1c, OAE1d, OAE3).

1406 The Aptian-Albian Cold Snap (C6, 118-111 Ma) separates the Selli/Goguel Thermal Maximum
1407 (OAE1a) from the remaining Late Cretaceous OAE’s. For a brief interval in the late Aptian and Early
1408 Albian, the global climate cooled off sufficiently for winter snow and ice to return to the northern
1409 and southern polar regions (Pucéat et al., 2003; Jenkyns et al., 2012; Erba et al., 2015; Herrle et al.,
1410 2015; O’Brien et al., 2017). Glendonites are reported from Ellesmere Island, Axel Heiberg Island,
1411 Svalbard, northern Greenland, and east-central Australia (Eromanga Sea) indicating that cool bottom
1412 waters once again had chilled the deep ocean basins (Frakes and Francis, 1988; Grasby et al., 2017;
1413 Vickers et al., 2019).

1414 The warmest Cretaceous temperatures occurred during the Cenomanian-Turonian Thermal
1415 Maximum (W6.2, 94 – 93 Ma). Second only to the Permo-Triassic Thermal Maximum (W13), the
1416 global average temperature reached 28°C and the pole-to equator temperature gradient was

1417 flattened with a temperature differential of only $\sim 20^{\circ}\text{C}$ degrees between the polar region (13°C) and
1418 the tropics (34°C). Not even a hint of ice existed at the poles during the Cenomanian-Turonian
1419 Thermal Maximum (Ziegler et al., 1985). The presence of tropical plants and dinosaurs on Antarctica
1420 (Dettmann, 1989; Cantrill and Poole, 2012) and above the Arctic Circle indicates that temperatures
1421 rarely fell below freezing even during the winter months (Wolfe and Upchurch, 1987; Parrish and
1422 Spicer, 1988). Recent descriptions of angiosperm leaf floras from Antarctica indicate that similar
1423 warm and wet conditions existed near the South Pole during the Late Cretaceous (Hayes *et al.*,
1424 2006). In general, during times of hothouse conditions, the equatorial and subtropical belts expand
1425 slightly poleward; the Polar and Cool Temperate belt are replaced by an expanded Warm Temperate
1426 belt that brings tropical conditions to latitudes above 50° north and south (Paratropical Belt of
1427 Boucot et al., 2013; the megathermal rainforests of Morley, 2011).

1428 Despite the overwhelming geological and paleontological evidence for warm polar regions during
1429 the Mid-Cretaceous Hothouse, early climate simulations tended to “run cold” and had a difficult
1430 time modeling these warmer polar temperatures (Barron and Washington, 1982). Various attempts
1431 have been made to modify the input parameters to the climate models to produce simulations more
1432 consistent with the geological data. Initial attempts to fix this problem used extremely elevated
1433 levels of greenhouse gases to warm the poles ($15\times$ modern CO_2 ; Bice and Norris, 2002). However,
1434 there is no geological support for CO_2 concentrations in the Cenomanian/Turonian much above $5\times$
1435 the modern value (van der Meer et al., 2014). The extreme high levels of CO_2 needed to keep the
1436 polar regions ice-free would necessarily make terrestrial and shallow marine habitats at low
1437 latitudes uninhabitable (Jacobs et al., 2005).

1438 Another way to make the polar regions warmer is to modestly increase the concentration of
1439 greenhouse gases and also modify the land cover in polar regions to a darker, denser vegetation
1440 (Upchurch *et al.*, 1999). The darker vegetation has a lower albedo and consequently more solar
1441 energy is absorbed at the surface. In this model, positive feedbacks between high-latitude forests,

1442 the atmosphere, and the ocean all contribute to significantly warmer temperatures at high latitudes
1443 during the Late Cretaceous (Upchurch *et al.*, 1999).

1444 A third explanation invokes a Late Cretaceous “Super-Gulf Stream” that vigorously carried warmth
1445 from the Equator to the Poles (Brady *et al.*, 1998). Though intuitively appealing, an analysis of the
1446 dynamics indicates that it is not possible to carry enough heat poleward using ocean currents alone.
1447 The atmosphere must also play an important role. In addition, much like today, the paleogeography
1448 of the Late Cretaceous presents a nearly landlocked polar region that would have been isolated from
1449 Gulf Stream-like ocean currents.

1450 One of the more promising approaches has been to change the high-altitude cloud parameterization
1451 that is used in climate models like the Community Climate System Model version 3 (CCSM3, Kiehl
1452 and Shields, 2013). The high albedo of low-altitude cumulus clouds reflects incoming sunlight back
1453 to space, which cools the Earth. Wispy, high-altitude clouds, on the other hand, reflect thermal
1454 energy back to the surface of the Earth resulting in net global warming (Kump and Pollard, 2008).
1455 Fewer “warm clouds” form in the modern world because anthropogenic atmospheric pollution
1456 reduces the amount of warm cloud condensation nuclei. When cloud parameters characteristic of
1457 pristine regions are introduced into the climate model, significant additional warming occurs,
1458 especially in polar regions (Upchurch *et al.*, 2015). Combined with a modest elevation in the
1459 concentration of atmospheric CO₂ (2x – 6x modern levels), the modelled temperature of polar
1460 regions remains above freezing throughout most of the year.

1461 The most radical hypothesis that has been proposed to explain the warm polar climates of the Late
1462 Cretaceous involves a fundamental rethinking of the way the atmosphere circulates. One of the
1463 basic features of the modern atmosphere is Hadley Cell circulation. In the Hadley Cell, warm air rises
1464 at the Equator, moves poleward, cools and descends over the subtropical desert belt (~35° N&S). In
1465 Hay’s model (Hay, 2008; Hay *et al.*, 2016), this simple, well-organized convective flow is replaced by a
1466 chaotic system of super-cyclonic eddies, which are like mega-hurricanes. Hundreds of these mega-

1467 hurricanes would have annually transferred vast amounts of heat from the Equator to the Poles
1468 during the Late Cretaceous. Though an intriguing and out-of-the-box proposition, no climate model
1469 can currently simulate this complex alternative to Hadley Cell circulation.

1470 After reaching peak Cretaceous temperatures during the Cenomanian-Turonian Thermal Maximum,
1471 temperatures gradually fell during the remainder of the Cretaceous. Maximum sea surface
1472 temperatures did not drop below 30°C until late in the Santonian (84 Ma) or early in the Campanian
1473 (O'Brien et al., 2017). This gradual cooling may have been punctuated by several, ephemeral cooling
1474 events at ~85Ma, ~76 Ma, and ~71 Ma (Miller et al., 1999, 2004, 2005a,b) as evidenced by $\delta^{18}\text{O}$
1475 temperature estimates from planktonic foraminifera. Also, an enigmatic dropstone deposit of
1476 Campanian – Maastrichtian age (75 – 70 Ma) has been reported from the region of the Anadyr River
1477 in Chukotka (Ahlberg et al., 2002).

1478 The modest, but steady, fall in temperatures during the Late Cretaceous was catastrophically
1479 interrupted by the arrival of the bolide that produced the 150 km diameter impact crater near the
1480 town of Chicxulub (Devil's Tail) in northern Yucatan (Alvarez and Alvarez, 1980; Schulte et al., 2010;
1481 Hildebrand et al., 1991). The Chicxulub impact is the largest known bolide impact of the Phanerozoic
1482 (Spray, 2020).

1483 The most likely scenario is that the impact event vaporized 3000 megatons of crustal material and
1484 injected this fine particulate matter high into the atmosphere. This material fell back to Earth
1485 forming a global "clay layer". The K/T boundary clay layer contains several unusual stratigraphic
1486 markers: 1) an iridium anomaly (Alvarez and Alvarez, 1980; Smit, 1999; Miller et al., 2010), 2)
1487 microtektites (Yancey and Guillemette, 2008), 3) shocked quartz (Bohor et al., 1987; Smit, 1999), and
1488 4) soot (from forest fires) that connect it directly to the Chicxulub impact event. (It should be noted that
1489 the authors prefer to use the term "K/T" rather than the more precise "K-Pg" to describe events
1490 occurring at the Cretaceous -Paleogene boundary. The term "K/T" has precedence, is still widely

1491 used, is more familiar to most readers, and is therefore a clearer descriptor than the technically
1492 correct, but more obscure and less euphonius, “K-Pg”.)

1493 While suspended in the atmosphere, this delicate shroud of material blocked the sun and turned day
1494 into night - a night that lasted several months to a year. Without sunlight, plants on land and
1495 plankton in the oceans died. Small and large herbivores gradually starved. Without herbivores to
1496 prey on, predators then starved - all the while, snow continued to fall (probably for several
1497 decades). As a consequence of the collapse of the food chain, ~75% of all species were wiped out
1498 (Sepkoski, 1996). The effect of this extinction event on global ecosystems was second only to the
1499 great Permo-Triassic Extinction (McGhee et al., 2013).

1500 The ensuing “Impact Winter” scenario plunged the Earth into a frigid deep-freeze comparable to the
1501 coldest glacial stages of any Phanerozoic ice age. The drastic cooling, however, was short-lived
1502 (Vellekoop et al., 2014, 2016) and was followed by an equally short-lived period of global warming
1503 triggered by the final, massive eruption of the Deccan LIP (Ernst, 2014; Keller et al., 2017). The first
1504 eruptions of the Deccan LIP predate the Chicxulub impact by 1-2 million years (Chenet et al., 2008;
1505 Keller et al., 2011, 2014). It has been proposed that an earlier impact event (Shiva impact) triggered
1506 the Deccan eruptions (Chatterjee et al., 2006), however this hypothesis has not received much
1507 support. It seems likely, however, that the Chicxulub impact did influence or enhance Deccan
1508 volcanism. It has been noted by several authors (E. Shoemaker, pers. comm.) that the impact site in
1509 Yucatan is nearly antipodal to the eruption site of the Deccan LIP in India. Though the antipodal
1510 paleolatitudes are identical (26° N vs 26° S), the antipodal paleolongitudes are offset by several
1511 thousand kilometers. Nevertheless, it seems plausible that shockwaves from the impact passed
1512 through the earth and were reconcentrated beneath the Deccan hotspot stimulating more
1513 voluminous eruptions (Richards et al., 2015; Renne et al., 2015). In any event, the excess
1514 atmospheric CO₂ from the Deccan eruptions caused a 4-8° spike in global temperatures (Petersen et
1515 al., 2016; Bond and Grasby, 2017) that ushered in the Paleogene Warm interval.

1516 Following the KT impact Winter, global temperatures warmed during the Paleocene, reaching a
1517 maximum during the early-middle Eocene (Paleocene - Eocene Hothouse, W5, 62 - 39.4 Ma). This
1518 period of global warmth was probably triggered by CO₂ injected into the atmosphere by massive
1519 volcanic eruptions in the North Atlantic Igneous Province (NAIP; Ernst, 2014). It was in this global,
1520 tropical "Garden of Eden" that our mammalian ancestors diversified, crossed newly-erupted volcanic
1521 land bridges between northern Europe and Greenland, and expanded across the globe (Wallace,
1522 2004).

1523 The classic record of deep ocean temperatures based on benthic foraminifera assembled by James
1524 Zachos (Zachos et al., 2001, 2008; also Westerhold et al., 2020) provides a framework for describing
1525 the temperature fluctuations during the Paleocene-Eocene Hothouse and the Late Cenozoic
1526 Icehouse (Koeberl and Montanari, 2009). These deep ocean temperatures have been converted to
1527 global average temperatures using the technique described in section 3.3.

1528 The three most prominent features of this detailed temperature record are: 1) the Paleocene-
1529 Eocene Thermal Maximum (W5.8, 55.6 Ma; Rea et al., 1990; Kennett and Stott, 1991; Wing et al.,
1530 2003; McInerney and Wing, 2011), 2) the Early Eocene Thermal Maximum (W5.5, ~50 Ma), and the
1531 Middle Eocene Thermal Maximum (W5.1, ~41 Ma). These are certainly "event" driven changes in
1532 climate. The one explanation for these spikes in temperature is the rapid release of massive
1533 amounts of methane hydrates (clathrates) from the deep sea (Zeebe et al., 2009). Methane is a
1534 powerful greenhouse gas and the release of gigatons of methane into the atmosphere would have
1535 produced the observed rapid rise in global temperature. Other hypotheses, summarized by Wing
1536 and McInerney (2011, p 494), suggest that the excess amount of greenhouse gases may have come
1537 from wildfires, volcanic intrusions into organic-rich sediments, drying of epicontinental seas, or the
1538 thawing of Antarctic permafrost. Most recently, Gutjhar et al. (2017) and Jones et al. (2019) have
1539 proposed that massive eruptive episodes associated with the North Atlantic Igneous Province (NAIP)
1540 provided the excess CO₂ responsible for these thermal maxima.

1541 A prominent feature of the early Eocene Hothouse is the broad, dome-shaped rise and fall in
 1542 temperature that defines the Middle Eocene Warm Interval (W5.4, 56-46 Ma). The shape of this
 1543 curve indicates that systematic changes were taking place over millions of years (Huber and
 1544 Caballero, 2011). These changes in global temperature were probably driven by gradually changing
 1545 paleogeographic, plate tectonic, or paleoceanographic conditions. The final notable feature of the
 1546 Zachos Curve is the rapid fall in temperature at the end of the Eocene (C4.3, Eocene Oligocene Rapid
 1547 Cooling, 33-34 Ma). It has been proposed by many authors that this cooling event was driven by the
 1548 development of a through-going Circum-Antarctic Current and the subsequent isolation and
 1549 refrigeration of Antarctica.

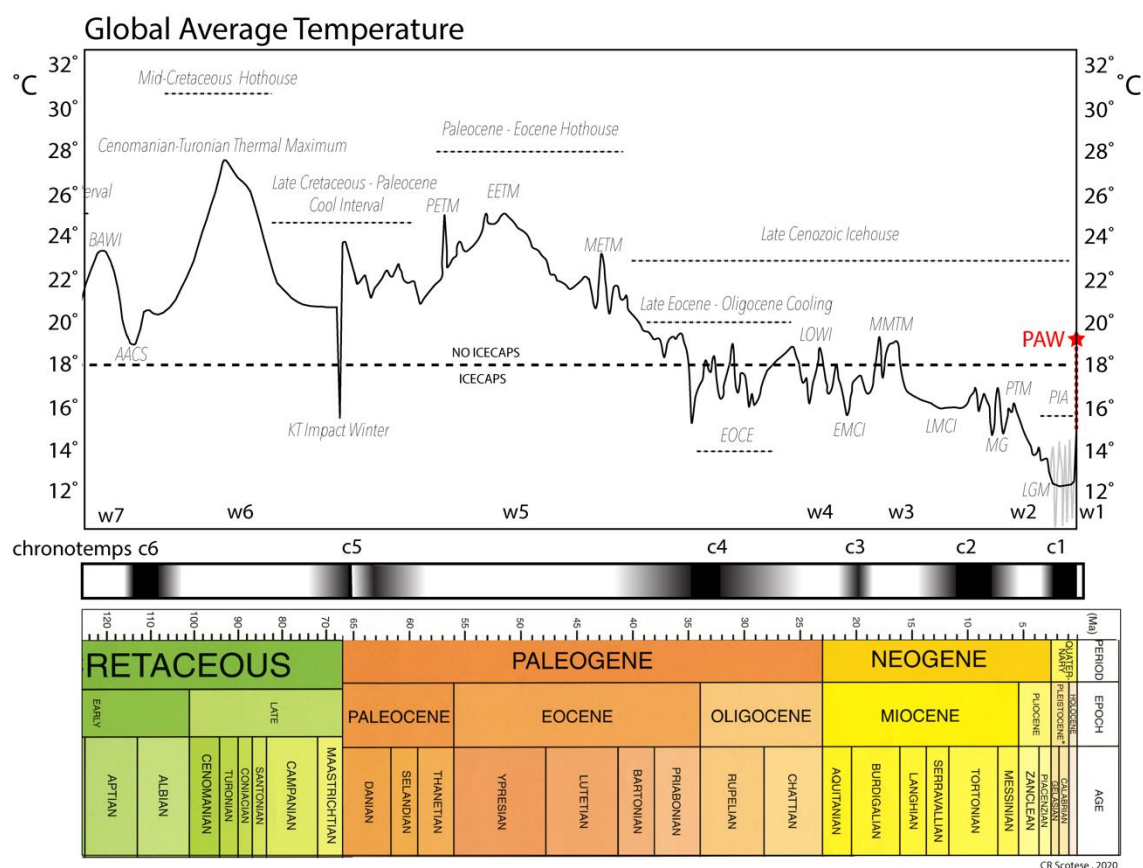


Figure 21. A Cenozoic Paleotemperature Timescale. white = warm time intervals, black = cool time intervals; Light gray jagged lines = a schematic representation of >50 glacial/interglacial cycles during the Plio-Pleistocene. Solid black line = Global Average Temperatures (GAT), < 18°C = large, permanent icecaps, > 18°C = no large, permanent icecaps. Timescale = International Chronostratigraphic Chart v2020/01. Refer to Table 3 for more information and sources for each chronotemp and abbreviations.

1550

1551 5.9 Late Cenozoic Icehouse (C1 – C4, 1880 CE – 39.4 Ma), Table 7, Figure 21

1552

"And now there came both mist and snow"

1553 *And it grew wondrous cold*
1554 *And ice, mast-high, came floating by*
1555 *As green as emerald."*
1556 Samuel Taylor Coleridge, Rime of the Ancient Mariner (1798)

1557

1558 As illustrated in Figure 21, the cooling trend that began after the Early Eocene Thermal Maximum
1559 (W5.5, 52-50 Ma) continued during the middle and late Eocene, though it was interrupted briefly by
1560 the Middle Eocene Thermal Maximum (W5.1, 41 Ma). What Earth System event initiated the Late
1561 Cenozoic Icehouse? The generally accepted explanation is that the collision of India, which took
1562 place at the height of the Early Eocene Thermal Maximum (~50 Ma; Molnar and Tapponier, 1975;
1563 Rowley, 1996, 1998), triggered a cascade of events that lead to global cooling (Raymo and
1564 Ruddiman, 1992). The collision of India with south-central Asia resulted in the rapid uplift of the
1565 Himalaya Mountains. By ~35 Ma (late Eocene – early Oligocene), the Himalayas and Tibetan plateau
1566 had achieved 90% of their modern height (Rowley and Currie, 2006), though the Tibetan plateau was
1567 less than half its present area. These young mountains were in the path of the Asian monsoon,
1568 which brought warm temperatures and abundant moisture. This lead to rapid mechanical and
1569 chemical weathering. The flux of calcium to the world's oceans increased and these calcium cations
1570 combined with carbonate ions to form limestone which drew-down the amount of CO₂ in the
1571 atmosphere. The gradual decrease in atmospheric CO₂ cooled the Earth.

1572 As global temperatures began to cool, the high altitude glaciers on the Gamburtsev mountains and
1573 Trans-Antarctic Ranges (> 1000 m) coalesced into ice sheets. At the Eocene-Oligocene boundary
1574 (C4.3, 34-33 Ma), temperatures plunged precipitously signalling the first major accumulation of ice
1575 on Antarctica. Permanent sea ice also formed around the periphery of Antarctica generating
1576 increasing amounts of cold bottom water. Icebergs coursed through the southern oceans and the
1577 first record of ice-rafted debris appeared in the deep-sea record. The global cooling also forced

1578 plants to adapt to the harsher winter conditions (Wolfe, 1971, 1978, 1992, 1994). Paleocceanographic
1579 events in the Southern Hemisphere, in particular the formation of the Circum-Antarctic Current,
1580 played a key role in the chronology of these events (Kennett, 1995).

1581 The Drake Passage is the seaway that flows between the southern tip of South America (Patagonia)
1582 and the northern tip of the West Antarctic Peninsula (Palmer Peninsula). In the early Mesozoic,
1583 these two regions were part of a continuous Andean mountain range. The ligation between
1584 Patagonia and the Palmer Peninsula was tested when Gondwana began to rift apart in the late
1585 Jurassic. Despite being stretched and extended as the Weddell Sea opened during the Cretaceous,
1586 Patagonia and the Palmer Peninsula were not completely separate until the late Eocene (~40 Ma).
1587 The best estimate for the age of the opening of the Drake Passage is 45 Ma (shallow water
1588 connection, <1000m) to 35 Ma (deep water connection, >1000 m) (Livermore *et al.*, 2005). An age
1589 of 41 Ma for the opening of the Drake Passage is based on the change in neodymium isotope ratios
1590 from sediments on the Agulhas Ridge that suggests an influx of shallow Pacific water (Scher and
1591 Martin, 2006).

1592 When the Southeast Indian Ocean between southern Australia and Antarctica (Wilkes Land) began
1593 to open in the Late Cretaceous, the eastern end of the rifted margin made a right-angle bend,
1594 hooking southward around Tasmania. This strike-slip boundary, the Tasman Fracture Zone,
1595 effectively closed off the eastern end of the Southeast Indian Ocean during the earliest phases of
1596 opening. When Australia began to move rapidly northward during the Late Eocene (40 Ma – 35 Ma),
1597 the overlapping bits of the Australian and Antarctic plates (South Tasman Rise and North Victoria
1598 Land, respectively) separated, allowing deep waters from the Indian Ocean and South Pacific Ocean
1599 to mix. The first deep water connection between the Indian Ocean and the South Pacific was
1600 through the Tasman Straits.

1601 Both the Drake Passage and the Tasman Gateway (Kennett *et al.*, 1974; Exon *et al.*, 2004; Kennett
1602 and Exon, 2004) were fully opened by the early Oligocene (34-30 Ma; Lawver and Gahagan, 2003).

1603 As a consequence, the Circum-Antarctic Current was able to isolate Antarctica from the world's
1604 oceans resulting in the "refrigeration" of Antarctica (C4.2, 34-28 Ma). The rapid growth of the
1605 Antarctic icecap during the Early Oligocene produced a major regression at the Rupelian/Chattian
1606 boundary (28.1 Ma). During the Oligocene, the massive Antarctic ice cap grew and shrank in fits and
1607 starts. These chaotic transitions are recorded in a dozen cooling and warming events (C4.1 and C4.2).
1608 Global temperatures remained cool until the end of the Oligocene when there was a slight warming
1609 (W4, 27-23 Ma). Though parts of West Antarctica were still forested during the Oligocene, mountain
1610 glaciers grew in the highlands of the Palmer Peninsula, reaching the ocean by the latest Oligocene. In
1611 the Northern Hemisphere there were local glaciers in Svalbard and central Greenland, but no
1612 permanent icecap.

1613 It is also worth noting that by the Early Oligocene, the collision between the Arabian peninsula and
1614 Iran was nearly complete. Though all the ocean floor had been subducted, a shallow seaway, the
1615 proto-Persian Gulf, filled the foredeep of the Zagros mountains of Iran and Iraq. During brief
1616 highstands of sea level during the late Oligocene and early Miocene, this shallow seaway connected
1617 with the deeper waters of the eastern Mediterranean. The closure of this westernmost extension of
1618 Tethys in the earliest Oligocene eliminated the westward flowing "Subtropical Eocene NeoTethys"
1619 (STENT) current. Some authors have speculated that this may have contributed to global cooling
1620 during the early Oligocene (Toggweiler et al. (2000), Hotinski and Toggweiler, 2003; Jovane et al.,
1621 2009).

1622 At the start of the Miocene, only Antarctica, straddling the South Pole, was covered by a permanent
1623 icecap. Cool conditions prevailed in the northern hemisphere as well, but there was no permanent
1624 ice. Global temperatures warmed in the middle Miocene (W3, 18 – 11 Ma), the Antarctic ice cap
1625 shrank and snow and ice disappeared from the northern hemisphere. By the end of the Miocene (~
1626 5 Ma), conditions had once again cooled (C2, 11 - 5.3Ma) and a permanent icecap had begun to form

1627 in the Arctic. The initiation of the Greenland ice sheet in the middle-late Miocene corresponds with
1628 the minimum sea level for the Miocene (~50 m; Miller et al., 2020).

1629 The growth of the Arctic icecap may have been triggered by two paleogeographic-
1630 paleoceanographic changes: 1) In the late Neogene (4-5 Ma), the Panama volcanic archipelago rose
1631 above sea level, creating the Panama land bridge. This land bridge connected North and South
1632 America, permitting the interchange of fauna and flora (Marshall *et al.*, 1982). More importantly,
1633 this land bridge served as a blockade, isolating the equatorial Atlantic and Pacific Oceans. Warm,
1634 equatorial Atlantic waters were diverted northward (the Gulf Stream). The warm waters of the Gulf
1635 Stream warmed the Arctic regions, but more importantly, provided a new source of moisture which
1636 fed winter snows. Increased snowfall led to the growth of glaciers and the Arctic ice sheets grew
1637 large. 2) In the eastern hemisphere, the northward movement of Australia during the early Miocene
1638 and the collision of Australia with Southeast Asia during the middle-late Miocene (~10-15 Ma)
1639 blocked equatorial circulation between the western Pacific Ocean and the Indian Ocean. As a
1640 consequence, the distance that ocean waters circulated along the Equator was shortened resulting
1641 in a net cooling of tropical surface waters. This reduction in the Earth's thermal budget, in turn, may
1642 have led to increased cooling at the poles.

1643 Global temperatures continued to plummet during the Pliocene. During the late Pliocene (~3.3 Ma),
1644 global temperatures warmed sufficiently to melt enough of the North and South polar icecaps so
1645 that sea level rose (~60 m), flooding the continental margins (W2.1, Pliocene Thermal Maximum).

1646 The Pleistocene Ice Age (C1) began in the latest Pliocene (2.7 Ma) and ended 11,700 years ago
1647 (Younger C1.1 Dryas). Driven by the tilt of the Earth (obliquity) and the shape of the Earth's orbit
1648 (eccentricity), the polar ice sheets waxed and waned causing global sea level to rise and fall (Miller et
1649 al., 2020). When ice sheets were at their maximum, sea level was ~100 meters lower than today.
1650 During the interglacial part of the cycle, when much of the polar ice caps had melted away, sea level
1651 was ~70 meters higher than today.

1652 Sea level has risen and fallen more than 50 times during the last 2 million years. This cycle of sea
1653 level change has been recorded in the changing ratio of the $^{18}\text{O}/^{16}\text{O}$ preserved in benthic/planktonic
1654 foraminifera (Lisiecki and Raymo, 2005). This fluctuating record begins nearly 2.7 million years ago;
1655 for the first ~ 2 million years, the cycle of icecap growth and retreat was modulated by the changing
1656 tilt of the Earth's axis (40,000 year obliquity cycle). Starting nearly one million years ago, the
1657 frequency of ice cap formation slowed from every 40,000 years to every 100,000 years, as the
1658 changing, eccentric shape of the Earth's orbit became the major forcing function. It should be noted
1659 that most of these marine isotopic sequences (MIS) match a similar cycle of changing CO_2
1660 concentration recorded in mile-long ice cores from Greenland and Antarctica (Barnola et al., 1987;
1661 Petit et al, 1999; Alley, 2000; EPICA Community Members, 2004; Jouzel et al, 2007).

1662 We are currently about halfway through a typical glacial/interglacial cycle. If humans did not inhabit
1663 the Earth, about 20,000 years from now, global temperatures would have once again begun to fall
1664 and ice sheets would have expanded into the oceans surrounding Antarctica and would have
1665 descended from the Arctic to begin a slow and steady march across the northern continents.
1666 However, this will not happen. The Earth has entered a "super-interglacial". The injection of CO_2
1667 into the atmosphere as a consequence of the burning of fossil fuels has warmed the Earth more than
1668 1°C and will continue to warm the Earth for another 300 years (~ 2300 CE). In the next section, we
1669 discuss how long anthropogenic global warming will continue and how warm the Earth will become.

1670

1671 5.10 Post-Anthropogenic Warming (W1) (2300 CE – 10,000 years in the future), Table 7, Figure 21

1672 It is well-established fact that burning fossil fuels releases CO_2 , a greenhouse gas, into the
1673 atmosphere, causing the Earth to warm faster than it would naturally (Archer, 2005; Archer et al.,
1674 2009a,b; Kidder and Worsley, 2012; Steffen et al., 2019). How warm will it get? How quickly will it
1675 warm to those new levels? In order to answer these questions, we need to know future trends in 1)
1676 global population (United Nations, 2019), 2) the average "energy footprint" per global resident

1677 (British Petroleum, 2019), 3) the future mix of energy sources (oil, gas, coal, hydroelectric, nuclear,
1678 and renewables; British Petroleum, 2019; Rogner, 2012; Shell,2018), 4) the rate at which the natural
1679 environment will absorb excess CO₂ emissions (Tans, 2009), and 5) the warming effect of
1680 greenhouse gases (climate sensitivity; Royer, 2016; Farnsworth et al., 2019). Though these
1681 parameters are not known with any certainty, we can nevertheless make an informed estimate of
1682 future trends and produce a reasoned prediction of the potential amount of global warming during
1683 the next 300 years (Scotese, 2020).

1684 We have estimated the amount of future global warming using a straightforward carbon budget
1685 model that predicts the changing amount of atmospheric CO₂. This CO₂ budget model is described in
1686 Table 8. Using these carbon budget equations, a dynamic model was constructed that predicts the
1687 amount of global warming during the next 300 years.

1688 Assuming that the Global Average Temperature (GAT) in 2000 was roughly 14.5°C (58° F), and the
1689 concentration of atmospheric CO₂ was 369 ppm. This model predicts that in 2200 the concentration
1690 of atmospheric CO₂ will be ~777 ppm, which is a little more than double the concentration of CO₂ in
1691 the year 2000 and the global temperature will rise about 5° C from 14.5°C (58°F) to 19.5°C (67° F).
1692 This change in temperature is indicated by the red star in Figure 21.

1693 As has been widely reported (Collins et al., 2013), most future warming takes place during the mid-
1694 to-late twenty-first century. Rapid global warming is nearly unavoidable because two key
1695 parameters - global population and energy use per capita - will rapidly rise during the next several
1696 decades.

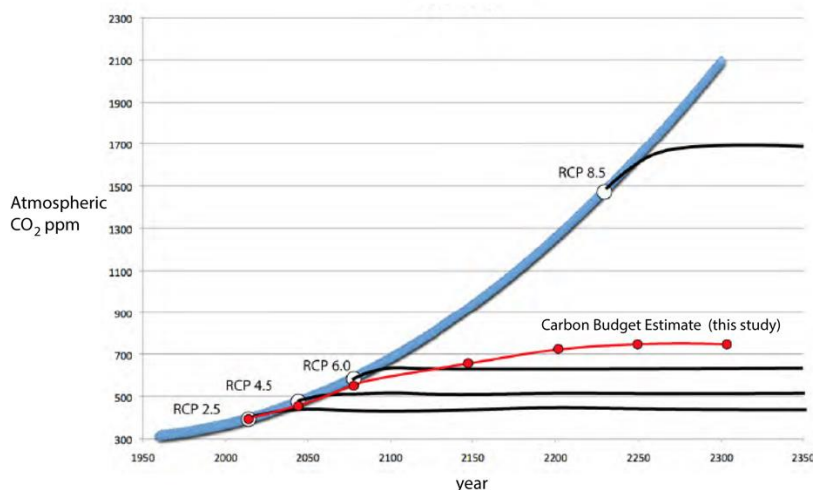


Figure 22. IPCC Estimates of Global Warming compared to the Results Predicted by the Carbon Budget Model (this study). The blue curve represents the projected increase in atmospheric CO₂ based on the continued burning of fossil fuels at the "modern rate" (1970 – 2020). The black curves are the CO₂ levels used in the IPCC models RCP 2.5, RCP 4.5, RCP 6.0, and RCP 8.5. The red curve is the projected CO₂ levels obtained in our model (between 750 ppm and 800 ppm at 2200 CE). Estimates from RCP 2.5 and RCP 4.5 are too low. The estimate of CO₂ used in RCP 8.5 is much too high. Estimates of CO₂ used in RCP 6.0 are about right.

1697

1698 According to the model, in the year 2100, global climate will have warmed beyond the 2°C limit
 1699 recommended by the Paris Accords (Figure 22). In 2200, after reaching a maximum temperature of
 1700 19.5°C, the global climate will begin to cool. This is due in part to natural processes, but most of the
 1701 modelled decrease in global temperature is the result of proposed human intervention (i.e. carbon
 1702 sequestration; Shell, 2018). If 10,000 carbon sequestration plants are built in the next 300 years, then
 1703 by 2300 the combined action of these carbon sequestration plants will have removed 1.8 trillion
 1704 gigatons of CO₂ from the atmosphere and the temperature will stabilize at 19.5°C (Shell, 2018). If no
 1705 carbon sequestration plants are built, then the projected future temperature will be closer to 20.5°C.
 1706 Both of these predictions are in line with IPCC estimates.

1707 What will the world be like after the Warming? This is the question that is probably the most on
 1708 people's minds. One can answer this question two ways. The first approach, taken by the
 1709 Intergovernmental Council on Climate Change (IPCC) and Burke et al. (2018), has been to run
 1710 hundreds of climate simulations that predict global climatic conditions using various global warming
 1711 scenarios (Figure 22). These results are very detailed and make explicit predictions (IPCC, 2007,
 1712 2018, 2019; Collins et al., 2013).

1713 Another way to understand our warmer future world is to compare the various possible warming
 1714 outcomes to the climates of the past. The area shaded in red on Figure 23 represents the
 1715 temperatures that lie within the range of the global warming predicted by the model presented here
 1716 (16.5°C – 19.5°C). You can see that this shaded region is much cooler than some of the hothouse
 1717 climates of the past. It is very good news that future global warming will likely not reach these
 1718 extreme hot house temperatures. Along the time-axis in Figure 23, several boxes highlight time
 1719 intervals in the deep past that had similar global climates. Of these, the Late Eocene – Miocene
 1720 Icehouse is probably the best analog to the climate we might experience after this period of Post-
 1721 Anthropogenic Warming (PAW).

1722

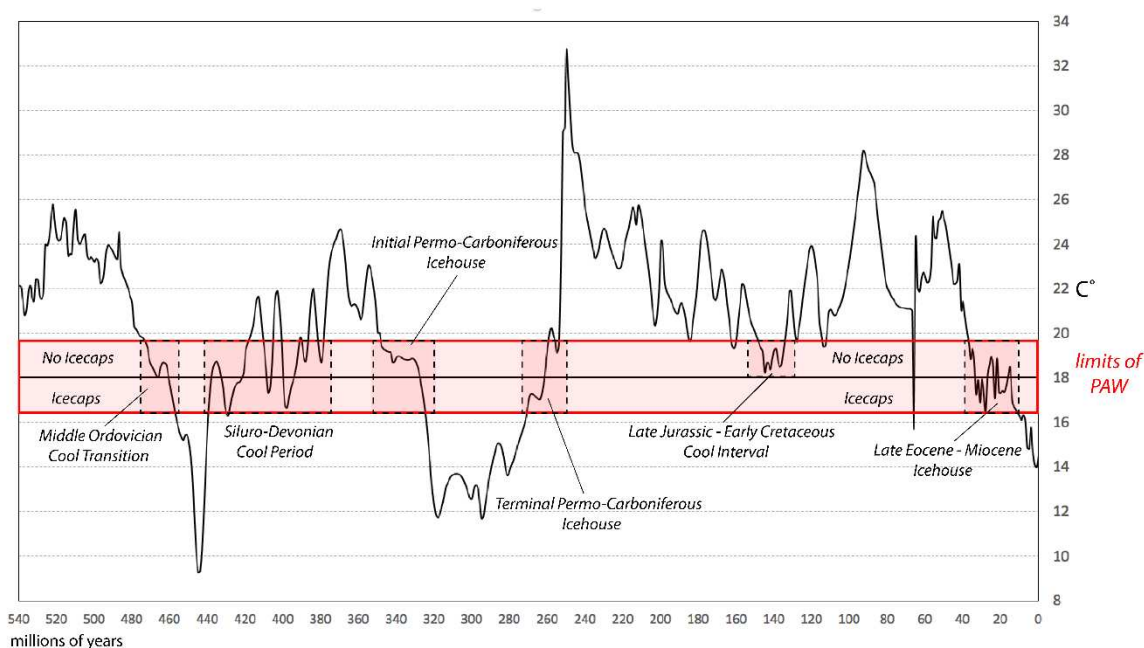


Figure 23. Projection of Future Global Warming onto Phanerozoic Temperature Time Scale. The likely amount of Post-Anthropogenic Warming (PAW) (red line). The boxes indicate times in the geological past when global temperatures were within the range of predicted PAW. When the Global Average Temperature is below 18°C large polar icecaps can form. When the Global Average Temperature is above 18°C large polar icecaps are unlikely to form.

1723

1724

1725 The geography of the early Oligocene world (30 million years ago) and the early Miocene world (15
 1726 Ma) resembled the modern world (Figure 24). The continents were essentially in the same places
 1727 and the oceans were about as wide as they are today. A large ice cap covered Antarctica, which was

1728 isolated from the other continents by the Circum-Antarctic Ocean. The northern hemisphere lacked
1729 any permanent ice cover, though snow covered the northernmost reaches of the continents during
1730 the winter.

1731 Unlike today's climate, the climate during the Oligocene and early Miocene was a little warmer near
1732 the Equator, and a diverse fauna thrived in tropical rain forests and in the oceans. Modern-sized
1733 desert belts separated the tropics from an expanded warm temperate belt that stretched across the
1734 northern hemisphere. The northern sub-polar regions, as well as Australia, were both wetter and
1735 warmer.

1736 These were worlds where land mammals thrived, diversified, and spread across the continents.
1737 Whales and enormous sharks ruled the seas. Plants also diversified. Grasslands covered the steppes
1738 and savannas and tropical and temperate forests provided a diverse set of habitats. All in all, the
1739 world was a reasonably nice place to live. Given enough time (5,000 -10,000 years; Archer, 2005;
1740 2009a,b), we might expect the same equable conditions to prevail after the Warming.

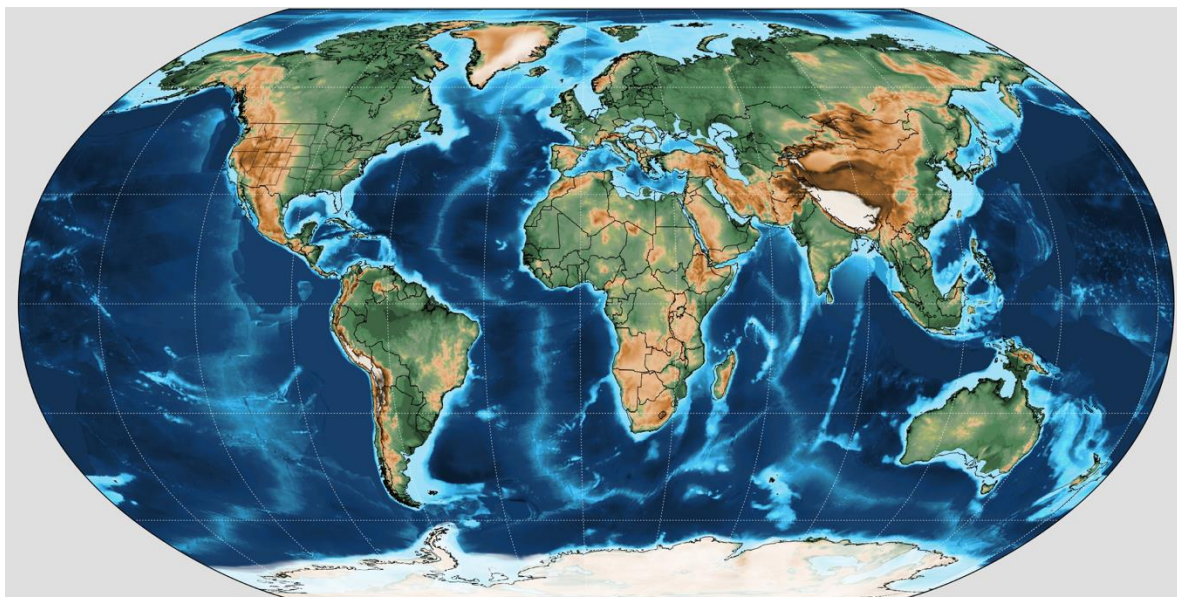
1741 The other five climatic "matches", though they had similar ranges of global temperature, had very
1742 different geographies. The climatic zones on a global Pangea would have been very different than
1743 the modern climatic belts.

1744 In conclusion, we are leaving our Ice Age heritage behind. A new, warmer world awaits us. The
1745 problem we face is not so much where we are headed, but rather how we will get there. The time
1746 for decisive action is quickly slipping away. Our stern challenge is to adapt to the rapid period of
1747 global warming that will take place during the next 100 years. To do this we must immediately take
1748 action to reduce our CO₂ emissions and take the steps needed to mitigate the undeniable damage
1749 that will be done to our environment, civilization, and society in the near future.

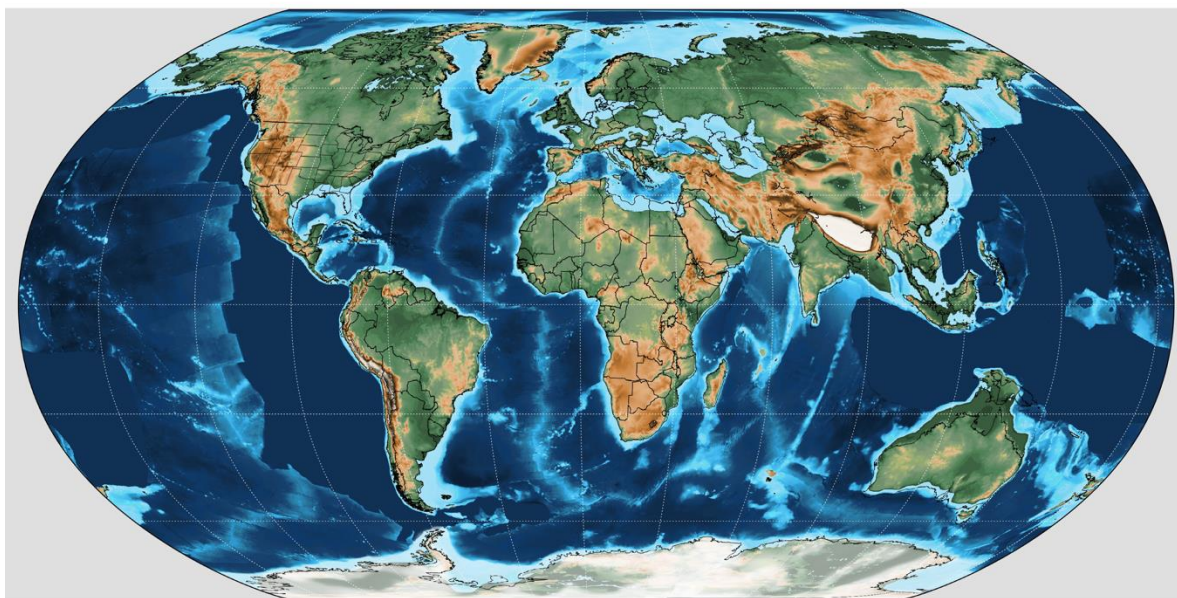
1750 **6. Summary and Conclusions**

1751 It has been long recognized that the Earth's climate, in particular the average global temperature,
1752 has alternated between "icehouse" and "hothouse" states. More than 70 years ago, Umbgrove
1753 (1947), and later Fischer (1981, 1982, 1984) recognized that these climatic "modes" varied on short-
1754 term, medium-term, and long-term timescales. During the past 20 years, beginning with the
1755 comprehensive pioneering work of Veizer et al. (1999) and followed by the insightful syntheses of
1756 Royer et al, (2004), Zachos et al. (2001, 2008), Grossman (2012 a,b), Boucot et al. (2013), Veizer and
1757 Prokoph (2015), O'Brien et al. (2017), Henkes et al. (2018), Valdes et al. (2018), and most recently
1758 Song et al. (2019), we now stand at the threshold to a deeper, more complete understanding of both
1759 the tempo and mode of global temperature change during the Phanerozoic.

1760 The goal of this essay has been to synthesize all of the available evidence for temperature change
1761 during the last 540 million years into a single, coherent, well-constrained global temperature curve
1762 (Figure 19-21, Table 3-7). Though the details may vary, there is good agreement between the
1763 temperature curve we present and earlier work (see Figure 1).



Middle Miocene Thermal Maximum (Langhian, 14.9 Ma)



Early Oligocene Cool Interval (Rupelian, 31 Ma)

Figure 24. Paleogeographic maps for the early Oligocene (30 Ma) and early Miocene (15 Ma). These past time periods are a good climatic match for world after Anthropogenic Warming.

1764

1765 We have produced this model of Phanerozoic temperatures by deconstructing temperature change

1766 into three components: 1) long-term (>50 million years) temperature changes, 2) medium-term (10

1767 – 20 million years), and 3) short-term temperature changes (a few million years or less).

1768 The Earth's long-term temperature change is controlled by multiple tectonic and environmental

1769 processes that drive the Earth's climate from icehouse to hothouse conditions, and vice versa. These

1770 changes can be described by mapping the changing Pole-to-Equator gradient revealed by
1771 paleogeographic distribution of lithologic indicators of climate such as: tillites, dropstones,
1772 glendonites, high latitude mangroves, palms, and crocodiles; temperate coal, evaporites, calcretes,
1773 tropical coals, bauxites, and laterites, (see Figures 4 and 5; Boucot et al., 2013). Long-term
1774 temperature changes occur due to changes in the Earth's "climatic equilibrium" which is controlled
1775 by the level of greenhouse gases in the atmosphere (principally CO₂), the geographic configuration of
1776 the continents and ocean basins (paleogeography and paleoceanography), the effectiveness of
1777 erosion and chemical weathering, and the reflectivity of the Earth's surface (albedo). Many of these
1778 factors are interconnected by a complex network of positive and negative feedback loops that can
1779 accelerate or decelerate changes in long-term global temperature (Hay, 2016; Ruddiman, 2001).
1780 Figure 13 illustrates our best estimate of the long-term temperature of the Earth during the past 540
1781 million years.

1782 Medium-term (10 – 20 million years) changes in the Earth's temperature are revealed by the record
1783 of isotopic temperatures measured in carbonate and phosphatic fossils. Recent global compilations
1784 of isotopic measurements of temperature (Grossman, 2012a&b, Veizer and Prokoph, 2015; Song et
1785 al., 2019; Grossman and Joachimski, 2020) have allowed us to generate a first-order model that
1786 describes the variation in tropical and polar temperatures for the last 540 million years (Figure 17).
1787 There are still numerous uncertainties regarding the interpretation of isotopic temperatures. For
1788 example, the isotopic composition of seawater can vary due to excess evaporation or the local influx
1789 of freshwater, as well as the removal of ¹⁶O from the oceans due to the growth of vast continental
1790 ice sheets. Also, the role that geographic and oceanographic variations play in δ¹⁸O variability has yet
1791 to be rigorously examined. Despite these caveats, we believe that the temperature record obtained
1792 from oxygen isotope data is robust and that a testable, first-order signal is generally recognizable
1793 (Figure 9).

1794 The causes of medium-term fluctuations in temperature are many and complex. We have not yet
1795 unravelled these forcing functions, but they are likely to include tectonic and geologic events such
1796 as: continental collisions and subsequent mountain building and unroofing, periods of ophiolite
1797 obduction and subsequent chemical weathering, the opening of oceanic gateways, and some mega-
1798 evolutionary events such as the evolution of land plants. One of the predictions made by our analysis
1799 of medium-term temperature changes is that there may have been several “mini-ice ages”,
1800 interspersed between the major glacial episodes (e.g. Hirnantian Ice Age, Late Paleozoic Icehouse,
1801 and Late Cenozoic Icehouse; Figure 16).

1802 Short-term changes in the Earth’s temperature are probably the most demonstrable because they
1803 are related to well-documented geologic events, namely the eruption of enormous volcanic
1804 provinces (LIPs) and the impact of large bolides. In this essay, we have documented that the
1805 eruption of ~20 large LIPs are strongly correlated with times of warmer global temperatures (Figure
1806 15 Tables 3-7). Conversely, it appears that large bolide impacts are well-correlated with cooler
1807 periods in Earth history (Figure 15, Tables 3-7), though a cause and effect relationship is less certain.
1808 It remains possible that a few of the most dramatic cooling events in Earth history may have been
1809 caused by as yet unrecognized large impact events (e.g. “Khione” event, Hirnantian Ice Age).

1810 In this essay, we combined the long-term, medium-term, and short-term changes in global
1811 temperature to produce the Phanerozoic Temperature Timescale (Figure 19-21, Tables 3-7). The
1812 Phanerozoic Temperature Timescale is divided into 24 “chronotemps”, or distinct warm and cool
1813 intervals. The youngest chronotemp (W1) is the current period of anthropogenic warming. The
1814 oldest postdates the Cryogenian “Snowball Earth”. Tables 3-7 list the names, timing, and
1815 temperatures associated with each chronotemp.

1816 It can certainly be argued that constructing a Phanerozoic Temperature Timescale is premature and
1817 an effort filled with error and unproven assumptions. Though this is probably true, we believe that
1818 the effort is worthwhile because we now have a structure that can be built upon, refined, corrected,

1819 expanded, and compared to other temperature models that use data sets that we did not use (i.e.,
1820 clumped isotopes, TEX₈₆). Moreover, having a paleotemperature timescale is essential if we are to
1821 understand the tempo and mode of climate change during the past 720+ million years. By
1822 characterizing, in a quantitative way, the pattern of paleotemperature change through time, we may
1823 be able to gain important insights into the history of the Earth System and the fundamental causes
1824 of climate change. These insights may be helpful guide as we traverse an uncertain path into the
1825 future.

1826

1827 7. Acknowledgements

1828 CRS would like to thank the past industrial sponsors of the PALEOMAP Project. H.S. is supported by
1829 the National Natural Science Foundation of China (41821001). B.J.W.M. is supported by the UK
1830 Natural Environment Research Council (NE/S009663/1). This work is part of the PhanTASTIC project
1831 led by Scott Wing and Brian Huber at the Smithsonian Institution National Museum of Natural
1832 History. The workshop was supported by a gift from Roland and Debra Sauermann. CRS especially
1833 benefitted from discussions of past climate with Dana Royer, Linda Ivany, Paul Valdes, Dan Lunt,
1834 Colin Summerhayes, Jan Veizer, and Ethan Grossman. CRS would like to thank Joseph Westrich,
1835 Colin Summerhayes, David Archer, Daniel Horton, and Peter Lange for their valuable scientific and
1836 critical input on the future global warming essay. Seth Stein and his class at Northwestern University
1837 (EPS 362) provided valuable feedback on my essay describing future global warming and convinced
1838 me to rewrite my initial essay as a do-it-yourself global warming calculator. Class members Peter
1839 Puleo, Tim Coston, and Chutian Chen provided especially helpful reviews. Special thanks to Phyllis
1840 Richmond for correcting grammar, clarifying prose, and corralling verbiage. This essay is dedicated
1841 to the life-long work and research of Larry Frakes.

1842

1843

1844 References Cited

- 1845 Ahlberg, A., Herman, A.B., Raikevich, M., Rees, A., and Spicer, R., 2002. Enigmatic Late Cretaceous
1846 high paleo-latitude limestones in Chukotka, northeasternmost Asia, *GFF*, v. 124, p. 197-199.
- 1847 Ahlberg, A., Olsson, I., Simkevicius, P., 2003. Triassic–Jurassic weathering and clay mineral dispersal
1848 in basement areas and sedimentary basins of southern Sweden. *Sedimentary Geology*, v. 161, p. 15–
1849 29.
- 1850 Alley, R.B., 2000. *The Two-Mile Time Machine*, Princeton University Press, Princeton, 229 pp.
- 1851 Alley, N.F., and Frakes, L.A., 2003. First known Cretaceous glaciation: Livingstone Tillite Member of
1852 the Cadna-owie formation, *Australian Journal of Earth Sciences*, v. 50, p. 139-144.
- 1853 Alsenz, H., Regnery, J., Ashckenazi-Polivoda, S., Meilijson, A., Ron-Yankovich, L., Abramovich, S.,
1854 Illner, P., Almogi-Labin, A., Feinstein, S., Berner, Z., Püttmann, W., 2013. Sea surface temperature
1855 record of a Late Cretaceous tropical southern Tethys upwelling system. *Palaeogeogr. Palaeoclimatol.*
1856 *Palaeoecol.* 392, 350–358.
- 1857 Alvarez, L.W., and Alvarez, W., Asaro, F., and Michel, H.V., 1980. Extraterrestrial cause for the
1858 Cretaceous-Tertiary extinction, *Science*, 208:1095-1107, doi: 10.1126/science.208.4448.1095
- 1859 Archer, D., 2005. Fate of fossil-fuel CO₂ in geologic time, *Journal of Geophysical Research, Oceans*,
1860 doi: 10.1029/2004JC002625.
- 1861 Archer, D., 2009. *The Long Thaw, How Humans Are Changing the Next 100,000 years of Earth's*
1862 *Climate*, Princeton University Press, Princeton, 180 pp.
- 1863 Archer, D., Eby, M., Brovkin, V., Ridgwell, A., Cao, I., Mikolajewicz, U., Caldiera, K., Matsumoto, K.,
1864 Munhoven, G., Montenegro, A., and Tokos, K., 2009. Atmospheric lifetime of fossil fuel carbon
1865 dioxide, *Annual Review of Earth and Planetary Sciences*, v. 37, pp. 117-134.
- 1866 Arthur, M.A., and Sageman, B.B., 1994. Marine black shales: Depositional mechanisms and
1867 environments of Ancient Deposits, *Annual Review of Earth and Planetary Sciences*, 22: 499-552.
- 1868 Azmy, K., Veizer, J., Bassett, M.G., Copper, P., 1998. Oxygen and carbon isotopic composition of
1869 Silurian brachiopods: Implications for coeval seawater and glaciations, *Geological Society of America*,
1870 v. 110, no. 11, p. 1499–1512.
- 1871 Balini, M., Lucas, S.G., Jenks, J.F, and Spielmann, J.A., 2010. Triassic ammonoid biostratigraphy: an
1872 overview, *Geological Society of London, Special Publications*, v.334:221–262.
- 1873 Bambach, R.K., Knoll, A.H., Wang, S.C., 2004. Origination, extinction, and mass depletions of marine
1874 diversity. *Paleobiology*, v. 30, p. 522–542.
- 1875 Barnola, J.M., Raynaud, D., Korotkevich, Y.S., and Lorius, C., 1987. Vostok ice core provides 160,000-
1876 year record of atmospheric CO₂, *Nature*, v. 329, p. 408-414
- 1877 Barral, A, Gomez, B., Legendre, S., Lécuyer, C., 2017. Evolution of the carbon isotope composition of
1878 atmospheric CO₂ throughout the Cretaceous. *Palaeogeography, Palaeoclimatology, Palaeoecology*,
1879 <http://dx.doi.org/10.1016/j.palaeo.2017.01.034>

- 1880 Barron, E.J. and Washington, W.M., 1982. Cretaceous climate: A comparison of atmospheric
1881 simulations with the geologic record, *Palaeogeography, Palaeoclimatology, and Palaeoecology*, v. 40,
1882 p. 103-133, doi: 10.1016/0031-0182(82)90086-4.
- 1883 Beerling, D.J., Berner, R.A., 2002. Biogeochemical constraints on the Triassic-Jurassic boundary
1884 carbon cycle event, *Global Biogeochemical Cycles*, v. 16, no. 3, p.1036, doi:10. 1029/2001GB001637
- 1885 Benedetto, J.L., and Sanchez, T.M., 1996. The "Afro-South American Realm" and Silurian "Clarkeia
1886 Fauna", in P. Copper and J. Jin (editors), *Brachiopods*, Balkema, p. 29-33.
- 1887 Benton M.J., 1993. Late Triassic extinctions and the origin of the dinosaurs, *Science*, v. 260, p. 769–
1888 770.
- 1889 Benton M.J., Zhang, Q., Hu, S., Chen, Z.Q., Wen, W., et al., 2013. Exceptional vertebrate biotas from
1890 the Triassic of China, and the expansion of marine ecosystems after the Permo-Triassic mass
1891 extinction. *Earth-Science Reviews*, v. 125, p. 199–243.
- 1892 Bergmann, K.D., Al Balushi, S.A.K., Macley, T., Grotzinger, J.P., and Eiler, J.M., 2018a. A 600-million
1893 year carbonate clumped-isotope record from the Sultanate of Oman, *Journal of Sedimentary
1894 Research*, v. 88, p. 960–979, doi:org/10.2110/jsr.2018.51.
- 1895 Bergmann, K.D., Finnegan, S., Creel, R., Eiler, J.M., Hughes, N.C., Popov, L.E., and Fischer, W.W., ,
1896 2018b. A paired apatite and calcite clumped isotope thermometry approach to estimating Cambro-
1897 Ordovician seawater temperatures and isotopic composition, *Geochimica et Cosmochimica Acta*, v.
1898 224, p.18-41, doi: 10.1016/j.gca.2017.11.015.
- 1899 Bernardi, M., Gianolla, P., Petti, F.M., Mietto, P., and Benton, M.J., 2018. Dinosaur diversification
1900 linked with the Carnian Pluvial Episode, *Nature Communications*, v. 9 :1499, doi: 10.1038/s41467-
1901 018-03996-1.
- 1902 Berner R. A., 1994. GEOCARB II: A revised model of atmospheric CO₂ over Phanerozoic time.
1903 *American Journal Science* 294(1):56–91.
- 1904 Berner, R.A., 2004. *The Phanerozoic Carbon Cycle: CO₂ and O₂*. Oxford University Press, New York.
- 1905 Berner, R.A., Lasaga, A.C., & Garrels, R.M. (1983). The carbonate silicate geochemical cycle and its
1906 effect on atmospheric carbon dioxide over the past 100 million years. *American Journal Science*, 283,
1907 641-683.
- 1908 Beuf, S., Biju-Duval, B., deCharpal, O., Rognon, P., Gariel, O., and Bennacef, A., 1971. Les Gres du
1909 Paleozoique inferieur au Sahara, Editions Technip, Paris, 464 pp
- 1910 Bice, K.L., and Norris, 2002, Possible atmospheric CO₂ extremes of the middle Cretaceous (late Albian
1911 to Turonian), *Paleoceanography*, 17:1-17.
- 1912 Black, B.A., and Gibson, S.A., 2019. Deep Carbon and the life cycle of Large Igneous Provinces,
1913 *Elements*, v. 15, p. 319-324.
- 1914 Bluth, G.J.D., & Kump, L.R., 1991. Phanerozoic paleogeology. *American Journal Science*, 291, 284-308
- 1915 Bohor, B.F., Triplehorn, D.M., Nichols, D.J., and Millard, H.T., Jr., 1987. Dinosaurs, spherules, and the
1916 "majic" layer: A new K-T boundary clay site in Wyoming, *Geology*, 15:896-899.

-
- 1917 Bond, D.P.G., and Grasby, S.E., 2017. On the causes of mass extinctions, *Palaeogeography,*
1918 *Palaeoclimatology, Palaeoecology*, v. 478, p. 3–29, doi.org/10.1016/j.palaeo.2016.11.005
- 1919 Bonis, N.R., Ruhl, M., Kurschner, W.M., 2010. Climate change driven black shale deposition during
1920 the end-Triassic in the western Tethys. *Palaeogeography, Palaeoclimatology, Palaeoecology*, v. 290,
1921 p. 151–159.
- 1922 Boucot, A.J., Chen Xu, and Scotese, C.R., 2013. *Phanerozoic Paleoclimate: An Atlas of Lithologic*
1923 *Indicators of Climate, SEPM Concepts in Sedimentology and Paleontology, (Print-on-Demand*
1924 *Version), No. 11, 478 pp., ISBN 978-1-56576-289-3, October 2013, Society for Sedimentary Geology,*
1925 *Tulsa, OK.*
- 1926 Boucot, A.J., 1990. Silurian biogeography, in W.S. McKerrow and C.R. Scotese (editors), *Palaeozoic*
1927 *Palaeogeography and Biogeography, Geological Society of London Memoir No. 12, p. 191-196.*
- 1928 Brady, E.C., DeConto, R., Thompson, S.L., 1998, Deepwater formation and poleward ocean heat
1929 transport in the warm climate extreme of the Cretaceous (80 Ma), *Geophysical Research Letters*, 25:
1930 4205-4208.
- 1931 Brand, U., Azmy, K., and Veizer, J., 2006. Evaluation of the Salinic I tectonic, Cancañiri glacial and
1932 Ireviken biotic events: Biochemostratigraphy of the Lower Silurian succession in the Niagara Gorge
1933 area, Canada and U.S.A., *Palaeogeography, Palaeoclimatology, Palaeoecology*, v. 241, p. 192–213,
1934 doi:10.1016/j.palaeo.2006.03.004
- 1935 Brass, G.W., Southam, J.R., Peterson, W.H., 1982. Warm Saline Bottom Water in the Ancient Ocean.
1936 *Nature* 296, 620-623.
- 1937 Brassell, S.C., 2009. Steryl ethers in a Valanginian claystone: molecular evidence for cooler waters in
1938 the central Pacific during the Early Cretaceous? *Palaeogeogr. Palaeoclimatol. Palaeoecol.* 282, 45–57.
- 1939 Brandley, R.T., and Krause, F.F., 1994. Thinolite-type pseudomorphs after ikait: indicators of cold
1940 water on the subequatorial western margin of Lower Carboniferous North America, *Canadian*
1941 *Society of Petroleum Geologists Memoir* 17, p. 333-334.
- 1942 Brenchley, P.J., Marshall, J.D., Carden, G.A.F., Robertson, D.B.R., Long, D.G., Meidla, T., Hints, L., and
1943 Anderson, T.F., 1994. Bathymetric and isotopic evidence for a short-lived Late Ordovician glaciation
1944 in a greenhouse period, *Geology*, v. 22, p. 295-298.
- 1945 Brett, C.E., Ivany, L.C., Bartholomew, A.J., Desantis, M.K., and Baird, G.C., 2009. Devonian ecological-
1946 evolutionary subunits in the Appalachian Basin: a revision and test of persistence and discreteness,
1947 in *Devonian Change: Case Studies in Palaeogeography and Palaeoecology*, P. Konigshof (editor),
1948 *Geological Society of London, Special Publication* v. 314, p. 7-36.
- 1949 British Petroleum (BP), 2019, “BP Energy Outlook, 2019”.
1950 [https://www.bp.com/content/dam/bp/business-sites/en/global/corporate/pdfs/energy-](https://www.bp.com/content/dam/bp/business-sites/en/global/corporate/pdfs/energy-economics/energy-outlook/bp-energy-outlook-2019.pdf)
1951 [economics/energy-outlook/bp-energy-outlook-2019.pdf](https://www.bp.com/content/dam/bp/business-sites/en/global/corporate/pdfs/energy-economics/energy-outlook/bp-energy-outlook-2019.pdf)
- 1952 Bruckschen, P., Oesmann, S., and Veizer, J., 1999. Isotope stratigraphy of the European
1953 Carboniferous: proxy signals for ocean chemistry, climate and tectonics, *Chemical Geology*, v. 161, p.
1954 127–163.

- 1955 Brune, S., Williams, S.E., Müller, R.D., 2017. Potential links between continental rifting, CO₂
1956 degassing and climate change through time,
- 1957 Buggisch, W., Joachimski, W.M., Sevastopulo, G., and Morrow, J.R., 2008. Mississippian $\delta^{13}\text{C}_{\text{carb}}$
1958 and conodont apatite $\delta^{18}\text{O}$ records - Their relation to the Late Palaeozoic Glaciation,
1959 Palaeogeography, Palaeoclimatology, Palaeoecology, v. 268, p. 273–292,
1960 doi:10.1016/j.palaeo.2008.03.043
- 1961 Burke, K.D., Williams, J.W. Chandler, M.A., Haywood, A.M., Lunt, D.J., and Otto-Bliesner, B.L., 2018.
1962 Pliocene and Eocene provide best analogs for near-future climates, Proceedings of the National
1963 Academy of Sciences, v. 115, no. 52, 13288-13293.
- 1964 Cantrill, D.J., and Poole, I., 2012. The Vegetation of Antarctica Through Geological Time, Cambridge
1965 University Press, Cambridge, England, 480 pp.
- 1966 Cao, W., Williams, S., Flament, N., Zahirovic, S., Scotese, C.R., and Müller, R.D., 2019. Paleolatitudinal
1967 distribution of lithologic indicators of climate in a paleogeographic framework, Geological Magazine,
1968 v. 156, no. 2, p. 331-354.
- 1969 Caputo, M.V., de Melo, J.H.G., StreeL, M., and Isbell, J.L., 2008. Late Devonian and Early
1970 Carboniferous glacial records of South America, in C.R. Fielding, T.D. Frank. and J.L. Isbell (editors),
1971 Resolving the Late Paleozoic Ice Age in Time and Space, Geological Society of America Special Paper
1972 v. 441, p. 161-174.
- 1973 Chamberlin, T.C., 1906. On a possible reversal of deep sea circulation and its influence on geologic
1974 climates, Proceedings of the American Philosophical Society, v. 45, n. 182, p. 33-43.
- 1975 Chatterjee, S., Guven, N., Yoshinobu, A., and Donofrio, R., 2006. Shiva structure: A possible KT
1976 boundary impact crater on the western shelf of India, Museum of Texas Tech University, Special
1977 Publication, 40 pp.
- 1978 Chen, B., Joachimski, M. M., Shen, S.-Z., Lambert, L. L., Lai, X.-L., Wang, X.-D., Chen, J., and Yuan, D.-
1979 X., 2013, Permian ice volume and palaeoclimate history: Oxygen isotope proxies revisited,
1980 Gondwana Research, v. 24, no. 1, p. 77-89.
- 1981 Chen, B., Joachimski, M. M., Wang, X.-D., Shen, S.-Z., Qi, Y.-P., and Qie, W.-K., 2016, Ice volume and
1982 paleoclimate history of the Late Paleozoic Ice Age from conodont apatite oxygen isotopes from
1983 Naqing (Guizhou, China), Palaeogeography, Palaeoclimatology, Palaeoecology, v. 448, p. 151-161.
- 1984 Chenet, A. L., Fluteau, F., Courtillot, V., Gerard, M., & Subbarao, K. V., 2008. Determination of rapid
1985 Deccan eruptions across the Cretaceous- Tertiary boundary using paleomagnetic secular variation:
1986 Results from a 1200-m-thick section in the Mahabaleshwar escarpment. Journal of Geophysical
1987 Research, 113, B04101. <https://doi.org/10.1029/2006JB004635>
- 1988 Clapham, M.E., and Renne, P.R., 2019. Flood Basalts and Mass Extinctions. Annual Review of Earth
1989 Planetary Sciences, v. 47, p. 275–303, doi: 10.1146/annurev-earth-053018-060136
- 1990 Clarkson, M.O., Kasemann, S.A., Wood, R.A., Lenton, T.M., Daines, S.J., et al., 2015. Ocean
1991 acidification and the Permo-Triassic mass extinction, Science, v. 348, p. 229–232,

- 1992 Cocks, L.R.M., 1972. The origin of the Silurian *Clarkeia* shelly fauna of South America, and its
1993 extension to West Africa, *Palaeontology*, v. 15, p.623-630.
- 1994 Cocks, L.R.M., and Fortey, R.A., 1990. Biogeography of Ordovician and Silurian faunas, in *Palaeozoic*
1995 *Palaeogeography and Biogeography*, W.S. McKerrow and C.R. Scotese (editors), Geological Society of
1996 London Memoir No. 12, p. 97-104.
- 1997 Colbath, G.K., 1986. Abrupt terminal Ordovician extinction in phytoplankton associations, southern
1998 Appalachians, *Geology*, v. 14, p. 943-946.
- 1999 Collins, M.R., R. Knutti, J. Arblaster, J.-L. Dufresne, T. Fichefet, P. Friedlingstein, X. Gao, W.J.
2000 Gutowski, T. Johns, G. Krinner, M. Shongwe, C. Tebaldi, A.J. Weaver, and M. Wehner, 2013: Long-
2001 term Climate Change: Projections, Commitments and Irreversibility. In *Climate Change 2013: The*
2002 *Physical Science Basis. Contribution of Working Group I to the Fifth Assessment Report of the*
2003 *Intergovernmental Panel on Climate Change* [Stocker, T.F., D. Qin, G.-K. Plattner, M. Tignor, S.K.
2004 Allen, J. Boschung, A. Nauels, Y. Xia, V. Bex, and P.M. Midgley (eds.)]. Cambridge University Press,
2005 Cambridge, United Kingdom and New York NY, USA.
- 2006 Courtillot, V., and Renne, X., 2003. On the ages of flood basalt events, *Comptes Rendus Geosciences*,
2007 v. 335, p. 113-140.
- 2008 Cramer, B.S., Toggweiler, J.R., Wright, J.D., Katz, M.E., and Miller, K.G., 2009. Ocean overturning since
2009 the Late Cretaceous: Inferences from a new benthic isotope compilation, *Paleoceanography* 6, v. 24,
2010 PA4216, p. 1-14, doi: 10.1029/2008PA001683.
- 2011 Crowley, T.J., 1994. Pangean Climates, in *Pangea: Paleoclimate, Tectonics, and Sedimentation*
2012 *during Accretion, Zenith, and Breakup of a Supercontinent*, (editor), G. D. Klein, Geological Society of
2013 America Special Paper 288, p. 25-39.
- 2014 Crowley, T.J., and Baum, S.K., 1991. Toward reconciliation of Late Ordovician (~440 Ma) glaciation
2015 with very high CO₂ Levels, *Journal of Geophysical Research*, v. 96, no. D12, p. 22,597-22,610.
- 2016 Crowley, T.J., and Baum, S.K., 1995. Reconciling Late Ordovician (440 Ma) glaciation with very high
2017 (14X) CO₂ Levels, *Journal of Geophysical Research*, v. 100, no. D1, p. 1093-1101.
- 2018 Dal Corso, J., Benton, M. J., Bernardi, M., Franz, M., Gianolla, P., Hohn, S., and Zhang, Y., 2018a. First
2019 Workshop on the Carnian Pluvial Episode (Late Triassic): a report, *Albertiana*, v. 44, p. 49-57.
- 2020 Dal Corso, J., Gianolla, P., Rigo, M., Franceschi, M., Roghi, G., Mietto, P., Manfrin, S., Raucsik, B.,
2021 Budai, T., Jenkyns, H.C., Reymond, C.E., Caggiati, M., Gattolini, G., Breda, A., Merico, A., Preto, N.,
2022 2018b. Multiple negative carbon-isotope excursions during the Carnian Pluvial Episode (Late
2023 Triassic), *Earth-Science Reviews*, v. 185, p. 732–750, doi:org/10.1016/j.earscirev.2018.07.004
- 2024 Davydov, V.I., and Cozar, P., 2017. The formation of the Alleghenian Isthmus triggered the Bashkirian
2025 glaciation: Constraints from warm-water benthic foraminifera, *Palaeogeography, Palaeoclimatology,*
2026 *Palaeoecology*, <http://dx.doi.org/10.1016/j.palaeo.2017.08.012>
- 2027 Davydov, V.I., 2014. Warm water benthic foraminifera document the Pennsylvanian–Permian
2028 warming and cooling events — The record from the Western Pangea tropical shelves,
2029 *Palaeogeography, Palaeoclimatology, Palaeoecology*, v. 414, p. 284-295,
2030 doi.org/10.1016/j.palaeo.2014.09.013

- 2031 Davydov, V.I., Korn, D., Schmitz, M.D., 2010. The Carboniferous Period, Chapter 23, in The Geologic
2032 Time Scale 2012, volume 2, F.M. Gradstein, J.G. Ogg, M.D. Schmitz, and G.M. Ogg (editors), Elsevier,
2033 Amsterdam, p. 603-651.
- 2034 De Lurio, J.L. and Frakes, L.A., 1999. Glendonites as a paleoenvironmental tool: Implications for early
2035 Cretaceous high latitude climates in Australia, *Geochimica et Cosmochimica Acta*, Vol. 63, No. 7/8,
2036 pp.
- 2037 Demaison, G.J., and Moore, G.T., 1980. Anoxic environments and oil source bed genesis, *American*
2038 *Association of Petroleum Geologists Bulletin*, 64:1179-1209.
- 2039 Dera, G., Brigaud, B., Monna, F., Laffont, R., Pucéat, E., Deconinck, J.-F., Pellenard, P., Joachimski,
2040 M.M., and Durllet, C., 2011. Climatic ups and downs in a disturbed Jurassic world, *Geology*, v. 39, no.
2041 3., p. 215-218, doi: 10.1130/G31579.1
- 2042 Dettmann, M.E., 1989. Antarctica: Cretaceous cradle of austral temperate rainforests?, in *Origins*
2043 *and Evolution of the Antarctic Biota*, Geological Society of London Special Publication, J.A. Crame
2044 (editor), v. 47, p. 89-105.
- 2045 Díaz-Martínez, E., and Grahn, I., 2007. Early Silurian glaciation along the western margin of
2046 Gondwana (Peru, Bolivia and northern Argentina): Palaeogeographic and geodynamic setting.
2047 *Palaeogeography, Palaeoclimatology, Palaeoecology*, v. 245, p. 62–81,
2048 doi:10.1016/j.palaeo.2006.02.018
- 2049 Duncan, R.A., and Huard, J., 1997. Trace metal anomalies and global anoxia: the OJP-Selli
2050 hydrothermal plume connection, *EOS Transactions American Geophysical Union*, 78, F774.
- 2051 Elliot, D.H., Fleming, T.H., Kyle, P.R., and Foland, K.A., 1999. Long-distance transport of magmas in the
2052 Jurassic Ferrar large igneous province, Antarctica, *Earth and Planetary Science Letters*, v. 167, p. 89-
2053 104.
- 2054 Elrick, M., and Scott, L. A., 2010, Carbon and oxygen isotope evidence for high-frequency (10^4 – 10^5 yr)
2055 and My-scale glacio-eustasy in Middle Pennsylvanian cyclic carbonates (Gray Mesa Formation),
2056 central New Mexico, *Palaeogeography, Palaeoclimatology, Palaeoecology*, v. 285, no. 3, p. 307-320.
- 2057 Emiliani, C. 1954. Temperatures of Pacific bottom waters and polar superficial waters during the
2058 Tertiary, *Science*, v. 119, issue 3103, p. 853-855, doi: 10.1126/science.119.3103.853
- 2059 Emiliani, C., 1955. Pleistocene temperatures, *Journal of Geology*, v. 63, no. 6, p. 538-578.
- 2060 EPICA Community Members, 2004. Eight glacial cycles from an Antarctic ice core, *Nature* 429: 623-
2061 628.
- 2062 Epstein, S. and Mayeda, T., 1953. Variation of O18 content of waters from natural sources,
2063 *Geochemica et Cosmochemica Acta*. 4 (5), 213-224.
- 2064 Erba, E., Bartolini, A., and Larson, R.L., 2004. Valanginian Weissert oceanic anoxic event, *Geology*
2065 32(2):149-152, doi 10.1130/G20008.1
- 2066 Erba, E., Duncan, R.A., Bottini, C., Tiraboschi, D., Weissert, H., Jenkyns, H.C., and Malinverno, A.,
2067 2015, Environmental consequences of Ontong Java Plateau and Kerguelen Plateau volcanism, in
2068 Neal, C.R., Sager, W.W, Sano, T., and Erba, E., eds., *The Origin, Evolution, and Environmental Impact*
2069 *of Oceanic Large Igneous Provinces: Geological Society of America Special Paper 511*, p. 271–303,
2070 doi:10.1130/2015.2511(15).

-
- 2071 Ernst, R.E., 2014. Large Igneous Provinces, Cambridge University Press, Cambridge, UK, 653 pp.
- 2072 Ernst, R.E., and Youbi, N., 2017. How Large Igneous Provinces affect global climate, sometimes cause
2073 mass extinctions, and represent natural markers in the geological record, *Palaeogeography,*
2074 *Palaeoclimatology, Palaeoecology*, v. 478, p. 30–52., doi:10.1016/j.palaeo.2017.03.014
- 2075 Erwin, D.H., 1993. *The Great Paleozoic Crisis: Life and Death in the Permian*, Columbia University
2076 Press, New York, 327 pp.
- 2077 Erwin, D.H., 1995. The End-Permian Mass Extinction, in *The Permian of the Northern Hemisphere*,
2078 volume 1: Paleogeography, Paleoclimates, Stratigraphy, P.A. Scholle, T.M. Peryt, D.S Ulmer-Scholle
2079 (editors), Springer-Verlag, Berlin, p. 3-19.
- 2080 Erwin, D.H., 2006. *Extinction: How Life on Earth Nearly Ended 250 Million Years Ago*, Princeton
2081 University Press, Princeton, 296 pp.
- 2082 Exon, N.F., Kennett, J.P., and Malone, M., 2004. *The Cenozoic Southern Ocean: Tectonics,*
2083 *Sedimentation, and Climate Change between Australia and Antarctica*, American Geophysical Union,
2084 Geophys. Monograph 151.
- 2085 Farnsworth, A., Lunt, D.J., O'Brien, C., Foster, G.L., Inglis, G.N., Markwick, P., Pancost, R.D., and
2086 Robinson, S.A., 2019. Climate sensitivity on geological timescales controlled by non-linear feedbacks
2087 and ocean circulation, *Geophysical Research Letters*.
- 2088 Fielding, C.R., Frank, T.D., Isbell, J.L., Henry, L.C., and Domack, E.W., 2010. Stratigraphic signature of
2089 the late Palaeozoic Ice Age in the Parmeener Supergroup of Tasmania, SE Australia, and inter-
2090 regional comparisons , *Palaeogeography, Palaeoclimatology, Palaeoecology*, v. 298, p. 70–90,
2091 doi:10.1016/j.palaeo.2010.05.023
- 2092 Fielding, C.R., Frank, T.D., Birgenheier, L.P., Rygel, M.C., Jones, A.T., and Roberts, J., 2008.
2093 Stratigraphic imprint of the Late Palaeozoic Ice Age in eastern Australia: a record of alternating
2094 glacial and nonglacial climate regime, *Journal of the Geological Society, London*, v. 165, p. 129–140.
- 2095 Fielding, C.R., Frank, T.D., Birgenheier, L.P., Rygel, M.C., Jones, A.T., and Roberts, J., 2008.
2096 Stratigraphic record and facies associations of the Late Paleozoic ice age in eastern Australia (New
2097 South Wales and Queensland), in C.R. Fielding, T.D. Frank. and J.L. Isbell (editors), *Resolving the Late*
2098 *Paleozoic Ice Age in Time and Space*, Geological Society of America Special Paper v. 441, p. 41-58.
- 2099 Finnegan, S., Bergmann, K., Eiler, J.M., Jones, D. S., Fike, D. A., Eisenman, I., Hughes, N. C., Tripathi, A.
2100 K., and Fischer, W. W., 2011. The magnitude and duration of Late Ordovician – Early Silurian
2101 Glaciation, *Science*, v. 331, no. 6019, p. 903-906, doi: 10.1126/science.12000803.
- 2102 Finnegan, S., Heim, N.A., Peters, S.E., Fischer, and Fischer, W.W., 2012. Climate change and selective
2103 signature of the Late Ordovician mass extinction, *Proceedings of the National Academy of Sciences*,
2104 v.109, no. 18, p. 6829-6834.
- 2105 Fischer, A. G., 1981. Climatic oscillations in the biosphere, in M.H. Nitecki (editor), *Biotic Crises in*
2106 *Ecological and Evolutionary Time*, Academic Press, pp. 103-131.
- 2107 Fischer, A. G., 1982. Long-term Climatic Oscillations Recorded in Stratigraphy, in *Studies in*
2108 *Geophysics: Climate in Earth History*, W.H. Berger and J.C. Crowell (editors), Chapter 9., National
2109 Academy Press, Washington, D.C., pp. 97-104.

-
- 2110 Fischer, A. G., 1984. The Two Phanerozoic Supercycles, in *Catastrophes and Earth History: The New*
2111 *Uniformitarianism*, W.A. Berggren and J.A. Van Couvering, (editors), Chapter 7, Princeton University
2112 Press, Princeton, N.J., pp. 129 – 150.
- 2113 Flügel, E., 1994. Pangean shelf carbonates: Controls and paleoclimatic significance of Permian and
2114 Triassic reefs, in *Pangea: Paleoclimate, Tectonics, and Sedimentation during the Accretion, Zenith,*
2115 *and Breakup of a Supercontinent*, George D. Klein (ed.), Geol. Soc. America Special Paper, 288: 247-
2116 266.
- 2117 Flügel, E., 2002. Triassic reef patterns, In Kiessling, W., Flügel,, E. & Golonka, J. (eds): *Phanerozoic*
2118 *Reef Patterns*. SEPM (Society for Sedimentary Geology) Special Publications 72, 391-464.
- 2119 Flügel,, E. & Kiessling, W., 2002. Patterns of Phanerozoic reef crises. In Kiessling, W., Flügel,, E. &
2120 Golonka, J. (eds): *Phanerozoic Reef Patterns*. SEPM (Society for Sedimentary Geology) Special
2121 Publications 72, 691-733.
- 2122 Foster, G.L., Royer, D.L., and Lunt, D.J., 2017. Future Climate Forcing Potentially without precedent in
2123 the last 420 million years, *Nature Communications*, v. 8, 14845, doi:10.1038/ncomms14845.
- 2124 Fraenkel, G., 1960. Lethal High Temperatures for Three Marine Invertebrates: *Limulus Polyphemus*,
2125 *Littorina littorea* and *Pagurus longicarpus*, *Oikos*, v. 11 fasc. 2, p. 171-182.
- 2126 Frakes, L.A., 1989. *Climates Through Geologic Time*, Elsevier, Amsterdam, 310 pp.
- 2127 Frakes, L., and Francis, J.E., 1988. A guide to Phanerozoic cold polar climates from high latitude ice-
2128 rafting in the Cretaceous. *Nature* 333, 547–549.
- 2129 Frakes L. A. and Francis J. E., 1990. Cretaceous palaeoclimates. In *Cretaceous Resources, Events, and*
2130 *Rhythms* (ed. R. N. Ginsburg and B. Beaudoin), pp. 373–287. Kluwer Academic Publishers.
- 2131 Frakes, L.A., Francis, J.E., and Syktus, J.I., 1992. *Climate Modes of the Phanerozoic*, Cambridge
2132 University Press, Cambridge, 274 pp. Freeman and Hayes
- 2133 Francis J. E. and Frakes L. A., 1993. Cretaceous climates. *Sediment. Rev.* **1**, 17–30.
- 2134 Frakes, L.A., Alley, N.F., and Deynoux, M., 1995. Early Cretaceous ice rafting and climate zonation in
2135 Australia, *International Geology Review*, v. 37, p. 567-583.
- 2136 Frank, T.D., Schultis, A.I., Fielding, C.R., 2015. Acme and demise of the late Palaeozoic ice age: A
2137 view from the southeastern margin of Gondwana, *Palaeogeography, Palaeoclimatology,*
2138 *Palaeoecology*, v. 418, p. 176–192, doi.org/10.1016/j.palaeo.2014.11.016
- 2139 Friedman, M., Sallan, L.C., 2012. Five hundred million years of extinction and recovery: a
2140 Phanerozoic survey of large-scale diversity patterns in fishes, *Palaeontology*, v. 55, p. 707–742.
- 2141 Galili, N., Shemesh, A., Yam, R., Brailovsky, I., Sela-Adler, M., Schuster, E.M., Collom, C., Bekker, A.,
2142 Planavsky, N., Macdonald, F.A., Pr eat, A., Rudmin, M., Trela, W., Stuesson, U., Heikoop, J.M., Aurell,
2143 M., Ramajo, J., and Halevy, I., 2019. The geologic history of seawater oxygen isotopes from marine
2144 iron oxides, *Science*, v. 365, p. 469–473.

- 2145 Gasson, E.G.W., and Kiessling, B.A., 2020. The Antarctic Ice Sheet, A Paleoclimate Modeling
2146 Perspective, *Oceanography*, June 2020 Online Release, pp. 11, doi.org/10.5670/oceanog.2020.208
- 2147 Gersonde, R. Kyte, F.T., Bleil, U., Diekmann, J.A., Flores, J.A., Gohl, K., Grahl, G., Hagen, R., Kuhn, G.,
2148 Sierro, F.J., Volker, D., and Bostwick, J.A., 1997. Geological record and reconstruction of the late
2149 Pliocene impact of the Eltanin asteroid in the Southern Ocean, *Nature*, 390: 357-363.
- 2150 Gibbs, M.T., Bluth, G.J.S., Fawcett, P.J., & Kump, L.R., 1999. Global chemical erosion over the last 250
2151 My: variations due to changes in paleogeography, paleoclimate, and paleogeology. *American Journal*
2152 *Science*, 299, 611–651.
- 2153 Girard, C., Klapper, G., and Feist, R., 2005. Subdivision of the terminal Frasnian linguiformis conodont
2154 Zone, revision of the correlative interval of Montagne Noire Zone 13, and discussion of
2155 stratigraphically significant Associated trilobites, in *Understanding Late Devonian and Permian-*
2156 *Triassic Biotic and Climatic Events; Towards an Integrated Approach*, D.J. Over, J.R. Morrow, and P.B.
2157 Wignall (editors), *Developments in Palaeontology & Stratigraphy*, v. 20, p. 181-198, Elsevier,
2158 Amsterdam.
- 2159 Godd ris, Y., Donnadi u, Y., Lefebvre, V., Le Hir, G., & Nardin, E., 2012. Tectonic control of
2160 continental weathering, atmospheric CO₂, and climate over Phanerozoic times: *Comptes Rendus*
2161 *Geoscience*, 344, 652–662.
- 2162 Godd ris, Y., Donnadi u, Y., Le Hir, G., Lefebvre, V., & Nardin, E., 2014. The role of palaeogeography
2163 in the Phanerozoic history of atmospheric CO₂ and climate. *Earth-Science Reviews*, 128, 122–138.
- 2164 Gough, D.O., 1981. Solar interior structure and luminosity variation, *Solar Physics*, v. 74, p. 21-34.
- 2165 Gradstein, F.M., Ogg, J.G., Schmitz, M.D., and Ogg, G.M., 2012. *The Geologic Time Scale 2012*, v. 1,
2166 Elsevier, 435 pp.
- 2167 Grahn, Y., Caputo, M.V., 1992. Early Silurian glaciations in Brazil Palaeogeography,
2168 Palaeoclimatology, Palaeoecology, v. 99, p. 9–15.
- 2169 Grahn, Y., Guti rrez, P., 2001. Silurian and Middle Devonian chitinozoa from the Zapla and Santa
2170 B rbara Ranges, Tarija Basin, northwestern Argentina. *Ameghiniana*, v. 38, p. 35–50.
- 2171 Grasby, S.E., McCune, G.E., Beauchamp, B., Galloway, J.M., 2017. Lower Cretaceous cold snaps led to
2172 widespread glendonite occurrences in the Sverdrup Basin, Canadian High Arctic. *Geol. Soc. Am. Bull.*
2173 129, 771–787. <http://dx.doi.org/10.1130/B31600.1>.
- 2174 Grice, K., Cao, C., Love, G.D., B ttcher, M.E., Twitchett, R.J., et al., 2005. Photic zone euxinia during
2175 the Permian- Triassic superanoxic event, *Science* v. 307, p. 706–709.
- 2176 Greene, A.R., Scoates, J.S., and Weis, D., 2008. Wrangellia flood basalts in Alaska: A record of plume-
2177 lithosphere interaction in a Late Triassic accreted oceanic plateau. *Geochemistry Geophysics*
2178 *Geosystems*, v. 9, Q12004, doi: 10.1029/2008GC002092.
- 2179 Greene, A.R., Scoates, J.S., Weis, D., and Israel, S., 2009a. Geochemistry of flood basalts from the
2180 Yukon (Canada) segment of the accreted Wrangellia oceanic plateau. *Lithos*, v. 110, p. 1–19, doi:
2181 10.1016/j.lithos.2008.11.010.

- 2182 Greene, A.R., Scoates, J.S., Weis, D., Nixon, G.T., and Kieffer, B., 2009b. Melting history and
2183 magmatic evolution of basalts and picrites from the accreted Wrangellia oceanic plateau, Vancouver
2184 Island, Canada: *Journal of Petrology*, v. 50, p. 467–505, doi: 10.1093/petrology/egp008.
- 2185 Greene, A.R., Scoates, J.S., Weis, D., Katvala, E.C., Israel, S., and Nixon, G.T. 2010. The architecture of
2186 oceanic plateaus revealed by the volcanic stratigraphy of the accreted Wrangellia oceanic plateau,
2187 *Geosphere*, v. 6, p. 47–73.
- 2188 Grossman, E. L., 1994. The carbon and oxygen isotope record during the evolution of Pangea
2189 Carboniferous to Triassic, in Klein, G. D., ed., *Pangea: Paleoclimate, Tectonics, and Sedimentation*
2190 *During Accretion, Zenith, and Breakup of a Supercontinent*: Boulder, Colorado, Geological Society of
2191 America Special Paper 288, p. 207-228.
- 2192 Grossman, E.L., 2012a. Oxygen Isotope Stratigraphy, in *The Geologic Time Scale 2012*, F. M.
2193 Gradstein, J.G. Ogg, M.D. Schmitz, and G.M. Ogg (editors), Elsevier, Amsterdam, volume 1, p. 181-
2194 206.
- 2195 Grossman, E.L., 2012b. Applying Oxygen Isotope Paleothermometry in Deep Time, in *Reconstructing*
2196 *Earth's Deep-Time Climate: State of the Art in 2012*, L. Ivany and B. Huber (editors), Paleontological
2197 Society Short Course, November 3, 2012, *The Paleontological Society Papers*, v. 18, pp. 39-67.
- 2198 Grossman, E.L., and Joachimski, M.M., 2020. Oxygen Isotope Stratigraphy, Chapter 10, in *The*
2199 *Geologic Time Scale 2020*, F. M. Gradstein, J.G. Ogg, M.D. Schmitz, and G.M. Ogg (editors), Elsevier,
2200 Amsterdam, volume 1, (in press).
- 2201 Grossman, E.L., Joachimski, M.M., Barney, B., Henkes, G.A., Ivany, L.C., Lunt, D.L., MacLeod, K.G.,
2202 Montañez, I.P., Scotese, C., and Wing, S.L., 2018. Toward a Phanerozoic History of Earth's Surface
2203 Temperature: The Oxygen Isotope Record of the Paleozoic to Early Cretaceous Time Slice (PaleCTS),
2204 (abstract), American Geophysical Union, Monday, December 10, 2018, Convention Center, Hall A-C
2205 (Poster Hall), Fall Meeting 2018, #PP11F-11319, Washington, D.C.
- 2206 Grossman, E.L., Yancey, T.E., Jones, T.E., Bruckschen, P., Chuvashov, B., Mazullo, S.J., and Mii,
2207 Horng-sheng, 2008. Glaciation, aridification, and carbon sequestration in the Permo-Carboniferous:
2208 The isotopic record from low latitudes, *Palaeogeography, Palaeoclimatology, Palaeoecology*, v. 268,
2209 p. 222–233, doi:10.1016/j.palaeo.2008.03.053
- 2210 Gruszczynski, M., Halas S., Hoffman, A., and Malkowski, K., 1989. A brachiopod calcite record of the
2211 oceanic carbon and oxygen isotope shifts at the Permian/Triassic transition. *Nature*, v. 337, p. 64-68.
- 2212 Gutjahr, M., Ridgwell, A., Sexton, P.F., anagnostou, E., Pearson, P.N., Pälike, H., Norris, R.D.,
2213 Thomas, E., and Foster, G.L., 2017. Very large release of mostly volcanic carbon during the
2214 Paleocene-Eocene Thermal Maximum, *Nature*, v. 548, p. 573-577.
- 2215 Haig, D.W., McCartain, E., Mory, A.J., Borges, G., Davydov, V.I., Dixon, M., Ernst, A., Groflin, S.,
2216 Håkansson, E., Keep, M., Dos Santos, Z., Shi, G.R., and Soares, J., 2014. Postglacial Early Permian (late
2217 Sakmarian–early Artinskian) shallow-marine carbonate deposition along a 2000 km transect from
2218 Timor to west Australia, *Palaeogeography, Palaeoclimatology, Palaeoecology*, v. 409, p. 180–204,
2219 doi.org/10.1016/j.palaeo.2014.05.009
- 2220 Hallam, A., 2002. How catastrophic was the end-Triassic mass extinction? *Lethaia*, v.35, p.147-157,
2221 doi: org/10.1111/j.1502-3931.2002.tb00075.x

-
- 2222 Hames, W., McHone, J.G., Renne, P., and Ruppel, C., 2003. The Central Atlantic Magmatic Province:
2223 Insights from Fragments of Pangea, American Geophysical Union, Geophys. Monogr. Ser., vol. 136,
2224 267 pp.
- 2225 Hammer, W.R., and Hickerson, W.J., 1996. Implications of an early Jurassic vertebrate fauna from
2226 Antarctica, in M. Morales (editor), The Continental Jurassic, Transactions of the Continental Jurassic
2227 Symposium, October 21-23, 1996, Museum of Northern Arizona, Flagstaff, Arizona, Museum of
2228 Northern Arizona Bulletin, v. 60, p. 215-218.
- 2229 Haq, B. U., & Schutter, S. R., 2009. A chronology of Paleozoic sea-level changes. *Science*, 322, 64-68.
- 2230 Haq, B. U., Hardenbol, J., & Vail, P. R., 1987. Chronology of fluctuating sea levels since the Triassic.
2231 *Science*, 235, 1156-1167.
- 2232 Hautmann, M., 2004. Effect of end-Triassic CO₂ maximum on carbonate sedimentation and marine
2233 mass extinction. *Facies* 50: 257–261.
- 2234 Hautmann, M., Benton, M.J., and Tomašových, A., 2008. Catastrophic ocean acidification at the
2235 Triassic-Jurassic boundary. *Neues Jahrb. Geologie Paläontologie*, v. 249, p.119–127.
- 2236 Hay, W.W., 2008. Evolving ideas about the Cretaceous climate and ocean circulation, *Cretaceous*
2237 *Research*, 29: 725-753.
- 2238 Hay, W.W., 2016. *Experimenting on a Small Planet: A History of Scientific Discoveries, a Future of*
2239 *Climate Change and Global Warming*, Springer, Switzerland, 819 pp.
- 2240 Hayes, P.A., Francis, J.E., Cantrill, D.J., and Crame, J.A., 2006. Palaeoclimate analysis of Late Cretaceous
2241 angiosperm leaf floras, James Ross Island, Antarctica, in *Cretaceous-Tertiary High-Latitude*
2242 *Palaeoenvironments, James Ross Basin, Antarctica*, J.E., Francis, D. Pirrie, and J.A. Crame, (editors),
2243 *Geol. Soc. London Special Publications* 258:49-62.
- 2244 Hays, P. D., and Grossman, E. L., 1991, Oxygen isotopes in meteoric calcite cements as indicators of
2245 continental paleoclimate, *Geology*, v. 19, no. 5, p. 441-444.
- 2246 Hearing, T.W., Harvey, T.H.P., Williams, M., Leng, M.J., Lamb, A.L., Wilby, P.R., Gabbott, S.E., Pohl, A.,
2247 and Donnadieu, Y., 2018. An early Cambrian greenhouse climate, *Science Advances*, 4:eaar5690 9.
- 2248 Heckel, P.H., 1994. Evaluation of evidence for glacio-eustatic control over marine Pennsylvanian
2249 cyclothem in North America and consideration of possible tectonic effects in J.M. Dennison and
2250 F.R. Etnesoohn (editors), *Tectonic and Eustatic Controls on Sedimentary Cycles*, SEPM Concepts in
2251 *Sedimentology and Paleontology*, v4, p. 65-87.
- 2252 Heckel, P.H., 2008. Pennsylvanian cyclothem in Midcontinent North America as far-field effects of
2253 waxing and waning of Gondwana ice sheets, in C.R. Fielding, T.D. Frank, and J.L. Isbell (editors),
2254 *Resolving the Late Paleozoic Ice Age in Time and Space*, Geological Society of America, Special Paper
2255 441, p. 275-289.
- 2256 Heckel, P.H., 2013. Pennsylvanian stratigraphy of Northern Midcontinent Shelf and biostratigraphic
2257 correlation of cyclothem, *Stratigraphy*, v. 10, no. 1–2, pp. 3–39.

- 2258 Henderson, C.M., Davydov, V.I., Wardlaw, B.R., 2012. The Permian Period, Chapter 24, in The
2259 Geologic Time Scale 2012, volume 2, F.M. Gradstein, J.G. Ogg, M.D. Schmitz, and G.M. Ogg (editors),
2260 Elsevier, Amsterdam, p.653-679.
- 2261 Henkes, G.A., Passey, B.H., Grossman, E.L., Shenton, B. J., Yancey, T. E., and Pérez-Huerta, A., 2018.
2262 Temperature evolution and oxygen isotope composition of Phanerozoic oceans from carbonate
2263 clumped isotope thermometry, *Earth and Planetary Science Letters*, v. 490, pp. 40-50,
2264 doi:10.1016/j.epsl.2018.02.001.
- 2265 Herrle, J.O., Schröder-Adams, C.J., Davis, W., Pugh, A.T., Galloway, J.M., and Fath, J., 2015. Mid-
2266 Cretaceous High Arctic stratigraphy, climate, and Oceanic Anoxic Events. *Geology*, 43(5): 403-406.
- 2267 Heydari, E., Arzani, N., and Hassanzadeh, J., 2008. Mantle plume: The invisible serial killer -
2268 Application to Permian-Triassic boundary mass extinction, *Palaeogeography, Palaeoclimatology,*
2269 *Palaeoecology*, v. 264, p. 147-162.
- 2270 Hildebrand, A.R., Penfield, G.T., Kring, D.A., Pilkington, M., Camargo, Z.A., Jacobsen, S.B., and Boynton,
2271 W.V., 1991. Chicxulub crater: A possible Cretaceous-Tertiary boundary impact crater on the Yucutan
2272 Peninsula, Mexico, *Geology*, 19:867-871.
- 2273 Hilgen, F.J., Lourens, L.J., and Van Dam, J.A., 2012. The Neogene Period, Chapter 29, in The Geologic
2274 Time Scale 2012, volume 2, F.M. Gradstein, J.G. Ogg, M.D. Schmitz, and G.M. Ogg, (editors), p. 923-
2275 978, Elsevier, Amsterdam.
- 2276 Hochuli, P.A., Hermann, E., Vigran, J.O., Bucher, H., and Weissert, H., 2010. Rapid demise and recovery
2277 of plant ecosystems across the end-Permian extinction event, *Global and Planetary Change*, v. 74, p.
2278 144-155.
- 2279 Hodel, F., Macouin, M., Trindade, R.I.F., Triantafyllou, A., Ganne, J., Chavagnac, V., Berger, J.,
2280 Rospabé, M., Destrienneville, C., Carlut, J., Ennih, N., and Agrinier, P., 2018. Fossil black smoker yields
2281 oxygen isotopic composition of Neoproterozoic seawater, *Nature Communications*, 9:1453, doi:
2282 10.1038/s41467-018-03890
- 2283 Hoffman, P.F., Kaufman, A.J., Halverson, G.P., and Schrag, D.P., 1998. A Neoproterozoic snowball
2284 Earth, *Science*, 281: 1342-1346.
- 2285 Hoffman, P.F., and Schrag, D.P., 2000. Snowball Earth, *Scientific American*, v. 282, p. 68-75.
- 2286 Hoffman, P.F., and Schrag, D.P., 2002. The snowball Earth hypothesis: testing the limits of global
2287 change, *Terra Nova*, v. 14, p. 129-155.
- 2288 Hoffman, P.F., and Li, Z.-X., 2009. A palaeogeographic context for Neoproterozoic glaciation,
2289 *Palaeogeography, Palaeoclimatology, Palaeoecology*, v. 277 (3-4), p 158-172.
- 2290 Hotinski, R., Bice, K.L., Kump, L.R., Najjar, R.G., and Arthur, M.A., 2001. Ocean stagnation and end-
2291 Permian anoxia. *Geology*, v. 29, p. 7-10.
- 2292 Hotinski, R.M., and Toggweiler, J.R., 2003. Impact of a Tethyan circumglobal passage on ocean heat
2293 transport and "equable" climates, *Paleoceanography*, 18:1007-1015.
- 2294 Hsu, K.J., Oberhänsli, H., Gao, J.Y., Shu, S., Haihong, C., and Krahenbuhl, U., 1985. 'Strangelove ocean'
2295 before the Cambrian. *Nature*, v. 316, p. 809-811.

- 2296 Huber, B.T., 1998. Tropical paradise at the Cretaceous poles?, *Science*, v. 282, p. 2199-2200.
- 2297 Huber, B.T., MacLeod, K.G., and Wing, S.L., 2000. *Warm Climates in Earth History*, Cambridge
2298 University Press, 462 pp.
- 2299 Huber, M., and Caballero, R., 2011. The early Eocene equable climate problem revisited: Climate of
2300 the Past Discussions, v.7., p. 241-304, doi: 10.5194/cpd-7-241-2011.
- 2301 Hughes, D.W., 2003. The approximate ratios between the diameters of terrestrial impact craters and
2302 the causative incident bolides, *Mon. Not. R. Astron. Soc.*, v. 338, p. 999-1003.
- 2303 IPCC 2007: Summary for Policymakers. IN: *Climate Change 2007: The Physical Science Basis.*
2304 *Contribution of Working Group I to the Fourth Assessment Report of the Intergovernmental Panel*
2305 *on Climate Change* [Solomon, S., D. Qin, M. Manning, Z. Chen, M. Marquis, K.B. Averyt, M. Tignor,
2306 and H.L. Miller (eds.)]. Cambridge University Press, Cambridge, United Kingdom and New York, USA.
- 2307 IPCC 2018: Summary for Policymakers. In: *Global Warming of 1.5°C. An IPCC Special Report on the*
2308 *impacts of global warming of 1.5°C above pre-industrial levels and related greenhouse gas emission*
2309 *pathways, in the context of strengthening the global response to the threat of climate change,*
2310 *sustainable development, and efforts to eradicate poverty* [Masson-Delmotte, V., P. Zhai, H.-O.
2311 Portner, D. Roberts, J. Skea, P.R. Sukla, A. Pirani, W. Moufouma-Okia, C. Pean, R. Pidcock, S. Connors,
2312 J.B.R. Matthews, Y. Chen, X. Zhou, M.I. Gomis, E. Lonnoy, T. Maycock, M. Tignor, and T. Waterfield
2313 (eds.)] Cambridge University Press, Cambridge, United Kingdom and New York, USA.
- 2314 IPCC 2019: Summary for Policymakers. In: *IPCC Special Report on the Ocean and Cryosphere in a*
2315 *Changing Climate* [H.-O. Portner, D.C. Roberts, V. Masson-Delmotte, P. Zhai, M. Tignor, E.
2316 Poloczanska, K. Mintenbeck, M. Nicolai, A. Okem, J. Petzold, B. Rama, N. Weyer(eds.)] Cambridge
2317 University Press, Cambridge, United Kingdom and New York, USA.
- 2318 Isozaki, Y., 1997. Permo-Triassic boundary superanoxia and stratified superocean: Records from Lost
2319 Deep Sea. *Science*, v. 276, p. 235-238.
- 2320 Jacobs, L.L., Polcyn, M.J., Taylor, L.H., and Ferguson, K., 2005, Sea-surface temperatures and
2321 paleoenvironments of dolichosaurs and early mosasaurs, *Netherlands Journal of Geosciences,*
2322 *Geologie en Mijnbouw*, 84-3:269-281.
- 2323 Jaffres, J.B.P., Shields, G.A., and Wallman, K., 2007. The oxygen isotope evolution of seawater: a critical
2324 review of a long-standing controversy and an improved geological water cycle model for the past 3.4
2325 billion years, *Earth-Science Reviews*, 83:83-122.
- 2326 Jenkyns, H.C., Jones, C.J., Grocke, D.R., Hesselbo, S.P., and Parkinson, D.N., 2002. Chemostratigraphy
2327 of the Jurassic System: applications, limitations and implications for palaeoceanography, *Journal of*
2328 *the Geological Society, London*, v. 159, p. 351–378.
- 2329 Jenkyns, H.C., 2010. Geochemistry of oceanic anoxic events. *Geochemical Geophysical Geosystems*,
2330 11:Q03004.
- 2331 Jenkyns, H.C., Schouten-Huibers, L., Schouten, S., and Sinninghe Damste, J.S., 2012. Warm Middle
2332 Jurassic–Early Cretaceous high-latitude sea-surface temperatures from the Southern Ocean, *Climate*
2333 *of the Past*, 8:215-226, doi:10.5194/cp-8-215-2012

- 2334 Joachimski, M. M., von Bitter, P. H., and Buggisch, W., 2006, Constraints on Pennsylvanian
2335 glacioeustatic sea-level changes using oxygen isotopes of conodont apatite, *Geology*, v. 34, no. 4, p.
2336 277-280.
- 2337 Joachimski, W.W., van Gelderin, R., Breisig, S., Buggisch, W., and Day, J., 2004. Oxygen isotope
2338 evolution of biogenic calcite and apatite during the Middle and Late Devonian, *International Journal*
2339 *of Earth Sciences (Geol Rundsch)*, v. 93, p. 542–553, doi: 10.1007/s00531-004-0405-8
- 2340 Joachimski, M.M., Breisig, S., Buggisch, W., Talent, J.A., Mawson, R., Gereke, M., Morrow, J.R., Day,
2341 J., and Weddige, K., 2009. Devonian climate and reef evolution: Insights from oxygen isotopes in
2342 apatite, *Earth and Planetary Science Letters*, v. 284, p. 599–609, doi:10.1016/j.epsl.2009.05.028
- 2343 Johnson, J.G., Klapper, G., Sandberg, C.A., 1985. Devonian eustatic fluctuations in Euramerica.
2344 *Geological Society of America Bulletin*, v. 96, p. 567–587.
- 2345 Johnson, J.G., 1988. Volcanism, eustasy, and extinctions. *Geology*, v. 16, p. 573–574.
- 2346 Jones, C.E., and Jenkyns, H.C., 2001. Seawater strontium isotopes, oceanic anoxic events, and
2347 seafloor hydrothermal activity in the Jurassic and Cretaceous, *American Journal of Science*, 301:112-
2348 149.
- 2349
- 2350 Jones, S.M., Hoggett, M., Greene, S.E., and Jones, T.D., 2019. Lareg Igneous Province thermogenic
2351 greenhouse gas flux could have initiated Paleocene-Eocene Thermal Maximum climate change,
2352 *Nature Communications*, v.10, article number 5547.
- 2353
- 2354 Jourdan, F., Féraud, G., Bertrand, H., Kampunzu, A.B., Tshoso, G., Watkeys, M.K., and Le Gall, B.
2355 2005. Karoo large igneous province: brevity, origin, and relation to mass extinction questioned by
2356 new $^{40}\text{Ar}/^{39}\text{Ar}$ age data. *Geology*, v. 33, p.745–748.
- 2357
- 2358 Jouzel, J., Masson-Delmotte, V., Cattani, O., Dreyfus, G., Falourd, S., Hoffmann, G., Minster, B.,
2359 Nouet, J., Barnola, J.M., Chappellaz, J., Fischer, H., Gallet, J.C., Johnsen, S., Leuenberger, M.,
2360 Loulergue, L., Luethi, D., Oerter, H., Parrenin, F., Raisbeck, G., Raynaud, D., Schilt, A., Schwander,
2361 J., Selmo, E., Souchez, R., Spahni, R., Stauffer, B., Steffensen, J.P., Stenni, B., Stocker, T.F., Tison, J.L.,
2362 Werner, M., and Wolff, E.W., 2007. Orbital and Millennial Antarctic Climate Variability over the Past
2363 800,000 Years, *Science*, v. 317, p.793-796.
- 2364
- 2365 Jovane, L., Coccioni, R., Marsili, A., Acton, G., 2009. The late Eocene greenhouse-icehouse transition:
2366 Observations from the Massignano global stratotype and point (GSSP), in C. Koeberl and A.
2367 Montanari, (eds.), *The Late Eocene Earth: Hot House, Ice House, and Impacts*, *Geol. Soc. America*,
2368 *Special Paper 452*149-168.
- 2369
- 2370 Judd, E., Bhattacharya, T., Ivany, L.C., 2020. A dynamical framework for interpreting ancient sea
2371 surface temperatures, *Geophysical Research Letters*, 47 (15):1-10, doi.org/10.1029/2020GL089044
- 2372
- 2373 Kamber, B.S., and Petrus, J.A., 2019. The influence of large bolide impacts on the Earth's Carbon
2374 Cycle, *Elements*, v.15, p.313-318.
- 2375
- 2376 Kamo, S.L., Czamanske, G.K., Amelin, Y., Fedorenko, V.A., Davis, D.W., and Trofimov, V.R., 2003.
2377 Rapid eruption of Siberian flood-volcanic rocks and evidence for coincidence with the Permian-
2378 Triassic boundary and mass extinction at 251 Ma. *Earth and Planetary Science Letters*, v. 214, p. 75-
91.

- 2379 Kasting, J.F., Howard, M.T., Wellman, K.T., Veizer, J., Shields, G., and Jaffres, J., 2006. Paleoclimates,
2380 ocean depth, and the oxygen isotopic composition of seawater, *Earth and Planetary Science Letters*,
2381 v. 252, p. 82-93.
- 2382 Keller, G., 2011. Defining the Cretaceous-Tertiary boundary: a practical guide and return to first
2383 principles. In: Keller, G., Adatte, T. (Eds.), *The KT Mass Extinction and the Chicxulub impact in Texas*.
2384 *SEPM Special Publication*, 100, 23-42.
- 2385 Keller, G., 2014. Deccan volcanism, the Chicxulub impact, and the end-Cretaceous mass extinction:
2386 Coincidence? Cause and effect? In: Keller, G., Kerr, A. (Eds.), *Volcanism, Impacts and Mass*
2387 *Extinctions: Causes and Effects*. *Geological Society of America Special Papers*, 505, 57-89,
2388 doi:10.1130/2014.2505(03).
- 2389 Keller, G., Mateo, P., Punekar, J., Khozyem, H., Gertsch, B., Spangenberg, J., Bitchong, A., and Adatte,
2390 T., 2017. Environmental Changes during the Cretaceous-Paleogene Mass Extinction and Paleocene-
2391 Eocene Thermal Maximum: Implications for the Anthropocene, *Gondwana Research*, v. 56, p. 69-89,
2392 doi.org/10.1016/j.gr.2017.12.002
- 2393 Kennett, J.P., and Stott, L.D., 1991. Abrupt deep-water warming, palaeoceanographic changes and
2394 benthic extinctions at the end of the Paleocene, *Nature*, v. 353, p.225-229.
- 2395 Kennett, J.P., Houtz, R.E., Andrews, P.B., Edwards, A. R., Gostin, V.A., Hajos, M., Hempton, M.A.,
2396 Jenkins, D.G., Margolis, S.V., Ovenshine, A.T., and Perch-Nielsen, K., 1974. Development of the Circum-
2397 Antarctic current, *Science*, 186:144-147.
- 2398 Kennett, J.P., 1995. A review of polar climate evolution during the Neogene based on the marine
2399 sediment record, in *Paleoclimate and Evolution with Emphasis on Human Origins*, E.S. Vrba, G.H.
2400 Denton, T.C. Patridge, and L.H. Burckle (eds.), Yale University Press, New Haven, p.49-64.
- 2401 Kennett, J.P., and Exon, N.F., 2004. Paleoceanographic evolution of the Tasmanian Seaway and its
2402 climatic implications, in N.F. Exon, J.P. Kennett and M. Malone, (eds.), *The Cenozoic Southern Ocean:*
2403 *Tectonics, Sedimentation, and Climate Change between Australia and Antarctica*, American
2404 Geophysical Union, *Geophys. Monograph* 151:345-367.
- 2405 Kidder, D.L. and Worsley, T.R., 2010. Phanerozoic Large Igneous Provinces (LIPs), HEATT (Haline
2406 Euxinic Acidic Thermal Transgression) episodes, and mass extinctions, *Palaeogeography*,
2407 *Palaeoclimatology, Palaeoecology*, v. 295, pp. 162-191.
- 2408 Kidder, D.L. and Worsley, T.R., 2012. A human-induced hothouse climate?, *GSA Today*, v. 22, no. 2,
2409 pp. 4 – 11, doi: 10.1130/G131A.1.
- 2410 Kiehl, J.T., and Shields, C., 2013. Sensitivity of the Palaeocene-Eocene Thermal Maximum climate to
2411 cloud properties: *Royal Society of London Philosophical Transactions*, ser. A, v. 371, 20130093,
2412 doi:10.1098/rsta.2013.0093.
- 2413 Kiessling, W., Flügel, and Golonka, J., 2002. Phanerozoic Reef Patterns, *SEPM (Society for*
2414 *Sedimentary Geology) Special Publication Number 72*, 775 pp.
- 2415 King, C., A., 2016. A Revised Correlation of Tertiary Rocks in the British Isles and adjacent areas of NW
2416 Europe, A.S. Gale & T.L. Barry (editors), *Geological Society Special Report no. 27*, 719 pp.
- 2417 Koeberl, C., and Montanari, A., 2009. *The Late Eocene Earth: Hot House, Ice House, and Impacts*, *Geol.*
2418 *Soc. America, Special Paper 452*, Boulder, Colorado, 322 pp.

- 2419 Köppen, W., 1918. Klassifikation der Klimate nach Temperatur, Niederschlag and Jahreslauf,
2420 Petermanns Geographische Mitteilungen, v. 64, pp.193-248.
- 2421 Korte, C., Hesselbo, S.P., Jenkyns, H.C., Rickaby, R.E.M., Spotl, C., 2009. Palaeoenvironmental
2422 significance of carbon- and oxygen-isotope stratigraphy of marine Triassic–Jurassic boundary
2423 sections in SW Britain, *Journal of the Geological Society of London*, v. 166, p. 431–445.
- 2424 Korte, C., Jones, P.J., Brand, U., Mertmann, D., and Veizer, J., 2008. Oxygen isotope values from high-
2425 latitudes: Clues for Permian sea-surface temperature gradients and Late Palaeozoic deglaciation,
2426 *Palaeogeography, Palaeoclimatology, Palaeoecology*, v. 269, p. 1–16,
2427 doi:10.1016/j.palaeo.2008.06.012
- 2428 Korte, C., Jasper, T., Kozur, H.W., and Veizer, J., 2005. $d^{18}\text{O}$ and $d^{13}\text{C}$ of Permian brachiopods: A
2429 record of seawater evolution and continental glaciation, *Palaeogeography, Palaeoclimatology,*
2430 *Palaeoecology*, v. 224, p. 333–351, doi:10.1016/j.palaeo.2005.03.01
- 2431 Kustatscher, E., Ash, S.R., Karasev, E., Pott, C., Vajda, V., Yu, J. & McLoughlin, S. 2018. Flora of the
2432 Late Triassic. In: Tanner, L. (ed.) *The Late Triassic World: Earth in a Time of Transition*, *Topics in*
2433 *Geobiology*, v. 46, p. 545-622, Springer, ISBN 978-3-319-68008-8.
- 2434 Kump, L.R., Arthur, M.A., Patkowsky, M.E., Gibbs, M.T., Pinkus, D.S., and Sheehan, P.M., 1999a. A
2435 weathering hypothesis for glaciation at high atmospheric CO_2 during the Late Ordovician,
2436 *Palaeogeography, Palaeoclimatology, and Palaeoecology*, v. 152, p. 173-187.
- 2437 Kump, L.R., Kasting, J.F., and Crane, R.G., 1999b. *The Earth System*, Prentice Hall, Upper Saddle River,
2438 N.J., 351 p.
- 2439 Kump, L.R., Arthur, M.A., 1999c. Interpreting carbon-isotope excursions: carbonates and organic
2440 matter. *Chemical Geology*, v. 161, p. 181–198.
- 2441 Kump, L.R., Gibbs, M.T., Arthur, M.A., Patzkowsky, M.E., and Sheehan, P.M., 1995. Hirnantian
2442 Glaciation and the Carbon Cycle, *Ordovician Odyssey: Short Papers for the Seventh International*
2443 *Symposium on the Ordovician System*, Las Vegas, Nevada, USA, June, 1995, (editors) J.D. Cooper,
2444 M.L. Droser, and S.C. Finney, p. 299-302, Society for Sedimentary Geology (SEPM), Pacific Section,
2445 Fullerton, CA.
- 2446 Kump, L.R., Pollard, D., 2008. Amplification of Cretaceous warmth by biological cloud feedbacks.
2447 *Science* 320, 195.
- 2448 Kump, L.R., 1991. Interpreting carbon-isotope excursions: Strangelove oceans. *Geology*, v. 19, p. 299-
2449 302.
- 2450 Ladant, J.-B., Donnadieu, Y., 2016. Palaeogeographic regulation of glacial events during the
2451 Cretaceous supergreenhouse. *Nat. Commun.* 7.
- 2452 Landing, E., 2012. Time-specific black mudstones and global hyperwarming on the Cambro-
2453 Ordovician slope and shelf of the Laurentia palaeocontinent, *Palaeogeog., Paleoclim., Palaeoecol.*,
2454 v. 367-368, p.256-272. Doi.org/10.1016/j.palaeo.2011.09.05
- 2455 Landing, E. 2018. Tropical weathering of the Taconic orogeny (i.e. “orogen”) as a driver for
2456 Ordovician cooling, *Geology Forum*, doi.org/10.1130/G3998.7c1

- 2457 Landing, E., Schmitz, M.D., Geyer, G., Traylor, R.B., and Bowring, S.A., 2020. Precise early Cambrian
2458 U–Pb zircon dates bracket the oldest trilobites and archaeocyathids in Moroccan West Gondwana,
2459 Geological Magazine <https://doi.org/10.1017/S0016756820000369>
- 2460 Landing E and Westrop SR, 2004. Environmental patterns in the origin and evolution loci of Early
2461 Cambrian skeletalized Metazoa: evidence from the Avalon microcontinent. In Neoproterozoic–
2462 Cambrian Biological Revolutions (eds JH Lipps and B Waggoner), pp. 93–105. Paleontological Society,
2463 Special Paper no. 10.
- 2464 Larson, R.L., 1991. Geological consequences of superplumes, *Geology*, 19:963-966.
- 2465 Larson, R.L., and Erba, E., 1999. Onset of the mid-Cretaceous greenhouse in the Barremian-Aptian:
2466 Igneous events and biological sedimentary, and geochemical responses, *Paleoceanography*, 14:663-
2467 678.
- 2468 Lawver, L.A., and Gahagan, L.M., 2003. Evolution of Cenozoic seaways in the circum-Antarctic region,
2469 *Palaeogeog., Paleoclim., Palaeoecol.*, 198:11-37.
- 2470 Lécuyer, C., Amiot, R., Touzeau, A., 2013. Calibration of the phosphate $\delta^{18}\text{O}$ thermometer with
2471 carbonate-water oxygen isotope fractionation equations, *Chemical Geology*, v. 347, pp. 217-226,
2472 doi:10.13039/501100004794.
- 2473 Legates, D.R., and Wilmott, C.J., 1990. Mean seasonal and spatial variability in global surface air
2474 temperature, *Theoretical and Applied Climatology*, v. 41, pp. 11-21.
- 2475 Lenton, T.M., Crouch, M., Johnson, M., Pires, N., and Dolan, L., 2012. First plants cooled the
2476 Ordovician, *Nature Geoscience*, v.5, p. 86-89.
- 2477 Ling, M.-X., Zhan, R.-B., Wang, G.-X., Wang, Y., Amelin, Y., Tang, P., Liu, J.-B., Jin, J., Huang, B., Wu, R.-
2478 C., Xue, S., Fu, B., Bennett, V.C., Wei, X., Luan, X.-C., Finnegan, S., Harper, D.A.T., Rong, J.-Y., 2019. An
2479 extremely brief end Ordovician mass extinction linked to abrupt onset of glaciation. *Solid Earth*
2480 *Sciences*, 4(4): 190-198.
- 2481 Lisiecki, L.E., and Raymo, M.E., 2005. A Pliocene-Pleistocene stack of 57 globally distributed benthic
2482 $\delta^{18}\text{O}$ records. *Paleoceanography* 20 (1), PA1003. <http://dx.doi.org/10.1029/2004PA001071>.
- 2483 Livermore, R., Nankivell, A., Eagles, G., And Morris, P., 2005. Paleogene opening of the Drake
2484 Passage, *Earth and Planetary Science Letters*, 236:459-470.
- 2485 Looy, C.V., Brugman, W.A., Dilcher, D.L., and Visscher, H., 1999. The delayed resurgence of equatorial
2486 forests after the Permian-Triassic ecologic crisis, *Proc. National Acad. Sci.*, 96:13857-13862.
- 2487 Luz, B., Kolodny, Y., and Kovach, J., 1984, Oxygen isotope variations in phosphate of biogenic
2488 apatites, III. Conodonts, *Earth and Planetary Science Letters*, v. 69, no. 2, p. 255-262.
- 2489 Malchus, N., and Steuber, T., 2002. Stable isotope records (O, C) of Jurassic aragonitic shells from
2490 England and NW Poland: palaeoecologic and environmental implications, *Geobios*, v. 35, p. 29–39.
- 2491 Marshall, H.G., Walker, J.C.G., & Kuhn, W.R., 1988. Long-term climate change and the geochemical
2492 cycle of carbon. *Journal of Geophysical Research*, 93, 791–801.
- 2493 Marshall, L.G., Webb, D.S., Sepkoski, J.J., Raup, D.M., 1982. Mammalian evolution and the Great
2494 American Interchange, *Science*, 215:1351-1357.

- 2495 Martinez-Peréz, C., Cascales-Minana, B., Plasencia, P., and Botella, H., 2014. Exploring the major
2496 depletions of conodont diversity during the Triassic, *Historical Biology*, v. 27, p. 503–507.
- 2497 Marzoli, A., Renne, P.R., Piccirillo, E.M., Ernesto, M., Bellieni, G., and DeMin, A., 1999. Extensive 200-
2498 million-year-old continental flood basalts of the Central Atlantic Magmatic Province (CAMP), *Science*,
2499 v 284, p. 616-618.
- 2500 McArthur, J.M., Janssen, N.M.M, Reboulet, S., Leng, M.J., Thirwall, M.F., van de Schootbrugge, B.,
2501 2007. Palaeotemperatures, polar ice-volume, and isotope stratigraphy (Mc/Ca, $\delta^{18}O$, $\delta^{13}C$,
2502 $^{87}Sr/^{86}Sr$): The Early Cretaceous (Berriasian, Valanginian, Hauterivian), *Palaeogeography*,
2503 *Palaeoclimatology*, *Palaeoecology*, v. 248, p. 391-430, doi:10.1016/j.palaeo.2006.12.015
- 2504
- 2505 McCune A.R., and Schaeffer, B., 1986. Triassic and Jurassic fishes: patterns of diversity in *The*
2506 *Beginning of the Age of Dinosaurs*, (editor), Kevin Pandian, p. 171–181, Cambridge University Press,
2507 Cambridge, UK.
- 2508 McElwain J.C., Beerling D.J., and Woodward F.I., 1999. Fossil plants and global warming at the
2509 Triassic-Jurassic boundary, *Science*, v. 285, p. 1386–1390.
- 2510 McElwain J.C., Punyasena S.W., 2007. Mass extinction events and the plant fossil record. *Trends in*
2511 *Ecology and Evolution*, v. 22, p. 548–557.
- 2512 McGhee, G.R., Clapham, M.E., Sheehan, P.M., Bottjer, D.J., and Droser, M.L., 2013. A new ecological-
2513 severity ranking of major Phanerozoic biodiversity crises, *Palaeogeography*, *Palaeoclimatology*,
2514 *Palaeoecology* 370: 260–270
- 2515 McGhee, G.R., Jr., 1996. *The Late Devonian Mass Extinction: The Frasnian/Famennian Crisis*, *Critical*
2516 *Moments in Paleobiology and Earth History Series*, D. J. Bottjer and R.K. Bambach (editors), Columbia
2517 University Press, New York, 303 pp.
- 2518 McGhee, G.R., Jr., 2005. Modelling Late Devonian extinction hypotheses, in *Understanding Late*
2519 *Devonian and Permian-Triassic Biotic and Climatic Events; Towards an Integrated Approach*, D.J.
2520 Over, J.R. Morrow, and P.B. Wignall (editors), *Developments in Palaeontology & Stratigraphy*, v. 20,
2521 p. 37 – 50. Elsevier, Amsterdam.
- 2522 McHone, J.G., and Puffer, J.H., 2003. Flood Basalt Provinces of the Pangean Atlantic Rift: Regional
2523 Extent and Environmental Significance, in P.M. LeTourneau & P.E. Olsen (eds.), *The Great Rift*
2524 *Valleys of Pangea in Eastern North America: Tectonics, Structure, and Volcanism*, Volume 1,
2525 Columbia University Press, New York, p.141-154.
- 2526 McInerney, F.A., Wing, S.L., 2011. The Paleocene-Eocene Thermal Maximum: a perturbation of
2527 carbon cycle, climate, and biosphere with implications for the future. *Annual Review of Earth*
2528 *Planetary Sciences*, v. 39, p. 489–516.
- 2529 McKenzie, N.R., and Jiang, H., 2019. Earth’s outgassing and climatic transitions: The slow burn
2530 towards environmental “catastrophes”?, *Elements*, v.15, p.325-330.
- 2531 McKerrow, W.S., Scotese, C.R., and Brasier, M., 1992. Early Cambrian continental reconstructions,
2532 *Journal of the Geological Society of London*, v. 149, p. 599-606.

- 2533 McLaren, D.J., 1970. Presidential address: Time, Life and Boundaries, *Journal of Paleontology*, v. 48,
2534 p. 801-815.
- 2535 McLaren, D., 1983. Bolides and biostratigraphy. *Geol. Soc. Am. Bull.* 94, 313–324.
- 2536 Melosh, H.J., 1989. *Impact Cratering, A Geologic Process*, Oxford University Press, New York, 253 p.
- 2537 Meyer, K.M., and Kump, L.R., 2008. Oceanic Euxinia in Earth History: Causes and Consequences,
2538 *Annual Review of Earth and Planetary Sciences*, 36:251-288.
- 2539
- 2540 Mii, H.-S., Shi, G.R., Wang, C.-A., 2013. Late Paleozoic middle-latitude Gondwana environment-
2541 stable isotope records from Western Australia, *Gondwana Research*, v. 24, p. 125–138,
2542 doi.org/10.1016/j.gr.2012.10.013
- 2543 Mii, H.-S., Grossman, E.L., and Yancey, T.E., 1999. Carboniferous isotope stratigraphies of North
2544 America: Implications for Carboniferous paleoceanography and Mississippian glaciation, *Geological*
2545 *Society of America Bulletin*, v. 111, no. 7, p. 960–973.
- 2546 Mii, H.-S., Shi, G.R., Cheng, C.-J., and Chen, Y.-Y., 2012. Permian Gondwanaland paleoenvironment
2547 inferred from carbon and oxygen isotope records of brachiopod fossils from Sydney Basin, southeast
2548 Australia, *Chemical Geology*, v. 291, p. 87–103, doi:10.1016/j.chemgeo.2011.10.002
- 2549 Milankovitch, M., 1920. *Theorie Mathematique des Phenomenes Thermiques produits par la*
2550 *Radiation Solaire*, Gauthier-Villars, Paris, 340 p.
- 2551 Miller, C.S., Petersen, F., da Silva, A.-C., Baranyi, V., Reichart, G.J., and Kürschner, W.M., 2017.
2552 Astronomical age constraints and extinction mechanisms of the Late Triassic Carnian crisis. *Nature*,
2553 *Scientific Reports* 7: doi:10.1038/s41598-017-02817-7.
- 2554 Miller, K.G., Fairbanks, R.G., and Mountain, G.S., 1987. Tertiary oxygen isotope synthesis, sea level
2555 history, and continental margin erosion, *Paleoceanography*, v. 2, p. 1-19.
- 2556 Miller, K.G., Barrera, E., Olsson, R.K., Sugarman, P.J., Savin, S.M., 1999. Does ice drive early
2557 Maastrichtian eustasy? *Geology* 27, 783–786.
- 2558 Miller, K.G., Sugarman, P.J., Browning, J.V., Kominz, M.A., Olsson, R.K., Feigenson, M.D., Hernández,
2559 J.C., 2004. Upper Cretaceous sequences and sea-level history, New Jersey coastal plain. *Geol. Soc.*
2560 *Am. Bull.* 116, 368–393.
- 2561 Miller, K.G., Kominz, M.A., Browning, J.V., Wright, J.D., Mountain, G.S., Katz, M.E., Sugarman, P.J.,
2562 Cramer, B.S., Christie-Blick, N., Pekar, S.F., 2005a. The Phanerozoic record of global sea-level change.
2563 *Science* 310, 1293–1298.
- 2564 Miller, K.G., Wright, J.D., J. V. Browning, J.V., 2005b. Visions of ice sheets in a greenhouse world.
2565 *Mar. Geol.* 217, 215–231.
- 2566 Miller, K.G., Sherrell, R.M., Browning, J.V., Field, M.P., Gallagher, W., Olsson, R.K., Sugarman, P.J.,
2567 Tuorto, S., and Wahyudi, H., 2010. Relationship between mass extinction and iridium across the
2568 Cretaceous-Paleogene boundary in New Jersey, *Geology*, 38:867-870.

- 2569 Miller, K.G., Browning, J.V., Scmetz, W.J., Kopp, R.E., Mountain, G.S., and Wright, J.D., 2020.
2570 Cenozoic sea-level and cryosphere evolution from deep-sea geochemical and continental margin
2571 records, *Science Advances*, 6, eaaz1346.
- 2572 Mills, B.J.W., Krause, A.J., Scotese, C.R., Hill, D.J., Shields, G.A., and Lenton, T.M., 2019. Modelling the
2573 long-term carbon cycle, atmospheric CO₂, and Earth surface temperature from late Neoproterozoic
2574 to present-day, *Gondwana Research*, v. 67, p. 172-186, doi: 10.1016/j.gr.2018.12.001 1342-937.
- 2575 Molnar, P., and Tapponnier, P., 1975. Cenozoic tectonics of Asia: Effects of a continental collision,
2576 *Science*, 189:419-426.
- 2577 Montañez, I.P., Tabor, N.J., Niemeier, D., DiMichele, W.A., Frank, T.D., Fielding, C.R. Isbell, J.L.,
2578 Birgenheier, L.P., and Rygel, M.C., 2007. CO₂ -Forced Climate and Vegetation Instability During Late
2579 Paleozoic Deglaciation, *Science*, v. 315, n. 5808, p. 87-91, doi: 10.1126/science.1134207
- 2580 Montañez I.P., McElwain, J.C., Poulsen, C.J., White, J.D., DiMichele, W.A., Wilson, J.P., Griggs, G., and
2581 Hren, M.T., 2016. Climate, p CO₂, and terrestrial carbon cycle linkages during late Palaeozoic glacial-
2582 interglacial cycles, *Nature Geoscience*, v.9, p. 824-828, doi :10.1038/NGEO2822
- 2583 Montañez, I.P., and J.C., Poulsen, 2013. The Late Paleozoic Ice Age: An Evolving Paradigm, *Annual*
2584 *Reviews of Earth and Planetary Sciences*, v41, p.629-656.
- 2585 Moore, G.T., Hayashida, D.N., Ross, C.A., and Jacobson, S.R., 1992, Paleoclimate of the
2586 Kimmeridgian/Tithonian (Late Jurassic) world: I. Results using a general circulation model,
2587 *Palaeogeography, Palaeoclimatology, and Palaeoecology*, 93:113-150.
- 2588 Moore, G.T., Jacobson, S.R., Ross, C.A., and Hayashida, D.N., 1994. A paleoclimate simulation of the
2589 Wenlockian (late Early Silurian) world using a general circulation model with implications for early land
2590 plant paleoecology, *Palaeogeog., Paleoclim., Palaeoecol.*, 110:115-144.
- 2591 Morley, R.J., 2011. Cretaceous and Tertiary climate change and the past distribution of megathermal
2592 rainforests, in *Tropical Rainforest Responses to Climatic Change*, M.B. Bush, J.R. Flenley, W.D.
2593 Gosling, (editors), p. 1-34, Springer-Verlag, Berlin.
- 2594 Mory, A.J., Redfern, J., and Martin, J.R., 2008. A review of Permian-Carboniferous glacial deposits in
2595 Western Australia, in C.R. Fielding, T.D. Frank. and J.L. Isbell (editors), *Resolving the Late Paleozoic*
2596 *Ice Age in Time and Space*, Geological Society of America Special Paper v. 441, p. 29-40.
- 2597 Mueller, S., Krystyn, L., and Kürschner, W.M. 2016a. Climate variability during the Carnian Pluvial
2598 Phase – a quantitative palynological study of the Carnian sedimentary succession at Lunz am See,
2599 Northern Calcareous Alps, Austria, *Palaeogeography, Palaeoclimatology, Palaeoecology*, v. 441, p.
2600 198–211.
- 2601 Mueller, S., Hounslow, M.W., and Kürschner, W.M. 2016b. Integrated stratigraphy and
2602 palaeoclimate history of the Carnian Pluvial Event in the Boreal realm; new data from the Upper
2603 Triassic Kapp Toscana Group in central Spitsbergen (Norway), *Journal of the Geological Society*, v.
2604 173, p. 186–202.
- 2605 Munnecke, A., Calner, M., Harper, D.A.T., and Servais, T., 2010. Ordovician and Silurian sea–water
2606 chemistry, sea level, and climate: A synopsis, *Palaeogeography, Palaeoclimatology, Palaeoecology*, v.
2607 296, p. 389–413, doi:10.1016/j.palaeo.2010.08.001

- 2608 Mutterlose, J., Pauly, S., and Steuber, T., 2009. Temperature controlled deposition of early
2609 Cretaceous (Barremian–early Aptian) black shales in an epicontinental sea, *Palaeogeography,*
2610 *Palaeoclimatology, Palaeoecology*, 273:330-345, doi:10.1016/j.palaeo.2008.04.026
- 2611 Nance, R.D., Murphy, J.B., Santosh, M., 2014. The supercontinent cycle: A retrospective essay,
2612 *Gondwana Research*, v. 25, p. 4-29, doi: 10.1016/j.gr.2012.12.026.
- 2613 Nance, R.D., and Murphy, J.B., 2018. Supercontinents and the case for Pannotia, in *Fifty Years of the*
2614 *Wilson Cycle Concept in Plate Tectonics*, R.W. Wilson, G.A. Houseman, K.J.W. McCaffrey, A.G. Dore,
2615 and S.J.H. Butler, Geological Society, London, Special Publications, 470, p. 1-17,
2616 doi:/10.1144/SP470.5.
- 2617 Nardin, E., Godd ris, Y., Donnadi u, Y., Le Hir, G., & Blakey, R.C., 2011. Modeling the early Paleozoic
2618 long-term climatic trend. *Geological Society of America Bulletin*. doi: 10.1130/B30364.1
- 2619 Navarro-Ramirez, J.P., Bodin, S., Consorti, L., and Immenhauser, A., 2017. Response of western South
2620 American epeiric-neritic ecosystem to middle Cretaceous Oceanic Anoxic Events, *Cretaceous*
2621 *Research*, v. 75, p. 61–80
- 2622 O’Brien, C.L., Robinson, S.A., Pancost, R.D., Sinninghe Damst , J. S., Schouten, S., Lunt, D. J., Alsenz,
2623 H., Bornemann, A., Bottini, C., Brassell, S. C., Farnsworth, A., Forster, A., Huber, B. T., Inglis, G. N.,
2624 Jenkyns, H. C., Linnert, C., Littler, K., Markwick, P., McAnena, A., Mutterlose, J., Naafs, B. D. A.,
2625 P ttmann, W., Sluijs, A., van Helmond, N. A. G. M., Vellekoop, J., Wagner, T., and Wrobel, N. E.,
2626 2017. Cretaceous sea-surface temperature evolution: Constraints for TEX 86 and planktonic
2627 foraminiferal Oxygen isotopes, *Earth-Science Reviews*, v. 172, p. 224-247, doi:
2628 10.1016/j.earscirev.2017.07.012. 2018
- 2629 Ogg, J.G. 2015. The mysterious Mid-Carnian “Wet Intermezzo” global event, *Journal of Earth Science*,
2630 v. 26, p. 181–191.
- 2631 Ogg, J.G., Ogg, G.M., and Gradstein, F.M., 2016. *A Concise Geological Time Scale 2016*, Elsevier,
2632 Amsterdam, 234 pp.
- 2633 Otto-Bliesner, B.L., 1995. Continental drift, runoff, and weathering feedbacks: Implications from
2634 climate model experiments. *Journal of Geophysical Research*, 100, 11,537-11,548
- 2635 Pankhurst, R.J., Leat, P.Y., Sruoga, P., et al., 1998. The Chon Aike province of Patagonia and related
2636 rocks in West Antarctica: a silicic large igneous province, *Journal of Volcanology and Geothermal*
2637 *Research*, 81: 113-136.
- 2638 Pankhurst, R.J., Riley, T.R., Fanning, C.M., and Kelley, S.P., 2000. Episodic silicic volcanism in
2639 Patagonia and the Antarctic peninsula: chronology of magmatism associated with the break-up of
2640 Gondwana, *Journal of Petrology*, 41:605-625.
- 2641 Park, J., and Royer, D.L., 2011. Geological constraints on the glacial amplification of Phanerozoic
2642 climate sensitivity, *American Journal of Science*, v. 311, p. 1-26, doi: 10.2475/01.2011.01.
- 2643 Parrish, J.T., 1993, Climate of the supercontinent Pangea, *J. Geology*, v. 101, p. 217-235.
- 2644 Parrish, J.T., 1998. *Interpreting Pre-Quaternary Climate from the Geologic Record*, Columbia
2645 University Press, New York, 338 pp.
- 2646 Parrish, J.T., and Spicer, R.A., 1988, Late Cretaceous terrestrial vegetation: A near polar temperature

- 2647 curve, *Geology*, 16:22-25.
- 2648 Peng, S., Babcock, L.E., and Cooper, R.A., 2012. The Cambrian Period, Chapter 19, in *The Geologic*
2649 *Time Scale 2012*, volume 2, F.M. Gradstein, J.G. Ogg, M.D. Schmitz, and G.M. Ogg (editors), Elsevier,
2650 Amsterdam, p. 437-488.
- 2651 Petersen, S.V., Dutton, A., Lohmann, K.C., 2016. End-Cretaceous extinction in Antarctica linked to
2652 both Deccan volcanism and meteorite impact via climate change, *Nature Communications*, 7:12079
2653 doi: 10.1038/ncomms12079
- 2654 Petit J.R., Jouzel, J., Raynaud, D., Barkov, N.I., Barnola, J.-M., Basile, I., Bender, M., Chappellaz, J.,
2655 Davis, M., Delaygue, G., Delmotte, M., Kotlyakov, V.M., Legrand, M., Lipenkov, V.Y., Lorius, C., Pépin,
2656 L., Saltzman, E., and Stievenard, M., 1999. Climate and atmospheric history of the past 420,000 years
2657 from the Vostok ice core, Antarctica, *Nature*, V. 299, p. 429-436.
- 2658 Pillans, B., and Gibbard, P., 2012. The Quaternary Period, Chapter 30, in *The Geologic Time Scale 2012*,
2659 volume 2, F.M. Gradstein, J.G. Ogg, M.D. Schmitz, and G.M. Ogg, (editors), p. 855-922, Elsevier,
2660 Amsterdam.
- 2661 Pirrie, D., Doyle, P., Marshall, J., Ellis, G., 1995. Cool Cretaceous climates: new data from the Albian
2662 of Western Australia. *J. Geol. Soc.* 152: 739–742.
- 2663 Pirrie, D., Marshall, J., Doyle, P., Riccardi, A., 2004. Cool early Albian climates; new data from
2664 Argentina. *Cretaceous Research* 25:, 27–33.
- 2665 Podlaha, O.G., Mutterlose, J., and Veizer, J., 1998. Preservation of $\delta^{18}\text{O}$ and $\delta^{13}\text{C}$ in belemnite
2666 rostra from Jurassic/early Cretaceous successions, *American Journal of Science*, v. 298, p. 324-347.
- 2667 Powell, C. McA., Li, Z.X., McElhinny, M.W., Meert, J.G., and Park, J.K., 1993. Paleomagnetic
2668 constraints on the timing of the Neoproterozoic breakup of Rodinia and the Cambrian formation of
2669 Gondwana, *Geology*, v. 21, pp. 889-892.
- 2670 Powell, C. McA., 1995. Are Neoproterozoic glacial deposits preserved on the margins of North
2671 America related to the fragmentation of two supercontinents (Comment), *Geology*, v. 23, pp. 1053-
2672 1054.
- 2673 Preto, N., Kustatscher, E., and Wignall, P.B. 2010. Triassic climates—state of the art and
2674 perspectives. *Palaeogeography, Palaeoclimatology, Palaeoecology*, 290:1–10.
- 2675 Price, G.D., 1999. The evidence and implications of polar ice during the Mesozoic. *Earth Sci. Rev.* 48,
2676 183–210.
- 2677 Price, G., Mutterlose, J., 2004. Isotopic signals from late Jurassic–early Cretaceous (Volgian–
2678 Valanginian) sub-Arctic belemnites, Yatria River, Western Siberia. *J. Geol. Soc.* 161, 959–968.
- 2679 Price, G.D., Nunn, E.V., 2010. Valanginian isotope variation in glendonites and belemnites from Arctic
2680 Svalbard: transient glacial temperatures during the Cretaceous greenhouse. *Geology* 38, 251–254.
- 2681 Price, G.D., Passey, B.H., 2013. Dynamic polar climates in a greenhouse world: evidence from
2682 clumped isotope thermometry of Early Cretaceous belemnites. *Geology* 41, 923–926.

- 2683 Prokoph, A., Shields, G. A., and Veizer, J., 2008, Compilation and time-series analysis of a marine
2684 carbonate $\delta^{18}\text{O}$, $\delta^{13}\text{C}$, $^{87}\text{Sr}/^{86}\text{Sr}$ and $\delta^{34}\text{S}$ database through Earth history, *Earth-Science Reviews*, v. 87,
2685 no. 3, p. 113-133.
- 2686 Pucéat, E., Lécuyer, C., Sheppard, S.M., Dromart, G., Reboulet, S., Grandjean, P., 2003. Thermal
2687 evolution of Cretaceous Tethyan marine waters inferred from oxygen isotope composition of fish
2688 tooth enamels. *Paleoceanography* 18, 1029. <http://dx.doi.org/10.1029/2002PA000823>.
- 2689 Punekar, J., Mateo, P., and Keller, G., 2014. Effects of Deccan volcanism on paleoenvironment and
2690 planktic foraminifera: A global survey, *Geological Society of America Special Paper*, v. 505, p. 91-116,
2691 doi:10.1130/2014.2505(04)
- 2692 Quiron, P.C., and MacLeod, K.G., 2014. Oxygen isotopes from conodont apatite of the midcontinent,
2693 US: Implications for Late Ordovician climate evolution, *Palaeogeography, Palaeoclimatology,*
2694 *Palaeoecology*, v. 404, p. 57–66, doi.org/10.1016/j.palaeo.2014.03.036
- 2695 Racki, G., 2020. A volcanic scenario for the Frasnian–Famennian major biotic crisis and other Late
2696 Devonian global changes: More answers than questions?, *Global and Planetary Change*, v. 189,
2697 doi.org/10.1016/j.gloplacha.2020.103174
- 2698 Racki, G., 2005. Toward understanding Late Devonian global events: few answers, many questions,
2699 in *Understanding Late Devonian and Permian-Triassic Biotic and Climatic Events; Towards an*
2700 *Integrated Approach*, D.J. Over, J.R. Morrow, and P.B. Wignall (editors), *Developments in*
2701 *Palaeontology & Stratigraphy*, v. 20, p. 5-36, Elsevier, Amsterdam.
- 2702 Rampino. M.R., 2020. Relationship between impact-crater size and severity of related mass
2703 extinction episodes (in press).
- 2704 Rampino. M.R., Caldiéra, K., and Prokoph, A., 2019. What causes mass extinctions? Large
2705 asteroid/comet impacts, flood-basalt volcanism, and ocean anoxia— Correlations and cycles, *in*
2706 Koeberl, C., and Bice, D.M., eds., *250 Million Years of Earth History in Central Italy: Celebrating 25*
2707 *Years of the Geological Observatory of Coldigioco: Geological Society of America Special Paper 542,*
2708 p. 1–32, [https://doi.org/10.1130/2019.2542\(14\)](https://doi.org/10.1130/2019.2542(14)).
- 2709 Rampino, M.R., and Self, S., 2015. Large Igneous Provinces and Biotic Extinctions, in *The*
2710 *Encyclopedia of Volcanoes*, second edition, H. Sigurdsson, B. Houghton, H. Rymer, J. Stix, and S.
2711 McNutt (editors), p.1049-158, Elsevier, Amsterdam.
- 2712 Rampino. M.R., and Shen, S.-Z., 2019. The end-Guadalupian (259.8 Ma) biodiversity crisis: the sixth
2713 major mass extinction?, *Historical Biology*, doi: 10.1080/08912963.2019.1658096
- 2714 Raup, D.M., 1979. Size of the Permo-Triassic bottleneck and its evolutionary implications. *Science*, v.
2715 206, p. 217-218.
- 2716 Raymo, M.E., Kozdon, R. , Evans, D., Lisiecki, L., and Ford, H.L., 2018. The accuracy of mid-Pliocene
2717 $\delta^{18}\text{O}$ -based ice volume and sea level reconstructions, *Geochimica et Cosmochimica Acta*, Vol. 63,
2718 No. 7/8, pp. 1039–1048.
- 2719 Raymo, M.E., and Ruddiman, W.F., 1992. Tectonic forcing of Late Cenozoic Climate, *Nature* 359:117-
2720 122.

- 2721 Raymo, M.E., Ruddiman, W.F., & Froelich, P.N. 1988. Influence of late Cenozoic mountain building on
2722 ocean geochemical cycles. *Geology*, 16, 649–653.
- 2723 Rea, D.K., Zachos, J.C., Owen, R.M., and Gingerich, P.D., 1990. Global change at the Paleocene-
2724 Eocene boundary: climatic and evolutionary consequences of tectonic events, *Palaeogeography*,
2725 *Palaeoclimatology*, *Palaeoecology* 79:117-128.
- 2726 Rees, P.McA., Ziegler, A.M., and Valdes, P.J., 2000, Jurassic phytogeography and climates: new data
2727 and model comparisons, in *Warm Climates in Earth History*, BT. Huber, K.G. MacLeod, and S. Wing
2728 (editors), Cambridge University Press, Cambridge, p. 297-318.
- 2729 Reichow, M.K., Saunders, A.D., White, R.V., Al'Mukhamedov, A.I., and Medvedev, A.Ya., 2005.
2730 Geochemistry and petrogenesis of basalts from the West Siberia Basin: an extension of the Permo-
2731 Triassic Siberian Traps, Russia. *Lithos*, v. 79, p. 425-452.
- 2732 Reichow, M. K., Pringle, M. S., Al'Mukhamedov, A. I., Allen, M. B., Andreichev, V. L., Buslov, M. M.,
2733 Davies, C. E., Fedoseev, G. S., Fitton, J. G., Inger, S., Medvedev, A. Y., Mitchell, C., Puchkov, V. N.,
2734 Safonova, I. Y., Scott, R. A., and Saunders, A. D., 2009, The timing and extent of the eruption of the
2735 Siberian Traps large igneous province: Implications for the end-Permian environmental crisis, *Earth*
2736 *and Planetary Science Letters*, v. 277, no. 1-2, p. 9-20.
- 2737 Renne, P.R., Sprain, C.J., Richards, M.A., Self, S., Vanderkluysen, L., and Pande, K., 2015. State shift in
2738 Deccan volcanism at the Cretaceous-Paleogene boundary, possibly induced by impact, *Science* 350
2739 (6256):76-78.
- 2740 Retallack, G., 2013. Permian and Triassic greenhouse crises, *Gondwana Research*, v. 24, p. 90–103,
2741 doi:10.1016/j.gr.2012.03.003.
- 2742 Retallack, G.J., Sheldon, N.D., Carr, P.F., Fanning, M., Thompson, C.A., Williams, M.L., Jones, B.J., and
2743 Hutton, A., 2011. Multiple Early Triassic greenhouse crises impeded recovery from Late Permian
2744 mass extinction, *Palaeogeography*, *Palaeoclimatology*, *Palaeoecology*, v. 308, 233–251, doi:
2745 10.1016/j.palaeo.2010.09.022
- 2746 Richards, M.A., Alvarez, W., Self, S., Karlstrom, L., Renne, P.R., Manga, M., Sprain, C.J., Smit, J.,
2747 Vanderkluysen, L., and Gibson, S.A., 2015. Triggering of the largest Deccan eruptions by the
2748 Chicxulub impact, *Geological Society of America Bulletin*, 127 (11-12):1507-
2749 1520, doi:10.1130/B31167.1
- 2750 Rigo, M., and Joachimski, M.M., 2010. Palaeoecology of Late Triassic conodonts: constraints from
2751 oxygen isotopes in biogenic apatite, *Acta Palaeontologica Polonica*, v. 55, p. 471–478.
- 2752 Rigo, M., Preto, N., Roghi, G., Tateo, F., and Mietto, P. 2007. A rise in the Carbonate Compensation
2753 Depth of western Tethys in the Carnian (Late Triassic): deep-water evidence for the Carnian Pluvial
2754 Event, *Palaeogeography*, *Palaeoclimatology*, *Palaeoecology*, v. 246, p. 188–205.
- 2755 Roghi, G., Gianolla, P., Minarelli, L., Pilati, C., and Preto, N., 2010. Palynological correlation of Carnian
2756 humid pulses throughout western Tethys, *Palaeogeography*, *Palaeoclimatology*, *Palaeoecology*, v.
2757 290, p. 89–106.
- 2758 Rogner, H.H., 2012. Energy Resources and Potential, Chapter 7, in Yeager, Kurt, Dayo, Felix, Fisher,
2759 Brian, Fouquet, Roger, Gilau, Asmerom, Rogner, Hans-Holger, Haug, Marianne, Hosier,
2760 Richard, Miller, Alan, Schnitteger, Sabine, Lustig, Nora, Johansson, Thomas B., Nakicenovic,

- 2761 Nebojsa, Patwardhan, Anand and Gomez-Echeverri, Luis (2012) *Energy and economy*. In: Global
2762 Energy Assessment (Gea). Cambridge University Press, Cambridge, UK, pp. 385-422. ISBN
2763 9780511793677
- 2764 Rosenau, N. A., Tabor, N. J., and Herrmann, A. D., 2014, Assessing the paleoenvironmental
2765 significance of middle–late Pennsylvanian conodont apatite $\delta^{18}\text{O}$ values in the illinois basin conodont
2766 apatite $\delta^{18}\text{O}$ values, *Palaios*, v. 29, no. 6, p. 250-265.
- 2767 Rowley, D.B., 1996. Age of initiation of collision between India and Asia: A review of stratigraphic
2768 data, *Earth and Planetary Sciences*, v. 145: 1-13.
- 2769 Rowley, D.B., 1998. Minimum age of initiation of collision between India and Asia north of Everest
2770 based on the subsidence history of the Zhepure mountain section, *Journal of Geology*, v. 106: 229-
2771 235.
- 2772 Rowley, D.B. and Currie, B.S., 2006. Palaeo-altimetry of the late Eocene to Miocene Lunpola basin,
2773 central Tibet, *Nature*, v. 439/9, p. 677-681, doi:10.1038/nature04506
- 2774 Royer, D.L., Berner, R.A., Montañez, I.P., Tabor, N.J., and Beerling, D.J., 2004. CO₂ as a primary driver
2775 of Phanerozoic climate, *GSA Today*, v. 14, no. 3, p. 4-10, doi: 10.1130/1052-5173 (2004) 014<0004:
2776 CAAPDO>2.0.CO:2.
- 2777 Royer, D., 2016. Climate Sensitivity in the Geological Past, *Annual Review of Earth and Planetary
2778 Sciences*, v. 44, pp. 277-293., <https://doi.org/10.1146/annrev-earth-100815-024150>.
- 2779 Ruddiman, W.F., 2001. *Earth's Climate: Past and Future*, W.H. Freeman and Company, New York, NY,
2780 465 pp.
- 2781 Ruffell, A., Simms, M.J., and Wignall, P.B., 2015. The Carnian Humid Episode of the late Triassic: a
2782 review, *Geological Magazine*, v. 153, p. 271–284.
- 2783 Sandberg, C.A., Morrow, J.R., Ziegler, W., 2000. Late Devonian events and mass extinc- tions. In:
2784 Catastrophic Events and Mass Extinctions: Impacts and Beyond. 1053. Lunar and Planetary Institute
2785 Contribution, Houston, Texas, pp. 188–189.
- 2786 Sandberg, C.A., Morrow, J.R., Ziegler, W., 2002. Late Devonian sea-level changes, catastrophic
2787 events, and mass extinctions. In: Koeberl, C., MacLeod, K.G. (Eds.), *Catastrophic Events and Mass
2788 Extinctions: Impacts and Beyond*, Geological Society of America Special Paper 356, p. 473–487.
- 2789 Sanei, H., Grasby, S., and Beauchamp, B., 2012. Latest Permian mercury anomalies. *Geology*, v. 40, p.
2790 63-66.
- 2791 Saunders, A.D., England, R.W., Reichow, M.K., and White, R.V., 2005. A mantle plume origin for the
2792 Siberian traps: uplift and extension in the West Siberian Basin, *Russia, Lithos*, 79:407-424.
- 2793 Suarez, C.A., Edmonds, M., and Jones, A.P., 2019. Earth catastrophes and their impact on the
2794 Carbon Cycle, *Elements*, v.15, p. 301-306.
- 2795 Savin, S.M., Douglas, R.G., and Stehli, F.G., 1975. Tertiary marine paleotemperatures, *Geological
2796 Society of America Bulletin*, v. 86, p. 1499-1510.

- 2797 Savin, S.M., 1977. The history of the Earth's surface temperature during the past 100 Ma, Annual
2798 Reviews of Earth and Planetary Sciences, v. 5, p. 319-355.
- 2799 Savitsky, A., and Golay, M.J.E., 1964. Smoothing and Differentiation of Data by Simplified Least
2800 Squares Procedures, Analytical Chemistry, v. 36, no. 8, pp. 1627-1639.
- 2801 Scher, H.D., and Martin, E.E., 2006. Timing and Climatic Consequences of the opening of Drake
2802 Passage, Science, 312:428-430.
- 2803 Schlanger, S.O., and Jenkyns, H.C., 1976. Cretaceous oceanic anoxic events: causes and
2804 consequences, Geol. Mijnbouw, 55:179-184.
- 2805 Schmitz, M.D., and Davydov, V.I., 2012. Quantitative radiometric and biostratigraphic calibration of
2806 the Pennsylvanian–Early Permian (Cisuralian) time scale and pan-Euramerican chronostratigraphic
2807 correlation, Geological Society of America Bulletin, v. 124, no. 3/4, p. 549–577, doi: 10.1130/B30385.
- 2808 Schobben, M., van de Schootbrugge, B., Wignall, P.B., 2019. Interpreting the carbon isotope record
2809 of mass extinctions, Elements, v. 15, p.331-337.
- 2810 Scholle, P.A., 1995. Carbon and sulfur isotope stratigraphy of the Permian and Adjacent Intervals, in
2811 *The Permian of the Northern Hemisphere*, volume 1: Paleogeography, Paleoclimates, Stratigraphy, P.A.
2812 Scholle, T.M. Peryt, D.S Ulmer-Scholle (editors), Springer-Verlag, Berlin, p. 133-149.
- 2813 Schouten, S., Hopmans, E.C., Schefuß, E., Sinninghe Damsté, J.S., 2002. Distributional variations in
2814 marine crenarchaeotal membrane lipids: a new tool for reconstructing ancient sea water
2815 temperatures? Earth Planet. Sci. Lett. 204, 265–274.
- 2816 Schuchert, C., 1910. Palaeogeography of North America, Geological Society of America Bulletin, 20,
2817 427-606.
- 2818 Schuchert, C., 1955. (published posthumously), Atlas of paleogeographic Maps of North America, C.
2819 O. Dunbar & C. M. Levene (Eds.), John Wiley & Sons, New York, and Chapman & Hall, Ltd., London,
2820 177 pp.
- 2821 Schulte, P., Alegret, L., Arenillas, I., et al., 2010. The Chicxulub asteroid impact and mass extinction at
2822 the Cretaceous-Paleogene boundary, Science, 327:1214-1218.
- 2823 Scotese, C.R., Boucot, A.J., and McKerrow, W.S., 1999. Gondwanan paleogeography and
2824 paleoclimatology, in Gondwana 10: Event Stratigraphy, Journal of African Earth Sciences, v. 28, issue
2825 1, pp. 99-114.
- 2826 Scotese, C.R., 2009. Late Proterozoic plate tectonics and paleogeography: A tale of two
2827 supercontinents, Rodinia and Pannotia, in Global Neoproterozoic petroleum systems: The emerging
2828 potential in North Africa, J. Craig, J. Thurow, A. Whitman, and Y. Abutarruma (editors), Geological
2829 Society of London Special Publication 326, pp. 67-83.
- 2830 Scotese, C.R., 2014. Atlas of Permo-Carboniferous Paleogeographic Maps (Mollweide Projection),
2831 Maps 53-64, volume 4, The Late Paleozoic, PALEOMAP Project Atlas for ArcGIS, PALEOMAP Project,
2832 Evanston, IL.
- 2833 Scotese, C.R., 2016. A New Global Temperature Curve for the Phanerozoic, (abstract), Geological
2834 Society of America Annual Meeting, Sunday, September 25, 2016, Session no. 74, #287, Recent

- 2835 Advances in Paleoclimatology and Paleoceanography (Posters). Exhibit Hall E/F (Colorado
2836 Convention Center), Geological Society of America Annual Meeting, Denver, CO.
- 2837 Scotese, C.R., 2020. Global Warming during the next 300 years, A Global Warming Calculator
2838 (student exercise with Excel spreadsheet), PALEOMAP Project, Evanston, IL. 49 pp.
- 2839 Sellwood, B.W., and Valdes, P.J., 2006. Mesozoic climates: General circulation models and the rock
2840 record, *Sedimentary Geology* 190:269–287, doi:10.1016/j.sedgeo.2006.05.013
- 2841 Şengör, A.M.C., and Atayman, S., 2009. The Permian Extinction and the Tethys: An exercise in global
2842 geology, *Geological Society of America Special Papers*, v. 448, 96 pp.
- 2843 Sepkoski, J.J., Jr., 1989. Periodicity in extinction and the problem of catastrophism in the history of life.
2844 *Journal of the Geological Society of London*, v. 146, p. 7-19.
- 2845 Sepkoski Jr., J.J., 1996. Patterns of Phanerozoic extinction: a perspective from global data bases, in
2846 O.H. Walliser (editor), *Global Events and Event Stratigraphy in the Phanerozoic*, Springer-Verlag,
2847 Berlin, pp. 35–51.
- 2848 Sheehan, P.M., 2001. The Late Ordovician Mass Extinction, *Annual Reviews of Earth and Planetary
2849 Sciences*, v. 29, p. 331–364.
- 2850 Sheehan, P.M., and Coorough, P.J., 1990. Brachiopod zoogeography across the Ordovician – Silurian
2851 extinction event, in *Palaeozoic Palaeogeography and Biogeography*, W.S. McKerrow and C.R. Scotese
2852 (editors), *Geological Society Memoir No. 12*, p. 181-187.
- 2853 Shi, G.R., 2001. Possible influence of Gondwanan glaciation on low-latitude carbonate sedimentation
2854 and trans-equatorial faunal migration: the Lower Permian of South China, *Papers from IGCP Project
2855 No. 411 on the Geodynamic Processes of Gondwanaland-derived Terranes in Eastern Asia*,
2856 *Geosciences Journal*, v. 5, no. 1, p. 57-63.
- 2857 Simms, M.J., and Ruffell, A.H. 1989. Synchronicity of climatic change and extinctions in the Late
2858 Triassic, *Geology*, v. 17, p. 265–268.
- 2859 Shell (2018), Shell Scenarios: SKY, Meeting the Goals of the Paris Agreement,
2860 [https://www.shell.com/promos/business-customers-promos/download-latest-scenario-
2861 sky/ jcr_content.stream/1530643931055/eca19f7fc0d20adbe830d3b0b27bcc9ef72198f5/shell-
2862 scenario-sky.pdf](https://www.shell.com/promos/business-customers-promos/download-latest-scenario-sky/jcr_content.stream/1530643931055/eca19f7fc0d20adbe830d3b0b27bcc9ef72198f5/shell-scenario-sky.pdf)
- 2863 Sloss, L.L., 1963. Sequences in the cratonic interior of North America, *Geological Society of America
2864 Memoir* 39, pp. 91-124.
- 2865 Smit, J., 1999. The global stratigraphy of the Cretaceous Tertiary boundary impact ejecta, *Annual
2866 Review of Earth and Planetary Sciences*, 27:75-91, doi:10.1146/annrev.earth.27.1.75.
- 2867 Song, H., Wignall, P.B., Chu, D., Tong, J., Sun, Y., He, W., and Tian, L., 2014. Anoxia/high temperature
2868 double whammy during the Permian-Triassic marine crisis and its aftermath, *Scientific Reports*,
2869 4:4132, doi: 10.1038/srep04132
- 2870 Song, H., Wignall, P.B., Song, H., Dai, X., and Chu, D., 2019. Seawater temperature and dissolved
2871 oxygen over the past 500 million years, *Journal of Earth Sciences*, v.30, no. 2, p. 236-243,
2872 doi:10.1007/s12583-028-1002-2.

- 2873 Song, H., Huang, S., Jia, E., Dai, X., Wignall, P.B., Dunhill, A.M., 2020. Flat latitudinal diversity gradient
2874 caused by the Permian–Triassic mass extinction. *Proceedings of the National Academy of Sciences*,
2875 117(30): 17578-17583.
- 2876 Spicer, R.A., Ahlberg, A., Herman, A.B., Hofmann, C.C., Raikevich, M., Valdes, P.J., and Markwick, P.J.,
2877 2008. The Late Cretaceous continental interior of Siberia: A challenge for climate models, *Earth and*
2878 *Planetary Science Letters*, v. 267, p. 228-235, doi:10.1016/j.espl.2007.11.049.
- 2879 Spray, J., 2020. Earth Impact Database (EID),
2880 http://passc.net/EarthImpactDatabase/New%20website_05-2018/Index.html
- 2881 Stanley, G. D., 2003. The evolution of modern corals and their early history, *Earth Science Reviews*, v.
2882 60, p. 195–225.
- 2883 Stanley, S.M., 2016. Estimates of the magnitudes of major marine mass extinctions in earth history,
2884 *Proceedings of the National Academy of Sciences, USA.*, v. 113, E6325–E6334.
2885
- 2886 Steffen. W., Rockstrom, J., Richardson, K., Lenton, T.M., Folke, C., Liverman, D., Summerhayes, C.P.,
2887 Barnosk, A.D., Cornell, S.E., Crucifix, M., Donges, J.F., Fetzer, I., Lade, S.J., Scheffer, M., Winkelmann,
2888 R., and Schellnhuber, H.J., 2019. Trajectories of the Earth System in the Anthropocene, *Proc.*
2889 *National Academy of Sciences*, www.pnas.org/cgi/doi/10.1073/pnas.1810141115, 8 p.
2890
- 2891 Stock, C.W., 2005. Devonian stromatoporoid originations, extinctions, and paleobiogeography: how
2892 they relate to the Frasnian-Famennian extinction, in *Understanding Late Devonian and Permian-*
2893 *Triassic Biotic and Climatic Events; Towards an Integrated Approach*, D.J. Over, J.R. Morrow, and P.B.
2894 Wignall (editors), *Developments in Palaeontology & Stratigraphy*, v. 20, p. 71 – 92, Elsevier,
2895 Amsterdam.
2896
- 2897 Sullivan, D.L., Brandon, A.D., Eldrett, J., Bergman, S.C., Wright, S., and Minisini, D., 2020. High
2898 resolution osmium data record three distinct pulses of magmatic activity during Cretaceous Oceanic
2899 Anoxic Event 2 (AOE-2), *Geochimica et Cosmochimica Acta*, v. 285, p. 257-273.
- 2900 Summerhayes, C.P., 2015. *Earth’s Climate Evolution*, Wiley-Blackwell, Chichester, UK, 394 pp.
- 2901 Sun, Y., Joachimski, M.M., Wignall, P.B., Yan, C., Chen, Y., Jiang, H., Wang, L., and Lai, X., 2012.
2902 *Lethally Hot Temperatures During the Early Triassic Greenhouse*, *Science*, v. 338, p. 366-370.
- 2903 Sun, Y.D., Wignall, P.B., Joachimski, M.M., Bond, D.P.G., Grasby, S.E., Lai, X.L., Wang, L.N., Zhang,
2904 Z.T., Sun, S., 2016. Climate warming, euxinia and carbon isotope perturbations during the Carnian
2905 (Triassic) Crisis in South China, *Earth and Planetary Science Letters*, v. 444, p. 88-100,
2906 doi:org/10.1016/j.epsl.2016.03.037
- 2907 Swanson-Hysell, N.L., and Macdonald, F.A., 2017. Tropical weathering of the Taconic Orogeny as a
2908 driver for Ordovician cooling, *Geology*, v.45, p. 719-722., doi.org/10.1130/G38985.1
- 2909 Tans, P. 2009. An accounting of the observed increase in oceanic and atmospheric CO₂ and an
2910 outlook for the future, *Oceanography*, v. 22, No.4, pp. 26 -35.
- 2911 Taylor, B., 2006. The single largest oceanic plateau: Ontong Java–Manihiki–Hikurangi. *Earth and*
2912 *Planetary Science Letters*, v. 241, p. 372–380.

- 2913 Taylor, E.L., Taylor, T.N., and Cuneo, R., 2000. Permian and Triassic high latitude paleoclimates:
2914 evidence from fossil biotas, in Huber, B.T., MacLeod, K.G., and Wing, S.L., (editors), *Warm Climates in*
2915 *Earth History*, Cambridge University Press, p. 321-350.
- 2916 Toggweiler, J.R., and Bjornsson, H., 2000. Drake Passage and palaeoclimate, *Journal of Quaternary*
2917 *Science*, 15:319-328.
- 2918 Tollefsen, E., Balic-Zunic, T., Mörth, C. et al., 2020.
- 2919 Torsvik, T.H., Svensen, H. H., Steinberger, B., Royer, D. L., Jerram, D.A., Jones, M.T, and Domeier,
2920 M., 2020. Connecting the Deep Earth and the Atmosphere, in *Mantle Convection and Surface*
2921 *Expression* S. Cottaar et al. (editors), AGU Monograph (in press).
- 2922 Trotter, J., Williams, I.S., Barnes, C.R., Männik, P., and Simpson, A., 2016. New conodont $\delta^{18}\text{O}$
2923 records of Silurian climate change: Implications for environmental and biological events,
2924 *Palaeogeography, Palaeoclimatology, Palaeoecology*, v. 443, p.34–48,
2925 doi.org/10.1016/j.palaeo.2015.11.011
- 2926 Trotter, J.A., Williams, I.S., Barnes, C.R., Lécuyer, C., and Nicoll, R.S., 2008. Did Cooling Oceans
2927 Trigger Ordovician Biodiversification? Evidence from Conodont Thermometry, *Science*, v. 321, no.
2928 5888, p. 550-554, DOI: 10.1126/science.1155814
- 2929 Trotter, A.J., Williams, S.I., Nicora, A., Mazza, M., and Rigo, M., 2015, Long-term cycles of Triassic
2930 climate change: A new $\delta^{18}\text{O}$ record from conodont apatite, *Earth and Planetary Science Letters*, v.
2931 415, p. 165–174.
- 2932 Umbgrove, J.H.F., 1947. *The Pulse of the Earth*, Martinus Nijhoff, The Hague, Netherlands, 358 pp.
- 2933 United Nations, 2019. *United Nations Report on World Population*,
2934 ([https://www.un.org/development/desa/publications/world-population-prospects-2019-](https://www.un.org/development/desa/publications/world-population-prospects-2019-highlights.html)
2935 [highlights.html](https://www.un.org/development/desa/publications/world-population-prospects-2019-highlights.html)).
- 2936 Upchurch, G.R., Otto-Bliesner, B.L., and Scotese, C.R., 1999, Terrestrial vegetation and its effects on
2937 climate during the latest Cretaceous, in *Evolution of the Cretaceous Ocean-Climate System*, E.
2938 Barrera and C. Johnson, (editors), Geological Society of America, Special Paper 332, pp.407-426.
- 2939 Upchurch, G.R., Kiehl, J., Shields, C., Scherer, J., and Scotese, C.R., 2015. Latitudinal temperature
2940 gradients and high latitude temperatures during the latest Cretaceous: Congruence of geologic data
2941 and climate models, *Geology*, v. 43, no. 9, p. 683-686.
- 2942 Urey, H.C., Lowenstam, H.A., Epstein, S., McKinney, C.R., 1951. Measurements of paleotemperatures
2943 and temperatures of the Upper Cretaceous of England, Denmark, and the southeastern United
2944 States, *Geological Society of America Bulletin*, v. 62, p. 399-416.
- 2945 Valdes, P.J., 1994, Atmospheric general circulation models of the Jurassic, in *Palaeoclimates and their*
2946 *modeling: with special reference to the Mesozoic Era*, J.R.L. Allen, B.J. Hoskins, B.W. Sellwood, R.A.
2947 Spicer, and P.J. Valdes (editors), Chapman and Hall, London, p. 109-118.
- 2948 Valdes, P.J., Lunt, D.L., and Scotese, C.R., 2018. Modelling the Climate History of the Phanerozoic,
2949 (abstract), American Geophysical Union, Monday, December 10, 2018, Convention Center, Hall A-C
2950 (Poster Hall), Fall Meeting 2018, #PP11F-1031, Washington, D.C.

- 2951 Valdes, P.J., Scotese, C.R., and Lunt, D.J., 2020. Deep ocean temperatures through time, *Climates of*
2952 *the Past* (in press).
- 2953 Valdes, P.J. and Sellwood, B.W., 1992, A palaeoclimate model for the Kimmeridgian, *Palaeogeography,*
2954 *Palaeoclimatology, and Palaeoecology*, 95:47-72.
- 2955 Vandenberghe, N., Hilgen, F.J., Speijer, R.P., 2012. The Paleogene Period, Chapter 28, in *The Geologic*
2956 *Time Scale 2012*, volume 2, F.M. Gradstein, J.G. Ogg, M.D. Schmitz, and G.M. Ogg, (editors), p. 855-
2957 922, Elsevier, Amsterdam.
- 2958 van der Meer, D.G., Zeebe, R.E., van Hinsbergen, J.J., Sluijs, A., Spakman, W., and Torsvik, T., 2014.
2959 Plate tectonic controls on atmospheric CO₂ levels since the Triassic, *Proceedings of the National*
2960 *Academy of Sciences*, v. 111, no. 12, p. 4380-4385, doi/10.1073/pnas.1315657111
- 2961 van der Meer, D.G., van den Berg van Saparoea, A.P.H., van Hinsbergen, D.J.J., van de Weg, R.M.B.,
2962 Godderis, Y., Le Hir, G., and Donnadieu, Y., 2017. Reconstructing first-order changes in sea level
2963 during the Phanerozoic and Neoproterozoic using strontium isotopes, *Gondwana Research*, v. 44,
2964 22-34.
- 2965 van de Schootbrugge, B., Tremolada, F., Rosenthal, Y., Bailey, T.R., Feist-Burkhardt, S., Brinkhuis, H.,
2966 Pross, J., Kent, D.V., and Falkowski, P.G., 2007. End-Triassic calcification crisis and blooms of organic-
2967 walled 'disaster species', *Palaeogeography, Palaeoclimatology, Palaeoecology* 244:126–141,
2968 doi:10.1016/j.palaeo.2006.06.026
- 2969 van de Schootbrugge, B., Quan, T.M., Lindström, S., Püttmann, W., Heunisch, C., Pross, J., Fiebig, J.,
2970 Petschick, R., Röhling, H.-G., Richoz, S., Rosenthal, Y., Falkowski, P.G., 2009. Floral changes across the
2971 Triassic/Jurassic boundary linked to flood basalt volcanism, *Nature Geoscience*, v.2, p. 589-594.
- 2972 van de Schootbrugge, B., Bachan, A., Suan, G., Richoz, S., and Payne, J.L., 2013. Microbes, mud and
2973 methane: cause and consequence of recurrent Early Jurassic anoxia following the end-Triassic mass
2974 extinction, *Palaeontology*, v. 56, p. 685–709.
- 2975 van Gelderin, R., Joachimski, M.M., Day, J., Jansen, U., Alvarez, F., Yolkin, E.A., and Ma, X.-P., 2006.
2976 Carbon, oxygen and strontium isotope records of Devonian brachiopod shell calcite,
2977 *Palaeogeography, Palaeoclimatology, Palaeoecology*, v. 240, p. 47–67.
2978 doi:10.1016/j.palaeo.2006.03.045
- 2979 Vaughan, A.P.M., 2007. Climate and geology – A Phanerozoic perspective, in *Deep-Time Perspectives*
2980 *on Climate Change: Marrying the Signal from Computer Models and Biological Proxies*, Williams, M.,
2981 Haywood, A.M., Gregory, F.J., and Schmidt, D.N., (editors), p. 5-59, *Micropalaeontological Society*
2982 *Special Publication*, Geological Society of London, London.
- 2983 Veevers, J.J., Conaghan, P.J., and Shaw, S.E., 1994. Turning point in Pangean environmental history at
2984 the Permian/Triassic (P/Tr) boundary, in *Pangea: Paleoclimate, Tectonics, and Sedimentation during*
2985 *the Accretion, Zenith, and Breakup of a Supercontinent*, George D. Klein (ed.), *Geol. Soc. America*
2986 *Special Paper*, 288: 187-196.
- 2987 Veizer, J., Fritz, P., and Jones, B., 1986. Geochemistry of brachiopods – oxygen and carbon isotopic
2988 records of Paleozoic oceans, *Geochemica et Cosmochemica Acta*, v. 40, pp. 1387-1395.

- 2989 Veizer, J., Ala, D., Azmy, K., Bruckschen, P., Buhl, D., Bruhn, F., Carden, G.A.F., Diener, A., Ebner, S.,
2990 Godderis, Y., Jasper, T., Korte, C., Pawellek, F., Podlaha, O.G., and Strauss, H., 1999. $^{87}\text{Sr}/^{86}\text{Sr}$, $\delta^{13}\text{C}$
2991 and $\delta^{18}\text{O}$ evolution of Phanerozoic seawater, *Chemical Geology*, v. 161, no. 1-3, pp. 59-88.
- 2992 Veizer, J.T., Godderis, Y., Francois, L.M., 2000. Evidence for decoupling of atmospheric CO_2 and
2993 global climate during the Phanerozoic Eon, *Nature*, v. 408, no. 6813, p. 698-701, doi:
2994 10.1038/35047044. 2000
- 2995 Veizer, J., and Hoefs, J., 1976, The nature of $\text{O}^{18}/\text{O}^{16}$ and $\text{C}^{13}/\text{C}^{12}$ secular trends in sedimentary
2996 carbonate rocks, *Geochimica et Cosmochimica Acta*, v. 40, no. 11, p. 1387-1395.
- 2997 Veizer, J.T., and Prokoph, A., 2015. Temperatures and Oxygen isotopic composition of Phanerozoic
2998 oceans, *Earth-Science Reviews*, v. 146: p. 92-104, doi: 10.1016/j.earscirev.2015.03.008.
- 2999 Vellekoop, J., Sluijs, A., Smit, J., Schouten, S., Weijers, J.W.H., Sinninghe Damsté, and Brinkhuis, H.,
3000 2014. Rapid short-term cooling following the Chicxulub impact at the Cretaceous-Paleogene
3001 boundary, *Proceedings of the National Academy of Science*, v. 111, n. 21, pp. 7537-7541.
- 3002 Vellekoop, J., Esmeraysenlet, S., Miller, K.G., Browning, J.V., Sluijs, A., De Schootbrugge, B.V.,
3003 Damsté, J.S.S., Brinkhuis, H., 2016. Evidence for Cretaceous-Paleogene boundary bolide "impact
3004 winter" conditions from New Jersey, USA. *Geology*, 44(8): 619-622.
- 3005 Verard, C. and Veizer, J., 2019. On plate tectonics and ocean temperatures, *Geology*, v. 47, p. 881-
3006 885.
- 3007 Vickers, M.L., Bajnai, D., Price, G.D., Linckens, J., and Fiebig, J., 2019. Southern high-latitude warmth
3008 during the Jurassic–Cretaceous: New evidence from clumped isotope thermometry, *Geology*,
3009 doi.org/10.1130/G46263.1
- 3010 Walker, J.C.G., Hays, P.B., and Kasting, J.F., 1981. A negative feedback mechanism for the long-term
3011 stabilization of Earth's surface temperature. *Journal of Geophysical Research*, 86, 9776–9782.
- 3012 Wallace, D.R., 2004. *Beasts of Eden, Walking Whales, Dawn Horses, and Other Enigmas of Mammal*
3013 *Evolution*, University of California Press, Berkeley, 340 pp.
- 3014 Wanless, H.R. and Shepherd, F.P., 1936. Sea level and climatic changes related to late Paleozoic
3015 cycles. *Geological Society of America Bulletin*, v. 47, p. 1177-1206.
- 3016 Wanless, H.R. and Weller, J.M., 1932. Correlation and extent of Pennsylvanian cyclothems.
3017 *Geological Society of America Bulletin*, v. 43, p. 1003-1016.
- 3018 Waterhouse, J.B., and Shi, G.R., 2013. Climatic implications from the sequential changes in diversity
3019 and biogeographic affinities for brachiopods and bivalves in the Permian of eastern Australia and
3020 New Zealand, *Gondwana Research*, v. 24, p. 139–147, doi:10.1016/j.gr.2012.06.008
- 3021 Webby, B.D., Paris, F., Droser, M.L., and Percival, I.G., 2004. *The Great Ordovician Biodiversification*
3022 *Event*, Columbia University Press, New York, 884 pp.
- 3023 Weirzbowski, H., and Joachimski, M., Reconstruction of late Bajocian–Bathonian marine
3024 palaeoenvironments using carbon and oxygen isotope ratios of calcareous fossils from the Polish
3025 Jura Chain (central Poland), *Palaeogeography, Palaeoclimatology, Palaeoecology*, v. 254, p. 523–540,
3026 doi:10.1016/j.palaeo.2007.07.010

- 3027 Wenzel, B., LeCuyer, C., and Joachimski, M.M., 2000. Comparing oxygen isotope records of Silurian
3028 calcite and phosphate - $\delta^{18}\text{O}$ compositions of brachiopods and conodonts, *Geochimica et*
3029 *Cosmochimica Acta*, v. 64, no. 11, p. 1859–1872.
- 3030 Wenzel, B., and Joachimski, M.M., 1996. Carbon and oxygen isotopic composition of Silurian
3031 brachiopods (Gotland/Sweden)" palaeoceanographic implications, *Palaeogeography,*
3032 *Palaeoclimatology, Palaeoecology*, v. 122, p. 143-166.
- 3033 Westerhold, T., Marwan, N., Drury, A.J., Liebrand, D., Agnini, C., Anagnostou, E., Barnett, J.S.K.,
3034 Bohaty, S.M., De Vleeschouwer, D., Florindo, F., Frederichs, T., Hodell, D.A., Holbourn, A.E.,
3035 Kroon, D., Lauretano, V., Littler, K., Lourens, L.L., Lyle, M., Pälike, H., Röhl, U., Tian, J., Wilkens,
3036 R.H., Wilson, P.A., Zachos, J.C., 2020. An astronomically dated record of Earth's climate and its
3037 predictability over the last 66 million years, *Science* 369: 1383-1387.
- 3038 Whiteside, J.H., and Grice, K., 2016. Biomarker Records Associated with Mass Extinction Events,
3039 *Annual Review of Earth Planetary Sciences*, v. 44, p. 581–612, doi: 10.1146/annurev-earth-060115-
3040 012501
- 3041 Whiteside, J.H., Olsen, P.E., Eglinton, T., Brookfield, M.E., and Sambrotto, R.N., 2010. Compound-
3042 specific carbon isotopes from Earth's largest flood basalt eruptions directly linked to the end-Triassic
3043 mass extinction, *Proceedings of the National Academy of Sciences*, v. 107, p. 6721–6725.
- 3044 Wierzbowski, H., and Joachimsky, M., 2007. Reconstruction of the late Bajocian-Bathonian marine
3045 paleoenvironments using carbon and oxygen isotope ratios of calcareous fossils from the Polish Jura
3046 Chain (central Poland), *Palaeogeography, Palaeoclimatology, Palaeoecology*, v. 254, p. 523-540, doi:
3047 10.1016/j.palaeo.2007.07.010.
- 3048 Wignall, P.B., and Hallam, A., 1992. Anoxia as a cause of the Permian/Triassic mass extinction: facies
3049 evidence from northern Italy and the western United States. *Palaeogeography, Palaeoclimatology,*
3050 *Palaeoecology*, v. 93, p. 21-446.
- 3051 Wignall, P.B., 2001. Large igneous provinces and mass extinctions. *Earth-Science Reviews*, v. 53, p.1-
3052 33.
- 3053 Wignall, P.B., 2015. *The Worst of Times, How life on Earth Survived Eighty Million Years of*
3054 *Extinctions*, Princeton University Press, Princeton, NJ, 199 p.
- 3055 Wilf, P., Johnson, K., and Huber, B.T., 2003. Correlated terrestrial and marine evidence for global
3056 climate changes before mass extinction at the Cretaceous – Paleogene boundary, *Proceedings of the*
3057 *National Academy of Sciences*, v. 100, no. 2, p. 599-604, doi /10.1073/pnas.0234701100
- 3058 Willis, K.J., and McElwain, J.C., 2014. *The Evolution of Plants*, Oxford University Press, Oxford, UK,
3059 378 pp.
- 3060 Wing, S.L., Gingerich, P.D., Schmitz, B., and Thomas, E., 2003. Causes and Consequences of Globally
3061 Warm Climates in the Early Paleogene, *Geol. Soc. America, Special Paper 369*, Boulder, Colorado, 614
3062 pp.
- 3063 Wing, S., and Huber, B., 2019. *Earth's Temperature History Workshop*, Smithsonian National
3064 Museum of Natural History, March 30-31, 2018, Washington, D.C.

- 3065 Wolfe, J. A. and G. R. Upchurch, 1987. North American nonmarine climates and vegetation during
3066 the Late Cretaceous, *Palaeogeography, Palaeoclimatology, Palaeoecology* 61: 33-77.
- 3067 Wolfe, J.A., 1971. Tertiary climatic fluctuations and methods of analysis of Tertiary floras, *Palaeogeog.*,
3068 *Palaeoclim.*, *Palaeoecol.*, 9:27-57.
- 3069 Wolfe, J.A., 1978. A paleobotanical interpretation of Tertiary climates in the northern hemisphere,
3070 *American Scientist*, 66:694-703.
- 3071 Wolfe, J.A., 1992. Climatic, floristic, and vegetational changes near the Eocene/Oligocene boundary in
3072 North America, in *Eocene-Oligocene Climatic and Biotic Evolution*, D.R. Prothero and W.A. Berggren
3073 (eds.), Princeton University Press, Princeton, 421-436. pp.
- 3074 Wolfe, J.A., 1994. Tertiary climatic changes at middle latitudes of western North America, *Palaeogeog.*,
3075 *Palaeoclim.*, *Palaeoecol.*, 108:195-205.
- 3076 Worsley, T.R. & Kidder D.L., 1991. First-order coupling of paleogeography and CO₂, with global
3077 surface temperature and its latitudinal contrast. *Geology*, 19, 1161-1164.
- 3078 Yancey, T.E., and Guillemette, R.N., 2008. Carbonate accretionary lapilli in distal deposits of the
3079 Chicxulub impact event: *Geol. Soc. America Bulletin*, 120:1105-1118.
- 3080 Young, S.A., Saltzman, M.R., Foland, K.A., Linder, J.S., and Kump, L.R., 2009. A major drop in seawater
3081 ⁸⁷Sr/⁸⁶Sr during the Middle Ordovician (Darriwilian): Links to volcanism and climate?, *Geology* v. 9,
3082 no. 10, p. 951–954, doi: 10.1130/G30152A.1
- 3083 Zachos, J., Pagani, M., Sloan, L., Thomas, E., and Billups, K. 2001. Trends, rhythms and aberrations in
3084 global climate 65 Ma to present, *Science*, v. 292, p. 686-693.
- 3085 Zachos, J.C., Dickens, G.R., and Zeebe, R.E., 2008. An early Cenozoic perspective on greenhouse
3086 warming and carbon-cycle dynamics, *Nature*, v. 45117, p. 279-283.
- 3087 Zeebe RE, Zachos JC, Dickens GR. 2009. Carbon dioxide forcing alone insufficient to explain
3088 Palaeocene- Eocene Thermal Maximum warming. *Nat. Geosci.* 2:576–80
- 3089 Zeng, J., Cao, C.-Q., Davydov, V.I., and Shen, S.-Z., 2012. Carbon isotope chemostratigraphy and
3090 implications of palaeoclimatic changes during the Cisuralian (Early Permian) in the southern Urals,
3091 Russia, *Gondwana Research*, v. 21, p. 601–610, doi:10.1016/j.gr.2011.06.002
- 3092 Zhang, L., Chen, D., Huang, T., Yu, H., Zhou, X., Wang, J., 2020. An abrupt oceanic change and
3093 frequent climate fluctuations across the Frasnian–Famennian transition of Late Devonian:
3094 constraints from conodont Sr isotope. *Geol. J.* <https://doi.org/10.1002/gj.3657>. (in press).
- 3095 Zhang, R.M.J., Follows, Grotzinger, J., and Marshall, J., 2001. Could the Late Permian deep ocean
3096 have been anoxic? *Palaeogeography*, v. 16, p. 317-329.
- 3097 Zhu, M.-Y., Babcock, L.E., and Peng, S.-C., 2006. Advances in Cambrian stratigraphy and
3098 paleontology: Integrating correlation techniques, paleobiology, taphonomy and paleoenvironmental
3099 reconstruction, *Palaeoworld*, v.15, p. 217–222, doi:10.1016/j.palwor.2006.10.016
- 3100 Ziegler, A.M., Eshel, G., Rees, P.Mc., Rothfus, T.A., Rowley, D.B., and Sunderlin, D., 2003. Tracing the
3101 tropics across land and sea: Permian to present, *Lethaia*, v. 36, p. 227-254.

-
- 3102 Ziegler, A.M., Hulver, M.L., Rowley, D.B., 1997, Permian World Topography and Climate, in *Late Glacial*
3103 *and Postglacial Environmental Changes: Quaternary, Carboniferous-Permian, and Proterozoic*, I. Peter
3104 Martini (editor), Oxford University Press, Oxford, p. 111-146.
- 3105 Ziegler, A.M., Parrish, J.M., Jiping, Y., Gyllenhaal, E.D., Rowley, D.B., Parrish, J.T., Sahngyou, N.,
3106 Behher, A., and Hulver, M.L., 1994. Early Mesozoic phytogeography and climate, in Allen, J., Hoskins,
3107 B.J., Sellwood, B.W., Spicer, R.S., Valdes, P.J. (editors), *Paleoclimates and Their Modelling: with*
3108 *Spreial Reference to the Mesozoic Era*, Chapman and Hall, London, pp. 89-97.
- 3109 Ziegler, A.M., Rowley, D.B., Lottes, A.L., Sahagian, D.L., Hulver, and Gierlowski, T.C., 1985.
3110 *Paleogeographic Interpretation: With an Example from the Mid-Cretaceous*, *Annual Reviews of Earth*
3111 *and Planetary Sciences*, v. 13, p. 385-425
- 3112
- 3113
- 3114

3115

3116

Figure Captions

3117 Figure 1. Estimates of Phanerozoic Global Average Temperature (GAT). Sources: Wing and Huber
3118 (2019), Valdes et al. (2018), Mills et al. (2019), and This study.

3119 Figure 2. “Double Hump” pattern of Phanerozoic Climate (Fischer, 1981; 1982), I = icehouse, G =
3120 greenhouse.

3121 Figure 3. Modern Köppen belts and the average temperature of each belt.

3122 Figure 4. Early Permian (280 Ma) lithologic indicators of climate and continental paleo-Köppen Belts
3123 (Boucot et al., 2013).

3124 Figure 5. Mid-Cretaceous (100 Ma) lithologic indicators of climate and continental paleo-Köppen
3125 Belts (Boucot et al., 2013).

3126 Figure 6. Long-Term Phanerozoic temperature trend calculated by estimating the changing area of
3127 paleo-Köppen belts (see Supplementary Materials for data and details of calculations).

3128 Figure 7. Raw and mean values of oxygen isotopes from phosphatic and carbonate fossils for
3129 reconstructing sea surface temperatures over the past 500 million years (modified after Song et al.,
3130 2019). The scale of $\delta^{18}\text{O}_{\text{Phos}}$ is used for phosphatic fossils, i.e., phosphatic brachiopod, conodont, and
3131 fish. The scale of $\delta^{18}\text{O}_{\text{Carb}}$ is used for carbonate fossils, i.e., belemnite, bivalve, brachiopod, planktonic
3132 foraminifer, and others. Magenta curve represents the mean values of sea surface temperatures per
3133 million years. Shaded area represents 95% confidence intervals.

3134 Figure 8. Phanerozoic Isotopic Temperature (Song et al., 2019). A. = Each dot represents the
3135 average of all temperatures that fall within a given one million year interval. The best-fit curve was
3136 obtained using the Savitsky-Golay smoothing technique (window 11-15, degree 4). B. Change in
3137 Tropical Temperature ($\Delta T^{\circ}_{\text{trop}}$). The black dots along the x-axis are the times when no data are
3138 available.

3139

3140 Figure 9. Modifications to the Phanerozoic Isotopic Temperature Curve. The dashed line is the
3141 isotopic temperature curve (see Figure 8). The colored lines represent modifications and
3142 adjustments made to that curve based on geological and paleontological constraints.

3143 Figure 10. Comparison of isotopic temperature data from the late Pennsylvanian of South China
3144 (open dots) and the USA (black dots) (Song et al., 2019).

3145 Figure 11. Comparison of Cenozoic deep ocean isotopic temperatures and tropical temperatures A.
3146 gray line = low resolution Tropical Temperatures (this study), and the black line = high resolution Δ
3147 Tropical Temperatures for the Cenozoic. B. isotopic temperatures from deep ocean, benthic
3148 foraminifera (Zachos et al., 2001, 2008; Westerhold et al., 2020).

3149 Figure 12. Phanerozoic Global Average Temperature (GAT), blackline = Global Average Temperature,
3150 dashed line = Long-term temperature change derived from changes in the pole-to-Equator

3151 temperature gradient calculated from the changing area of Köppen Climatic Belts (see Figure 6).
3152 When the Global Average Temperature is below 18°C large polar icecaps can form. When the Global
3153 Average Temperature is above 18°C large polar icecaps are unlikely to form.

3154 Figure 13. Timing and magnitude of Large Igneous Provinces (rectangles) eruptions and bolide
3155 impacts (circles). The size of the rectangles indicates the relative eruptive intensity ($10^6 \text{ km}^2/\text{my}$)
3156 (left-hand scale). See Table 1 and 2 for abbreviations. Sources: Ernst (2014), Spray (2020).

3157 Figure 14. Comparison of the timing of LIPS (black squares, Table 1), large bolide impacts (circles
3158 with dots, Table 2), and putative large impact events (light gray circles with x's) with the changes in
3159 Tropical Temperature (ΔT_{trop}). The size of the lettering is roughly proportional to the size of the LIP
3160 or bolide impact. See Table 1 and 2 for abbreviations. Sources: Ernst (2014), Spray (2020).

3161 Figure 15. Phanerozoic Ice Ages. gray = global area of snow and ice cover (10^6 km^2), dotted line =
3162 snow and ice predicted by Global Average Temperatures ($\text{GAT} < 18^\circ\text{C}$, Figure 12), numbers =
3163 number of glacial deposits (tillites, dropstones, and glendonites). Note inverted temperature scale
3164 (left side).

3165 Figure 16. Tropical, Global Average, Deep Ocean, and Polar Temperatures. (a) red line = tropical
3166 temperature (15 N - 15 S), (b) black line = global average temperature (GAT), (c) blue line = deep
3167 ocean temperatures (after Valdes et al., 2020) (d) light blue line = polar temperature ($> 67 \text{ N\&S}$). The
3168 chronological resolution of this diagram, ~ 5 million years, matches the chronological resolution of
3169 the paleo-Köppen maps (see Supplementary Materials).

3170 Figure 17. The polar temperature and the Pole to Equator temperature gradient for different Global
3171 Average Temperatures (GAT). Polar Temperature = average temperature above 67° latitude (N&S),
3172 Deep Sea = the average temperature at the bottom of the oceans (after Valdes et al., 2020). Pole to
3173 Equator Gradient = the average change in temperature for every one degree of latitude measured
3174 between 30° and 60° latitude. The Pole to Equator temperature gradient is shallow near the Equator
3175 and steepens rapidly near the Pole. The plus signs are the combined average temperatures for the
3176 present-day northern and southern hemispheres. Frequency = the percent of the time during the
3177 Phanerozoic characterized by this Pole-to-Equator temperature gradient. All of these calculations
3178 are based on an average tropical temperature of 26°C (15 N – 15 S).

3179 Figure 18. Comparison of Phanerozoic global average temperatures (black line) with strontium flux
3180 ratio relative to the present-day flux (dashed line). Red line highlights when the trends are
3181 coincident.

3182 Figure 19. A Paleozoic Paleotemperature Timescale. white = warm time intervals, black = cool time
3183 intervals. Solid black line = Global Average Temperatures (GAT), $< 18^{\circ}\text{C}$ = large permanent,
3184 icecaps, $> 18^{\circ}\text{C}$ = no large, permanent icecaps. Light gray jagged lines = a schematic representation
3185 of >50 glacial/interglacial cycles during the Permo-Carboniferous. Timescale = International
3186 Chronostratigraphic Chart v2020/01. Refer to Table 3 for more information about each chronotemp
3187 and abbreviations.

3188 Figure 20. A Mesozoic Paleotemperature Timescale. white = warm time intervals, black = cool time
3189 intervals. Solid black line = Global Average Temperatures (GAT), $< 18^{\circ}\text{C}$ = large, permanent
3190 icecaps, $> 18^{\circ}\text{C}$ = no large, permanent icecaps. Timescale = International Chronostratigraphic Chart
3191 v2020/01. Refer to Table 3 for more information about each chronotemp and abbreviations.

3192 Figure 21. A Cenozoic Paleotemperature Timescale. white = warm time intervals, black = cool time
3193 intervals; Light gray jagged lines = a schematic representation of >50 glacial/interglacial cycles during
3194 the Plio-Pleistocene. Solid black line = Global Average Temperatures (GAT), $< 18^{\circ}\text{C}$ = large,
3195 permanent icecaps, $> 18^{\circ}\text{C}$ = no large, permanent icecaps. Timescale = International
3196 Chronostratigraphic Chart v2020/01. Refer to Table 3 for more information about each chronotemp
3197 and abbreviations.

3198 Figure 22. IPCC Estimates of Global Warming compared to the Results Predicted by the Carbon
3199 Budget Model (this study). The blue curve represents the projected increase in atmospheric CO_2
3200 based on the continued burning of fossil fuels at the “modern rate” (1970 – 2020). The black curves
3201 are the CO_2 levels used in the IPCC models RCP 2.5, RCP 4.5, RCP 6.0, and RCP 8.5. The red curve is
3202 the projected CO_2 levels obtained in our model (between 750 ppm and 800 ppm at 2200 CE).
3203 Estimates from RCP 2.5 and RCP 4.5 are too low. The estimate of CO_2 used in RCP 8.5 is much too
3204 high. Estimates of CO_2 used in RCP 6.0 are about right.

3205 Figure 23. Projection of Future Global Warming onto Phanerozoic Temperature Time Scale. The likely
3206 amount of Post-Anthropogenic Warming (PAW) (red line). The boxes indicate times in the geological
3207 past when global temperatures were within the range of predicted PAW. When the Global Average
3208 Temperature is below 18°C large polar icecaps can form. When the Global Average Temperature is
3209 above 18°C large polar icecaps are unlikely to form.

3210 Figure 24. Paleogeographic maps for the early Oligocene (30 Ma) and early Miocene (15 Ma). These
3211 past time periods are a good climatic match for world after Anthropogenic Warming.

3212